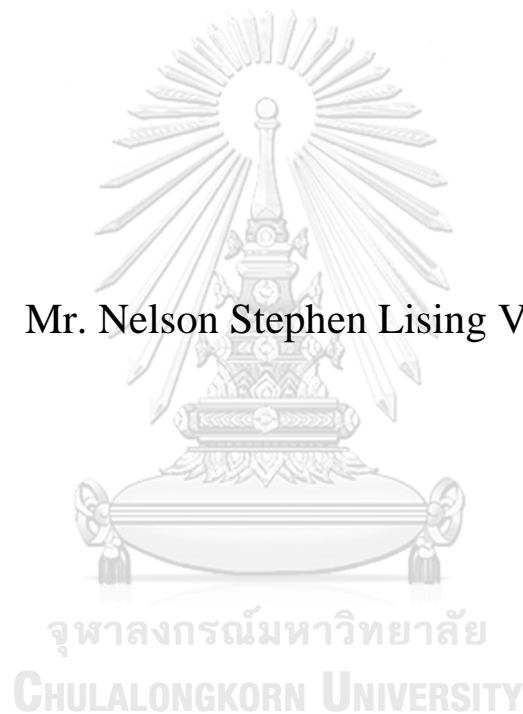


**BIAS CORRECTION OF SATELLITE PRECIPITATION  
ESTIMATES OVER THAILAND**

**Mr. Nelson Stephen Lising Ventura**



**A Thesis Submitted in Partial Fulfillment of the Requirements  
for the Degree of Master of Engineering in Water Resources Engineering  
Department of Water Resources Engineering  
FACULTY OF ENGINEERING  
Chulalongkorn University  
Academic Year 2020  
Copyright of Chulalongkorn University**

การปรับแก้ความเอนเอียงเชิงสถิติของการประมาณปริมาณฝนจากข้อมูลดาวเทียมในพื้นที่ประเทศไทย



วิทยานิพนธ์นี้เป็นส่วนหนึ่งของการศึกษาตามหลักสูตรปริญญาวิศวกรรมศาสตรมหาบัณฑิต  
สาขาวิชาวิศวกรรมแหล่งน้ำ ภาควิชาวิศวกรรมแหล่งน้ำ  
คณะวิศวกรรมศาสตร์ จุฬาลงกรณ์มหาวิทยาลัย  
ปีการศึกษา 2563  
ลิขสิทธิ์ของจุฬาลงกรณ์มหาวิทยาลัย

Thesis Title	BIAS CORRECTION OF SATELLITE PRECIPITATION ESTIMATES OVER THAILAND
By	Mr. Nelson Stephen Lising Ventura
Field of Study	Water Resources Engineering
Thesis Advisor	Assistant Professor PIYATIDA RUANGRASSAMEE, Ph.D.

---

Accepted by the FACULTY OF ENGINEERING, Chulalongkorn University  
in Partial Fulfillment of the Requirement for the Master of Engineering

..... Dean of the FACULTY OF  
ENGINEERING  
(Professor SUPOT TEACHAVORASINSKUN, D.Eng.)

THESIS COMMITTEE

..... Chairman  
(Assistant Professor ANURAK SRIARIYAWAT, Ph.D.)  
..... Thesis Advisor  
(Assistant Professor PIYATIDA RUANGRASSAMEE,  
Ph.D.)  
..... Examiner  
(Associate Professor TUANTAN KITPAISALSAKUL,  
D.Eng.)  
..... External Examiner  
(Thanapon Piman, Ph.D.)

จุฬาลงกรณ์มหาวิทยาลัย  
CHULALONGKORN UNIVERSITY

เนลสัน สตีเฟน ลิสซิ่ง เวนทูรา : การปรับแก้ความเอนเอียงเชิงสถิติของการประมาณปริมาณฝนจากข้อมูลดาวเทียมในพื้นที่ประเทศไทย. ( BIAS CORRECTION OF SATELLITE PRECIPITATION ESTIMATES OVER THAILAND) อ.ที่ปรึกษาหลัก : ผศ. ดร. ปิยธิดา เรืองรัมย์

ในช่วงหลายปีที่ผ่านมา ดาวเทียมอุตุนิยมวิทยาได้ทำให้เกิดการพัฒนาการประมาณปริมาณฝนจากข้อมูลดาวเทียมที่ให้อัตราความเข้มฝนที่ครอบคลุมพื้นที่ทั่วโลก อย่างไรก็ตาม ข้อมูลจากดาวเทียมมิได้เป็นการวัดปริมาณฝนตกในพื้นที่โดยตรง ดังนั้น จึงจำเป็นต้องมีการปรับแก้ความเอนเอียงเชิงสถิติของการประมาณปริมาณฝนจากข้อมูลดาวเทียมสำหรับการนำไปประยุกต์ใช้กับแบบจำลองทางอุทกวิทยาเพื่อให้ผลลัพธ์ที่สามารถนำไปใช้ประโยชน์ได้ วัตถุประสงค์ของการศึกษานี้เพื่อประเมินประสิทธิภาพของการปรับแก้ความเอนเอียงเชิงสถิติของการประมาณปริมาณฝนจากข้อมูลดาวเทียมในพื้นที่ประเทศไทย โดยประเมินข้อมูล 3 ข้อมูล ได้แก่ Precipitation Estimates from Remotely Sensed Information using Artificial Neural Networks – Cloud Classification System (PERSIANN-CCS), Global Satellite Mapping of Precipitation - Near Real Time (GSMaP\_NRT) และ Integrated Multi-satellite Retrievals for GPM (IMERG) Early version เปรียบเทียบกับข้อมูลฝนจากสถานีตรวจวัดของกรมอุตุนิยมวิทยา ในช่วงปีพ.ศ. 2546 – 2561 และปรับแก้การประมาณปริมาณฝนจากข้อมูลดาวเทียมด้วย 3 วิธี ได้แก่ Scaling, Quantile Mapping (QM) และ Artificial Neural Network (ANN) จากผลการศึกษาพบว่าโดยภาพรวมทั้งประเทศ PERSIANN-CCS และ IMERG Early มีปริมาณฝนที่สูงกว่าข้อมูลฝนจากสถานีตรวจวัด สำหรับ GSMaP\_NRT มีปริมาณฝนที่น้อยกว่าข้อมูลฝนจากสถานีตรวจวัด โดย IMERG Early มีค่า RMSE น้อยที่สุด รองลงมาคือ GSMaP\_NRT และ PERSIANN-CCS ตามลำดับ GSMaP\_NRT มีค่า Equitable Threat Score (ETS) สูงที่สุดในขณะที่ IMERG Early มีค่า ETS น้อยที่สุด เนื่องจากมีค่า false alarm ที่สูง ข้อมูลฝนจากดาวเทียมทั้ง 3 ข้อมูล มีความคลาดเคลื่อนสูงในช่วงฤดูฝน ในช่วงเหตุการณ์ฝนตกหนักและฝนตกหนักมากมีปริมาณฝนที่น้อยกว่าข้อมูลฝนจากสถานีตรวจวัด และมีความคลาดเคลื่อนสูงในบริเวณชายฝั่งซึ่งเป็นบริเวณที่มีปริมาณฝนตกหนัก IMERG Early มีค่า RMSE น้อยที่สุดในทุกกลุ่มน้ำ หลังการปรับแก้ความเอนเอียงเชิงสถิติทั้ง 3 วิธี พบว่า IMERG Early ที่ปรับแก้แล้วมีค่า RMSE น้อยที่สุดในทุกกลุ่มน้ำ เมื่อประเมินจาก RMSE วิธี ANN ให้ผลที่ดีที่สุดเมื่อเปรียบเทียบทั้ง 3 วิธี อย่างไรก็ตามในช่วงปริมาณฝนตกหนักมาก ปริมาณฝนที่ปรับแก้ความเอนเอียงเชิงสถิติด้วยวิธี ANN มีค่าน้อยกว่าข้อมูลฝนจากสถานีตรวจวัดมากขึ้น มีค่า RMSE สูงขึ้น และทำให้ข้อมูลฝนจากข้อมูลดาวเทียม PERSIANN-CCS และ GSMaP\_NRT ที่ปรับแก้ความเอนเอียงเชิงสถิติด้วยวิธี ANN มี ETS ที่น้อยลง มีเพียงการปรับแก้ความเอนเอียงเชิงสถิติด้วยวิธี QM ที่สามารถทำให้ความคลาดเคลื่อนของปริมาณฝนตกหนักมากลดลง และเพิ่ม ETS โดยภาพรวม การปรับแก้ความเอนเอียงเชิงสถิติของข้อมูลฝนจากดาวเทียม IMERG Early ด้วยวิธี ANN มีค่า RMSE ที่น้อยที่สุดในทุกกลุ่มน้ำ

สาขาวิชา           วิศวกรรมแหล่งน้ำ  
ปีการศึกษา        2563

ลายมือชื่อนิสิต .....  
ลายมือชื่อ อ.ที่ปรึกษาหลัก .....



# # 6170381321 : MAJOR WATER RESOURCES ENGINEERING

KEYWORD satellite precipitation estimates, bias correction, artificial neural networks, quantile mapping

D: Nelson Stephen Lising Ventura : BIAS CORRECTION OF SATELLITE PRECIPITATION ESTIMATES OVER THAILAND. Advisor: Asst. Prof. PIYATIDA RUANGRASSAMEE, Ph.D.

Over the years, meteorological satellite instruments have produced Satellite Precipitation Estimates (SPEs) that can supply rainfall intensity rates globally. However, these datasets do not directly reflect the actual values of ground measurements so it is imperative to correct the systematic biases of SPEs to produce reliable hydrologic models. Thus, the aim of this study is to assess the effectiveness of bias correction of SPE products over Thailand. The Precipitation Estimates from Remotely Sensed Information using Artificial Neural Networks – Cloud Classification System (PERSIANN-CCS), Global Satellite Mapping of Precipitation - Near Real Time (GSMaP\_NRT), and Integrated Multi-satellite Retrievals for GPM (IMERG) Early version were evaluated in comparison to the Thai Meteorological Department (TMD) gauge measurements from 2003 to 2018. Subsequently, the SPEs were corrected by using Scaling, Quantile Mapping (QM), and an Artificial Neural Network (ANN) correction. Both the original PERSIANN-CCS and IMERG Early generally exhibit overestimation over Thailand while the GSMaP\_NRT slightly underestimate rainfall. The original IMERG Early also shows the least RMSE overall, followed by GSMaP\_NRT, then by PERSIANN-CCS. GSMaP\_NRT shows the highest Equitable Threat Score (ETS) while IMERG Early has the lowest ETS because it has large amounts of false alarms. All products exhibit higher errors during the wet season, high underestimation during heavy and extreme rainfall, and higher errors near the coastal areas where high rainfall occurs. IMERG Early also shows the least RMSE in all river basins. After bias correction, the adjusted IMERG Early dataset still provides the least RMSE for all basins regardless of which correction method was applied. The ANN bias correction method performs the best among the three methods in terms of RMSE. However, it increases the underestimation and RMSE of extreme rainfall events and worsens ETS of PERSIANN-CCS and GSMaP\_NRT. Only the QM bias correction is able to consistently reduce errors of extreme rainfall and improve ETS. Overall, the ANN adjusted IMERG Early dataset has the least RMSE in all river basins.

Field of Study: Water Resources Engineering

Academic Year: 2020

Year:

Student's

Signature .....

Advisor's

Signature .....

## ACKNOWLEDGEMENTS

I would like to extend my deepest and humblest gratitude to the remarkable people and organizations of whom has aided and guided me throughout the whole three years of my study. If not for them, the study would not have been possible.

First of all, I would like to thank the ASEAN University Network/Southeast Asia Engineering Education Development Network (AUN/SEED-Net) of Japan International Cooperation Agency (JICA) for supporting my study in Chulalongkorn University through scholarship. Their profuse aid has been fundamental to the success of this study of which I am deeply appreciative.

I would also like to acknowledge the agencies that have provided data used in this study. Namely, I extend my gratitude to the Thai Meteorological Department (TMD) for providing the daily rainfall, maximum temperature, and minimum temperature data, and the University of California - Irvine (UCI) Center for Hydrometeorology and Remote Sensing (CHRS) for PERSIANN-CCS, Japan Aerospace Exploration Agency (JAXA) for GSMaP\_NRT, and National Aeronautics and Space Administration (NASA) for IMERG Early.

Moreover, I am sincerely grateful for the unwavering support, guidance, and supervision that Asst. Prof. Dr. Piyatida Rungrasamee, my advisor, has bestowed upon me. She has gone above and beyond in supporting me during my study. Amidst various trials and obstacles, she has steadfastly believed in her students and has always encouraged me to perform to the best of my abilities. Without her, I would never be able to accomplish this study. The experiences that I have gained and the help I have received from her are irreplaceable.

Furthermore, I would also like to thank the thesis committee composed of Asst. Prof. Dr. Anurak Sriariyawat, Assoc. Prof. Dr. Tuantan Kitpaisalsakul, and Dr. Thanapon Piman for imparting their invaluable insights and wisdom in shaping this research. The learnings I received from them has helped me improve both my study and myself as a researcher.

I would also like to acknowledge Distinguished Professor Soroosh Sorooshian, Professor Kuo-lin Hsu, Assistant Adjunct Professor Dr. Phu Nguyen, and all of the people in the Center of Hydrometeorology and Remote Sensing of University of California –

Irvine for allowing me to study about satellite precipitation estimation with them. Their support has further strengthened my knowledge and understanding of the concepts I needed for this research.

In addition, I would like to express my gratitude to my professors, the staff, my seniors, and my friends in the Department of Water Resources Engineering, Faculty of Engineering, Chulalongkorn University. Throughout these three years, they have continued to provide me with their support, especially during times of hardships. I am thankful to have met such amazing teachers and friends.

I would also like to thank my professors from De La Salle University – Manila, Dr. Renan Tanhueco and Dr. Mario De Leon, for giving me the opportunity to learn more about water resources engineering. I will always be grateful to them for introducing me to the scholarship and equipping me with the knowledge I needed to push forward.

Lastly, I am deeply grateful to my friends, my family, and those that stayed with me through it all. I am grateful my parents for unconditionally supporting my dreams and never giving up on me. I thank my long-time friends, as well as those I met along the way, for lifting me up and being there for me whenever I hit my lowest points. Most of all, I thank the God Almighty for giving me the strength to push through each day. I would not be able to accomplish anything if not for Him.



จุฬาลงกรณ์มหาวิทยาลัย Nelson Stephen Lising Ventura  
CHULALONGKORN UNIVERSITY

# TABLE OF CONTENTS

	<b>Page</b>
ABSTRACT (THAI) .....	i
ABSTRACT (ENGLISH).....	ii
ACKNOWLEDGEMENTS.....	iii
TABLE OF CONTENTS.....	v
LIST OF TABLES.....	viii
LIST OF FIGURES .....	ix
LIST OF ABBREVIATIONS.....	xiii
CHAPTER 1 INTRODUCTION.....	1
1.1. Background of the Study.....	1
1.2. Objectives of the Study .....	2
1.3. Scope and Limitations .....	3
1.4. Significance of the Study.....	5
CHAPTER 2 LITERATURE REVIEW.....	6
2.1. Satellite Precipitation Estimates .....	6
2.1.1. Tropical Precipitation Measurement Mission (TRMM) Multi- satellite Precipitation Analysis (TMPA) .....	9
2.1.2. Climate Prediction Center (CPC) Morphing Technique (CMORPH) .....	10
2.1.3. Precipitation Estimation from Remotely Sensed Information using Artificial Neural Network (PERSIANN) .....	11
2.1.4. Global Satellite Mapping of Precipitation (GSMaP).....	12
2.1.5. Integrated Multi-satellite Retrievals for GPM (IMERG).....	14
2.2. Satellite Precipitation Estimates Evaluation.....	16
2.3. Satellite Precipitation Estimates Bias Correction.....	23
2.3.1. Scaling Correction .....	24
2.3.2. Regression and Curve Fitting .....	26

2.3.3.	Quantile Mapping .....	27
2.4.	Bias Correction using Machine Learning .....	31
CHAPTER 3 METHODOLOGY .....		38
3.1.	Study Area .....	38
3.2.	Data Sources .....	40
3.3.	Methodology.....	41
CHAPTER 4 EVALUATION OF SATELLITE PRECIPITATION ESTIMATES OVER THAILAND .....		48
4.1.1.	Annual Precipitation .....	48
4.1.2.	Monthly Precipitation .....	50
4.2.	Daily Precipitation Assessment .....	52
4.2.1.	Over Whole Study Period.....	52
4.2.2.	By Month.....	53
4.2.3.	By Precipitation Intensity .....	55
4.2.4.	By Basin .....	57
4.3.	Precipitation Detection Assessment .....	59
4.3.1.	Over Whole Study Area .....	59
4.3.2.	By Month.....	60
4.3.3.	By Basin .....	62
4.4.	Summary of Evaluation .....	63
CHAPTER 5 BIAS CORRECTION OF SATELLITE PRECIPITATION ESTIMATES.....		65
5.1.	Calibration .....	65
5.2.	Validation .....	67
5.3.	Comparison of Bias Corrected SPE Products .....	69
5.3.1.	Annual and Monthly Precipitation Patterns.....	69
5.3.2.	Daily Precipitation and Detection Skill Analysis .....	77
5.3.3.	Precipitation and Detection Analysis by Month.....	82
5.3.4.	Precipitation and Detection Analysis by Basin .....	90
5.3.5.	Precipitation Analysis by Intensity.....	96

5.4. Comparison of Adjusted SPE Products .....	101
CHAPTER 6 Conclusions and Recommendations .....	106
6.1. Conclusions .....	106
6.2. Recommendations .....	109
REFERENCES .....	111
APPENDIX A: Table for Scaling Bias Factors .....	116
APPENDIX B: CDFs from Quantile Mapping.....	119
VITA.....	122



## LIST OF TABLES

	<b>Page</b>
Table 2-1. SPE Details and Information .....	12
Table 2-2. Equations for Evaluation of SPEs .....	18
Table 3-1. SPE Product Spatiotemporal Resolutions and Latency .....	41
Table 3-2. Categorical Statistics Formula and Optimal Values.....	44
Table 3-3. TMD Precipitation Intensity Ranges .....	44
Table 4-1. Annual Precipitation Quantitative Statistics.....	49
Table 4-2. Monthly Precipitation Quantitative Statistics.....	51
Table 4-3. Daily Precipitation Quantitative Statistics.....	53
Table 4-4. Precipitation Categorical Statistics.....	60
Table 5-1. Summary of strong and weak points of each bias correction method.....	102
Table 5-2. Basin RMSE (mm/day) for each adjusted SPE Product.....	104
Table 5-3. Basin Normalized RMSE for each adjusted SPE Product.....	105
Table A-1. Scaling Factors for PERSIANN-CCS .....	116
Table A-2. Scaling Factors for GSMaP_NRT .....	117
Table A-3. Scaling Factors for IMERG Early .....	118

CHULALONGKORN UNIVERSITY

## LIST OF FIGURES

	<b>Page</b>
Figure 1-1. Resolution of Rainfall Quantification over Spatiotemporal Representation (Kirstetter, 2019).....	2
Figure 2-1. GEO and LEO Satellite Orbits.....	7
Figure 2-2. Difference between VIS/IR and MW sensors on Satellites (Kirstetter, 2019).....	8
Figure 2-3. Timeline of SPE development in recent years. ....	10
Figure 2-4. GSMaP Algorithm Flowchart (Mega et al, 2019).....	14
Figure 2-5. IMERG Algorithm Flowchart (Huffman et al., 2015).....	16
Figure 2-6. 2x2 Contingency Table for Forecast-Event Pairs (Wilks, 2011).....	17
Figure 2-7. POD and FAR over increasing rainfall intensity (Behrangi et al., 2011).....	23
Figure 2-8. GPCP Gauges over the whole country of Malaysia (Tan & Santo, 2018).....	23
Figure 2-9. Curve fitting PI vs ME for a) $0 < PI \leq 20$ and b) $20 \text{ mm/day} < PI$ (Deng et al., 2018).....	26
Figure 2-10. Quantile Mapping Algorithm (Karbalaee et al., 2017).....	28
Figure 2-11. Mean Daily Accumulated Rainfall (Alharbi et al., 2018).....	30
Figure 2-12. CDF Calculation Procedure (Z. Yang et al., 2016).....	31
Figure 2-13. Difference between traditional programming and machine learning (Lee, 2019).....	32
Figure 2-14. Examples of Machine Learning Problem Types; (a) regression, (b) classification, and (c) clustering (Lee, 2019).....	32
Figure 2-15. Scheme of a sample neural network (Rebala et al., 2019).....	34
Figure 2-16. (a) Sigmoid and Hyperbolic Tangent vs (b) ReLU Activation Functions.....	36
Figure 3-1. Averaged Monthly Rainfall and Temperature Over Thailand.....	38
Figure 3-2. Thailand River Basin and TMD Station Locations.....	39
Figure 3-3. Temporal Coverage of Rain Gauge Data and SPE Products.....	41
Figure 3-4. Flowchart of the Methodology.....	43



Figure 3-5. Bias Correction – Interpolation Scheme Example .....	47
Figure 4-1. Annual Scatterplot of SPE Products .....	49
Figure 4-2. Average Annual Rainfall for PERSIANN-CCS (left), GSMaP_NRT (center), and IMERG Early (right).....	50
Figure 4-3. Monthly Scatterplot of SPE Products .....	51
Figure 4-4. Cumulative Average Monthly Rainfall over Thailand.....	52
Figure 4-5. Daily Scatterplot of SPE Products .....	53
Figure 4-6. BIAS of Daily Rainfall per Month.....	54
Figure 4-7. RMSE of Daily Rainfall per Month.....	54
Figure 4-8. CORR of Daily Rainfall per Month.....	55
Figure 4-9. BIAS of Daily Rainfall by Intensity.....	56
Figure 4-10. RMSE of Daily Rainfall by Intensity.....	56
Figure 4-11. CORR of Daily Rainfall by Intensity.....	57
Figure 4-12. BIAS of Daily Rainfall by Basin .....	58
Figure 4-13. RMSE of Daily Rainfall by Basin.....	58
Figure 4-14. CORR of Daily Rainfall by Basin.....	59
Figure 4-15. Precipitation Detection Skill of SPE Products .....	60
Figure 4-16. POD of Daily Rainfall per Month.....	61
Figure 4-17. FAR of Daily Rainfall per Month.....	61
Figure 4-18. ETS of Daily Rainfall per Month.....	61
Figure 4-19. POD of Daily Rainfall per Basin .....	62
Figure 4-20. FAR of Daily Rainfall per Basin.....	63
Figure 4-21. ETS of Daily Rainfall per Basin .....	63
Figure 5-1. Results of Initial ANN trials using varying number of hidden nodes.....	66
Figure 5-2. BIAS of Original and Adjusted SPE Products - Calibration.....	66
Figure 5-3. RMSE of Original and Adjusted SPE Products - Calibration.....	67
Figure 5-4. BIAS of Original and Adjusted SPE Products - Validation.....	68
Figure 5-5. RMSE of Original and Adjusted SPE Products - Validation.....	69
Figure 5-6. Annual Rainfall Scatterplot of Adjusted SPE Products .....	70

Figure 5-7. BIAS of Adjusted SPE Products Annual Rainfall .....	71
Figure 5-8. RMSE of Adjusted SPE Products Annual Rainfall.....	72
Figure 5-9. CORR of Adjusted SPE Products Annual Rainfall.....	72
Figure 5-10. Monthly Rainfall Scatterplot of Adjusted SPE Products .....	73
Figure 5-11. BIAS of Adjusted SPE Products Monthly Rainfall .....	74
Figure 5-12. RMSE of Adjusted SPE Products Monthly Rainfall.....	74
Figure 5-13. CORR of Adjusted SPE Products Monthly Rainfall.....	75
Figure 5-14. Monthly Rainfall Timeseries in each year for Adjusted PERSIANN- CCS .....	76
Figure 5-15. Monthly Rainfall Timeseries in each year for Adjusted GSMaP_NRT	76
Figure 5-16. Monthly Rainfall Timeseries in each year for Adjusted IMERG Early.	77
Figure 5-17. Daily Rainfall Scatterplot of Adjusted SPE Products .....	78
Figure 5-18. BIAS of Adjusted SPE Products Daily Rainfall .....	79
Figure 5-19. RMSE of Adjusted SPE Products Daily Rainfall .....	79
Figure 5-20. CORR of Adjusted SPE Products Daily Rainfall .....	80
Figure 5-21. POD of Adjusted SPE Products Daily Rainfall .....	81
Figure 5-22. FAR of Adjusted SPE Products Daily Rainfall.....	81
Figure 5-23. ETS of Adjusted SPE Products Daily Rainfall .....	82
Figure 5-24. BIAS of Adjusted PERSIANN-CCS Daily Rainfall by Month.....	83
Figure 5-25. RMSE of Adjusted PERSIANN-CCS Daily Rainfall by Month .....	83
Figure 5-26. CORR of Adjusted PERSIANN-CCS Daily Rainfall by Month .....	83
Figure 5-27. POD of Adjusted PERSIANN-CCS Daily Rainfall by Month .....	84
Figure 5-28. FAR of Adjusted PERSIANN-CCS Daily Rainfall by Month .....	84
Figure 5-29. ETS of Adjusted PERSIANN-CCS Daily Rainfall by Month.....	84
Figure 5-30. BIAS of Adjusted GSMaP_NRT Daily Rainfall by Month.....	85
Figure 5-31. RMSE of Adjusted GSMaP_NRT Daily Rainfall by Month.....	86
Figure 5-32. CORR of Adjusted GSMaP_NRT Daily Rainfall by Month.....	86
Figure 5-33. POD of Adjusted GSMaP_NRT Daily Rainfall by Month.....	86
Figure 5-34. FAR of Adjusted GSMaP_NRT Daily Rainfall by Month .....	87

Figure 5-35. ETS of Adjusted GSMaP_NRT Daily Rainfall by Month.....	87
Figure 5-36. BIAS of Adjusted IMERG Early Daily Rainfall by Month.....	88
Figure 5-37. RMSE of Adjusted IMERG Early Daily Rainfall by Month.....	88
Figure 5-38. CORR of Adjusted IMERG Early Daily Rainfall by Month.....	89
Figure 5-39. POD of Adjusted IMERG Early Daily Rainfall by Month.....	89
Figure 5-40. FAR of Adjusted IMERG Early Daily Rainfall by Month.....	89
Figure 5-41. ETS of Adjusted IMERG Early Daily Rainfall by Month.....	90
Figure 5-42. BIAS of Adjusted SPE Products Daily Rainfall by Basin.....	91
Figure 5-43. RMSE of Adjusted SPE Products Daily Rainfall by Basin.....	92
Figure 5-44. CORR of Adjusted SPE Products Daily Rainfall by Basin.....	93
Figure 5-45. POD of Adjusted SPE Products Daily Rainfall by Basin.....	94
Figure 5-46. FAR of Adjusted SPE Products Daily Rainfall by Basin.....	95
Figure 5-47. ETS of Adjusted SPE Products Daily Rainfall by Basin.....	96
Figure 5-48. BIAS of Adjusted SPE Products Daily Rainfall by Basin.....	98
Figure 5-49. RMSE of Adjusted SPE Products Daily Rainfall by Basin.....	99
Figure 5-50. CORR of Adjusted SPE Products Daily Rainfall by Basin.....	100
Figure B-1. PERSIANN-CCS CDF by Basin.....	119
Figure B-2. GSMaP_NRT CDF by Basin.....	120
Figure B-3. IMERG Early CDF by Basin.....	121

## LIST OF ABBREVIATIONS

AMW	-	Active Microwave
ANN	-	Artificial Neural Network
BF	-	Bias Factor
BIAS	-	Mean Error
CCS	-	(PERSIANN) Cloud Classification System
CDF	-	Cumulative Distribution Function
CDR	-	(PERSIANN) Climate Data Record
CHIRPS	-	Climate Hazards Group InfraRed Precipitation with Station
CHRS	-	Center for Hydrometeorology and Remote Sensing (UCI)
CMORPH	-	CPC Morphing Technique
CNES	-	Centre National d'Études Spatiales
CNN	-	Convolutional Neural Network
CORR	-	Correlation Coefficient
CPC	-	Climate Prediction Center
CSAV	-	Cloud System Advection Vectors
CSI	-	Critical Skill Index
CV	-	Coefficient of Variation
DPR	-	Dual-frequency Precipitation Radar
DT	-	Distribution Transformation
EGAT	-	Electricity Generating Authority in Thailand
ETS	-	Equitable Threat Score
EUMETSAT	-	European Organization for the Exploitation of Meteorological Satellites

FAR	-	False Alarm Ratio
GEO	-	Geostationary Satellite
GPM	-	Global Precipitation Mission
GSMaP	-	Global Satellite Mapping of Precipitation
GSS	-	Gilbert Skill Score
GW	-	Gaussian Weighing
HSS	-	Heidke Skill Score
IDW	-	Inverse Distance Weighing
IMERG	-	Integrated Multi-satellite Retrieval for GPM
IR	-	Infrared sensors
ISRO	-	Indian Space Research Organization
JAXA	-	Japan Aerospace Exploration Agency
KF	-	Kalman Filter
LEO	-	Low Earth Orbiting (Satellite)
MAE	-	Mean Absolute Error
MLP	-	Multilayer Perceptron
MW	-	Microwave
MWR	-	(GSMaP) Microwave Retrievals
NASA	-	National Aeronautics and Space Administration (USA)
NASDA	-	National Space Development Agency (Japan)
NOAA	-	National Oceanic and Atmospheric Administration (USA)
NRT	-	Near-Real Time
PERSIANN	-	Precipitation Estimation from Remotely Sensed Information using Artificial Neural Network

PI	-	Precipitation Intensity
PMW	-	Passive Microwave
POD	-	Probability of Detection
PR	-	Precipitation Radar
PSS	-	Peirce Skill Score
QM	-	Quantile Mapping
RBIAS	-	Relative Bias
RID	-	Royal Irrigation Department
RMSE	-	Root-Mean-Squared Error
RNN	-	Recurrent Neural Network
SPE	-	Satellite Precipitation Estimate
SVM	-	Support Vector Machine
TMD	-	Thai Meteorological Department
TMI	-	TRMM Microwave Imager
TMPA	-	TRMM Multi-Satellite Precipitation Analysis
TRMM	-	Tropical Precipitation Measurement Mission
TSF	-	Time-Space Fixed
TSV	-	Time-Space Variable
TV	-	Time Variable Only
TVSF	-	Time Variable Space Fixed
UCI	-	University of California Irvine
VIRS	-	Visible and Infrared Sensors
VIS	-	Visible sensors

# CHAPTER 1

## INTRODUCTION

### 1.1. Background of the Study

Precipitation is a key parameter for various field of study. Accurate quantification of precipitation over certain areas is one of the key factors required to obtain reasonable results from hydrologic analyses. There are various ways to measure and estimate rainfall over specific locations. However, as the spatiotemporal representation increases, the resolution of the measurements lowers as shown in Figure 1-1. One of the simplest and most accurate methods is by the use of rain gauges as it can physically measure the depth of rainfall over a given period. Consequently, since the measurement is only located in a point location, it can only be considered as accurate within the vicinity of the rain gauge station. Another way to estimate precipitation is through the use of ground-based radars. It gives a better spatial distribution of rainfall compared to a rain gauge while maintaining a significant amount of accuracy as the sensors are still ground-based. However, since the radar indirectly measures the rainfall through signals from the pulses of microwaves, interference and physical obstructions can reduce the accuracy of the precipitation estimates. Similarly, space-borne radars equipped on satellites can also estimate precipitation. One of the advantages of satellite-based precipitation estimates is its spatial coverage which provides rainfall measurements for almost anywhere around the whole globe. Nevertheless, the data from satellite sensors has its drawbacks since the estimates come from indirect measurements.

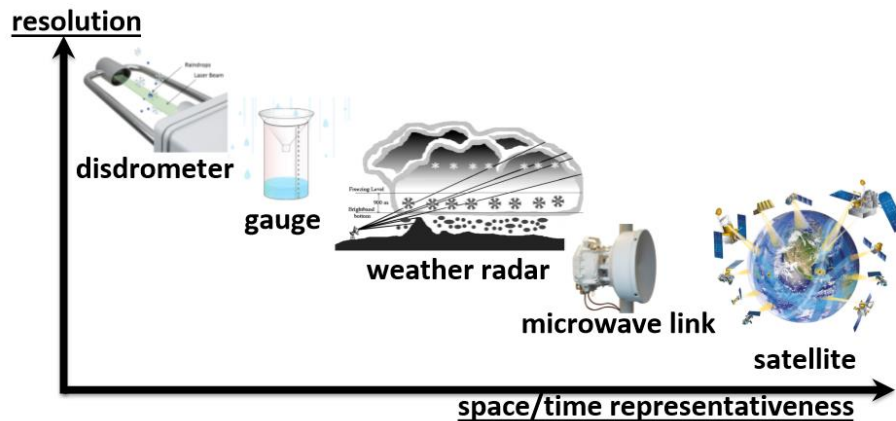


*Figure 1-1. Resolution of Rainfall Quantification over Spatiotemporal Representation (Kirstetter, 2019)*

Satellite precipitation estimates (SPEs) have the potential to provide rainfall data for almost every location in the world. However, these estimates contain systematic biases that need to be corrected. Moreover, other rainfall products have their own advantages and disadvantages. Combining different datasets may enhance the quality of precipitation estimates. Taking the spatial coverage of satellite rainfall data and the accuracy of rain gauge measurements can improve hydrologic models and simulations.

## **1.2. Objectives of the Study**

The main objective of this study is to assess the effectiveness of bias correction of satellite precipitation estimates. Specifically, the study aims:

1. To quantify the systematic bias of near-real-time (NRT) satellite precipitation estimates compared to rain gauges in Thailand;
2. To adjust the bias of the SPE products in each basin using Scaling, Quantile Mapping (QM), and Artificial Neural Network (ANN) bias correction methods; and
3. To determine which adjusted SPE product and its respective bias correction method has the least overall error in each basin within the country.



### 1.3. Scope and Limitations

The study focuses on the assessment of the performance of the original and corrected NRT SPE products at a daily timescale within the boundaries of Thailand. The 123 TMD synoptic stations are used as basis for the evaluation of SPE products. Selected gauges are to be filtered in accordance to a Double Mass Consistency Analysis with respect to the other Thai Meteorological Department (TMD) synoptic stations within the same basin. Precipitation Estimation from Remotely Sensed Information using Artificial Neural Network (PERSIANN-CCS), Global Satellite Mapping of Precipitation Near Real Time version (GSMaP\_NRT), and Integrated Multi-satellitE Retrievals for GPM (IMERG) Early Run from 2003 to 2018 at a daily time scale are the selected SPE products to be evaluated. The year 2003 has been selected to provide consistency in terms of temporal coverage for all the SPE dataset. In addition, the daily maximum and minimum temperatures at the same TMD stations are included in the study as additional input predictors for the ANN bias correction method. However, the temperature data available is only until the middle of 2017; therefore, the ANN testing/validation period would be shortened until the end of 2016.

SPEs are to be evaluated with quantitative statistics and categorical statistics. Quantitative statistics include computation of mean bias (BIAS), root-mean-squared error (RMSE), and correlation coefficient (CORR) while categorical statistics include determination of probability of detection (POD), false alarm ratio (FAR), and equitable threat score (ETS). In terms of comparison, the SPE product with the lowest RMSE would be selected as the best performing dataset within each river basin.

After the evaluation, all of the selected SPE products would be corrected within each river basin. Scaling correction, quantile mapping, and an ANN model would be utilized to adjust the SPE rainfall pixel with an available rain gauge station. The three bias correction methods would use the same datasets for their respective calibration phases. The scaling correction would utilize a Time-Space Variable (TSV) approach, wherein the bias factor applied to the data varies by month and by basin. Likewise, the QM correction would separate the data by basin to produce a cumulative distribution function (CDF) for each basin. Furthermore, the ANN correction would follow a backward-propagation Multi-layer Perceptron (MLP) regression model with the input vector containing the original satellite rainfall value, maximum temperature, and minimum temperature while the output value being the adjusted satellite rainfall value. All river basin would have its own ANN model with one hidden layer containing 8 hidden nodes to account for consistency as any additional number of hidden nodes to this does not lower the resulting error during the training phase for the datasets. The activation function used for the ANN model would be a Rectified Linear Unit instead of the sigmoid and hyperbolic tangent function in order to account for the vanishing gradient problem.

In addition, the error between the values of the original and corrected pixels would be interpolated using a simple inverse-distance weighing (IDW) interpolation method over the whole river basin. This error map would be used to adjust non-gauged pixels within the basin. The calibration (training) period for the bias correction would start from 2003 until 2010 while the validation (testing) period would be from 2011 to 2018. Any data that are not within the set time period (2003 to 2018) would not be included in the analysis. Moreover, gauge stations that are inconsistent with TMD synoptic

stations would be removed. Furthermore, although bias correction will significantly reduce its systematic errors and enhance its detection skills, these methods may not be able to correct the daily random errors

#### **1.4. Significance of the Study**

The improvement of the NRT daily SPE precipitation data would provide various development for many fields. In hydrology, the corrected SPE data would allow for better flood and drought models and warning systems as it could provide data to cover ungauged area. Other fields, such as in agriculture or in meteorology, may use the adjusted datasets for monitoring or forecasting. Furthermore, including an ANN model on correction would provide more insight to how machine learning methodologies could be used for water resources engineering.

## **CHAPTER 2**

### **LITERATURE REVIEW**

#### **2.1. Satellite Precipitation Estimates**

SPE products are estimated from space-borne radar instruments, sensors, and/or imagers. The greatest asset of estimations from satellites is that it can approximate the precipitation rate for the whole globe. Since the 1960s, satellite missions started aiming for the improvement of meteorological observations (Kidd & Huffman, 2011). Over the years, the technology greatly advanced with gave way for better measurement instruments.

The meteorological satellites can be classified into two types; geostationary (GEO) and Low Earth Orbiting (LEO) satellites (Hu et al., 2019; Kidd & Huffman, 2011) as shown in Figure 2-1. GEO satellites are positioned approximately 38500 kilometers above the equator and orbits at around the same speed as the rotation of the Earth. These satellites are equipped with visible (VIS) and infrared (IR) sensors which can provide images every 30 minutes. VIS images have a spatial resolution of approximately 1 km by 1 km while IR sensors has approximately 4 km by 4 km. On the other hand, LEO satellites can provide better measure precipitation with the addition of passive microwave (PMW) sensors which measures precipitation more directly. However, these satellites can only pass over a given location approximately twice every day. Unlike GEO satellites, these satellites are located at a lower altitude of approximately 850 kilometers above the surface of Earth and has an overpass twice a day. However, the products from LEO satellites provides higher resolution data of approximately 250 meters to 1 kilometer.

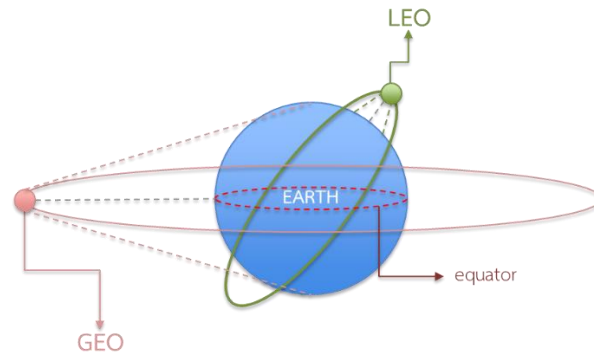


*Figure 2-1. GEO and LEO Satellite Orbits*

Thakur et al. (2017) classifies the satellite rainfall estimation into four methods using VIS/IR, PMW, active microwave (AMW) sensors, and blending multiple data from different sensors. Rainfall measurements estimated from VIS/IR are computed by establishing statistical relationships between the cloud parameters and rainfall intensity. VIS images are used to identify cloud classifications and delineate cloud area which sets apart the regions with and without rain. However, these images are limited as it is only visible during the day. IR images fill in the gaps by using cloud temperatures to supplement the estimate. VIS/IR algorithms are able to detect and produce continuous rainfall data. However, these products have low accuracy because cloud temperatures are not directly related to rainfall intensity (Hu et al., 2019). Kidd and Huffman (2011) stated that emission from precipitation particles can be used to quantify rainfall as emissions from rain droplets increase the MW radiation observed while precipitation ice particles cause scattering which reduces MW radiation. However, these techniques differ as rain drop emission relates to the measurements of rainfall throughout the whole atmosphere column while ice precipitation scattering occurs more at the upper parts of a cloud. One of the challenges for PMW rainfall products is that LEO satellites only

have up to two observations per day which cannot provide continuous retrievals. Figure 2-2 illustrates the difference between what these sensors can detect.

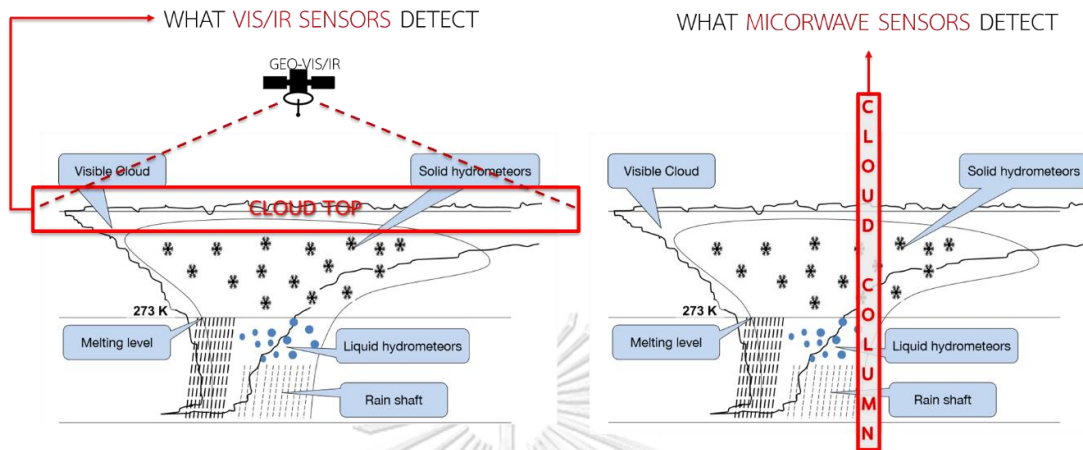


Figure 2-2. Difference between VIS/IR and MW sensors on Satellites (Kirstetter, 2019)

AMW observations provide the most direct rainfall estimation compared to VIS/IR and PMW retrievals. The precipitation radar (PR) on the satellite utilizes the relation between radar reflectivity and rain rate to estimate precipitation (Thakur et al., 2017). This radar measurement can provide data of the vertical structure of precipitation which improves the calculation for the precipitation rate. The first PR deployed into orbit was the Tropical Precipitation Measurement Mission (TRMM) PR. However, the TRMM ended last 2015 after depleting its fuel source. The single-frequency radar was then succeeded by the Global Precipitation Mission (GPM) dual-frequency precipitation radar (DPR). The DPR can improve the observations and retrievals for precipitation in cold seasons, especially in higher latitudes. However, similar to PMW retrievals, AMW observations cannot estimate rainfall intensity continuously.

Each SPE product has a particular algorithm which makes it distinct. For example, each sensor retrieval technique has its own advantages and disadvantages. Multi-sensor techniques are employed to overcome the gaps of the observations of each satellite. Combining the frequency of VIS/IR sample with the direct measurement of PMW improves the quality of precipitation estimation from satellite retrievals. There have also been techniques to calibrate IR observations with PMW. One of the most common techniques is using blended algorithms which produces calibration curves to map sensor observations to each other (e.g. IR with PMW). Various organizations and agencies have produced their own satellite rainfall products using diverse and complex techniques such as incorporating cloud processes or use of artificial neural network (ANN). Table 2-1 lists the details of the satellite-based rainfall products discussed. Moreover, Figure 2-3 illustrates the timeline for the improvements of SPEs over the recent years.

#### 2.1.1. Tropical Precipitation Measurement Mission (TRMM) Multi-satellite Precipitation Analysis (TMPA)

With the joint development of National Aeronautics and Space Administration (NASA) of the United States of America and the National Space Development Agency (NASDA) of Japan (which has now merged with into the Japan Aerospace Exploration Agency), TRMM was launched in 1997 and was the first dedicated precipitation mission to be launched (Li, Wang, Chen, & Austin, 2019). The mission officially ended after 17 years of service in 2015. The remains of the spacecraft and its instrument landed over the South Indian Ocean with majority of its part scorched from the entry into Earth. The TRMM satellite housed its PR, the TRMM Microwave Imager (TMI), and Visible and Infrared Scanner (VIRS). The mission produced various precipitation products

ranging from its single sensor retrieval to merged multi-satellite (Huffman et al., 2007). The TRMM Multi-satellite Precipitation Analysis (TMPA) product merged various satellite data and calibrated with the TMI observations in order to produce a high-quality estimate for precipitation. The two major datasets from TMPA were the NRT version 3B42-RT and the post-real-time 3B42-V7 which is mainly used for research (Maggioni, Meyers, & Robinson, 2016). The 3B42-RT product has a spatiotemporal resolution of 0.25° for every 3 hours which covers 50°S to 50°N from March 2000 to 2015 when the mission ended. The NRT product has a latency of approximately 9 hours. On the other hand, the 3B42-V7 has the same resolution and coverage but has longer latency at roughly 2 months. This late release is due to the bias adjustment using the Global Precipitation Climatology Centre (GPCC) gauge analysis.

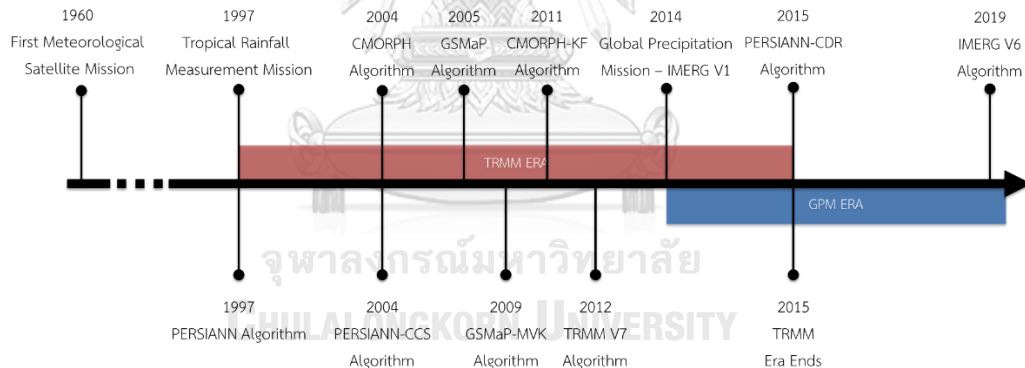


*Figure 2-3. Timeline of SPE development in recent years.*

### 2.1.2. Climate Prediction Center (CPC) Morphing Technique (CMORPH)

CMORPH is developed by the National Oceanic and Atmospheric Administration (NOAA). Its product directly utilizes the PMW observation with cloud motion from IR observations (Kidd & Huffman, 2011). The retrievals are computed by generating cloud system advection vectors (CSAV) from IR observations and morphing precipitation shape and rate by time-weighted linear interpolation between forward- and backward-



propagated PMW observations (Joyce, Janowiak, Arkin, & Xie, 2004). The produced estimate from CMORPH has a spatiotemporal resolution of  $0.25^\circ \times 0.25^\circ$  for every 30 minutes that covers  $60^\circ\text{S}$  to  $60^\circ\text{N}$  from 1998 to present at a latency of 18 hours. CMORPH-Kalman Filter (KF) is another CPC product that uses Kalman Filter to provide higher resolution data at 8km by 8km every thirty minutes (Joyce & Xie, 2011).

### 2.1.3. Precipitation Estimation from Remotely Sensed Information using Artificial Neural Network (PERSIANN)

In the early 1990s, integrating ANN into precipitation estimation has already been studied which showed promising results (Kidd & Huffman, 2011). Precipitation Estimation from Remotely Sensed Information using Artificial Neural Network (PERSIANN) has been produced by the Center for Hydrometeorology and Remote Sensing (CHRS) at the University of California Irvine (UCI) since 1997 (Hsu, Gao, Sorooshian, & Gupta, 1997). The PERSIANN algorithm utilizes the brightness temperature of the observed and neighboring pixels from longwave IR images to calculate the precipitation rate using ANN. Over the years, various developments of this satellite-based precipitation estimates have been produced (Nguyen et al., 2018). The family of products include PERSIANN, PERSIANN Cloud Classification System (PERSIANN-CCS), and PERSIANN Climate Data Record (PERSIANN-CDR). All of these products have a similar spatial coverage of  $60^\circ\text{S}$  to  $60^\circ\text{N}$  but differs in their spatiotemporal resolution and latency. The three products may be distinctly differentiated by its utilization purpose. PERSIANN and PERSIANN-CCS are more suitable for short-term applications (Hong, Hsu, Sorooshian, & Gao, 2004). PERSIANN incorporates quality control by calibration using PMW retrievals before it is released after 2 days. Moreover, it has a spatiotemporal resolution of  $0.25^\circ$  by  $0.25^\circ$

every hour. On the other hand, PERSIANN-CCS is available as an NRT product with latency of approximately 1 hour and a higher spatial resolution of 0.04° by 0.04°. Although this product is less calibrated than the original PERSIANN, Nguyen et al. (2018) states that PMW calibrated PERSIANN-CCS products are available for data after 2014. PERSIANN-CDR is a bias adjusted product that has a record since 1983 which makes it applicable for historical and long-term statistical analysis in hydrometeorological studies (Ashouri et al., 2015). PERSIANN-CDR has a similar spatiotemporal resolution with the original PERSIANN but its latency is approximately 3 months.

*Table 2-1. SPE Details and Information*

Product Detail	TMPA (TRMM)		CMORPH		PERSIANN			GSMaP				IMERG (GPM)		
	3B42-RT	3B42-V7	CMORPH	CMORPH-KF	Original	CCS	CDR	NRT	MVK	Gauge	NOW	Early	Late	Final
GEO-IR	✓	✓	✓	✓	✓	✓	✓	✓	✓	✓	✓	✓	✓	✓
LEO-PMW	✓	✓	✓	✓	✓	< 2014 x	> 2014 ✓	✓	✓	✓	✓	✓	✓	✓
AMW (PR/DPR)	✓	✓	x	x	x	x	x	x	x	x	x	✓	✓	✓
Ground Data	x	✓	x	x	x	x	✓	x	x	✓	x	x	x	✓
Key Algorithm	Merging Multiple Satellite Estimates		IR Cloud Motion Vector PMW Morphing		ANN			PMW Forward Propagation Kalman Filter				Merging Multiple Satellite Estimates IR Feature Segmentation PMW Morphing Kalman Filter		
					PMW Calibration	IR Feature Separation	PMW Calibration	x	Backward Propagation		Forward Extrapolation			
	x	Gauge Adjustment	x	Kalman Filter	x	x	Gauge Adjustment	x	x	Gauge Adjustment	x	x	x	Gauge Adjustment

#### 2.1.4. Global Satellite Mapping of Precipitation (GSMaP)

As early as 2002, Japan has been producing its own high-resolution satellite-based precipitation estimates. Currently, Global Satellite Mapping of Precipitation (GSMaP) utilizes PMW and IR observations for its rainfall estimates. GSMaP\_MWR (Microwave Retrievals) converts brightness temperatures to precipitation rate values (Mega et al., 2018). The algorithm of this product has been updated in order to incorporate the orographic effect on precipitation. It has a spatiotemporal resolution of

0.25° by 0.25° every hour covering 60°S to 60°N globally. GSMaP\_NRT offers a product for short-term applications at a latency of 4 hours and provides data from 2008 to present. It propagates precipitation rates from the previous product forward in time in accordance to cloud motion vectors which is then adjusted using Kalman filter, similar to the CMORPH methodology (Ushio et al., 2009). Contrarily, GSMaP\_MVK has a longer latency at 3 days but it delivers a more accurate precipitation estimate compared to the previous products. It also has precipitation estimates since 2000 to present. This product improves the described methodology as well as the morphing technique of CMORPH by including backward propagation. The overall flowchart is shown in Figure 2-4. A more recent product of JAXA is the GSMaP\_Gauge which utilizes gauge stations to remove the bias in the satellite-based estimate. The global gauge data of CPC has been used to adjust the GSMaP\_MVK and GSMaP\_NRT. In addition, a new product named GSMaP\_NOW has been released recently to provide actual real time precipitation half-hourly data with latency less than 1 hour. It utilizes extrapolation of half an hour into the future using cloud motion vector from GEO satellites (Japan Aerospace Exploration Agency, 2019). It currently provides data from 27 June 2019 to present.

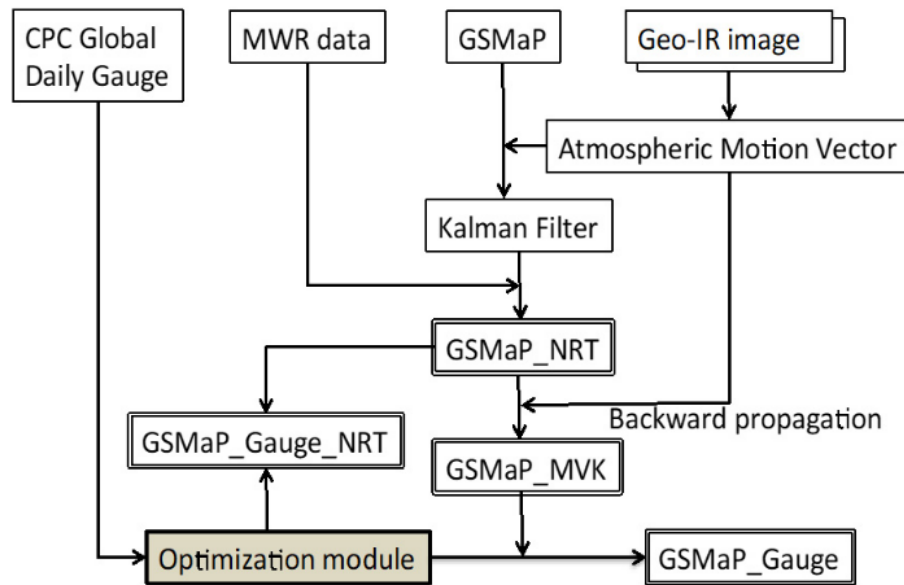


Figure 2-4. GSMaP Algorithm Flowchart (Mega et al, 2019)

#### 2.1.5. Integrated Multi-satellite Retrievals for GPM (IMERG)

With the success of TRMM, the Global Precipitation Mission (GPM) has been initiated by NASA and the Japan Aerospace Exploration Agency (JAXA) as its successor. Notably, other international space agencies such as the Centre National d'Études Spatiales (CNES), Indian Space Research Organization (ISRO), National Oceanic and Atmospheric Administration (NOAA), and European Organization for the Exploitation of Meteorological Satellites (EUMETSAT) have joined the mission. In this mission, the satellite instrument has been equipped with a dual-frequency precipitation radar (DPR) which provides better detection of precipitation occurrences by approximately 1.5 times compared to the TRMM PR (Gao, Tang, & Hong, 2017).

NASA has released its GPM era satellite precipitation estimate named Integrated Multi-Satellite Retrievals for GPM (IMERG). This satellite-based rainfall product utilizes global rain gauge, IR, PMW, and DPR datasets to estimate the precipitation (Huffman et al., 2015). Aside from building from the TRMM algorithm, it incorporates

multiple methodologies from satellite rainfall products of various agencies. The IMERG algorithm uses cloud motion vectors and Kalman filter to improve spatial resolution of the products similar to CMORPH-Kalman Filter (KF) and GSMaP-MVK products. Moreover, it applies the IR segmentation methodology of PERSIANN-CCS to fill in gaps within the data using microwave-calibrated IR retrievals. The process flow for IMERG are visualized in Figure 2-5. Similar to most satellite products, IMERG utilizes post-calibration by adjusting the satellite precipitation estimates using global gauge data. The output IMERG Version 6 (V6) product has a spatiotemporal resolution of  $0.1^\circ$  by  $0.1^\circ$  every 30 minutes with full global coverage from 1998 to present for the current version. There are three sub-product which differs in their latency. These datasets are 3B-HHR-E (Early), 3B-HHR-L (Late), and 3B-HHR (Final) with latencies of approximately 4 hours, 14 hours, and 3.5 months respectively. As the latency increase, more data are used to improve the precipitation estimates. Although Early and Late datasets are both NRT products, the former may be utilized for potential flood or landslide warnings while latter would be more applicable for agricultural forecasting or drought monitoring (Sungmin et al., 2017). Similar to the TMPA algorithm, the Final product is adjusted with the expectation that its monthly sum would be equal to the monthly satellite-gauge combination of IMERG.

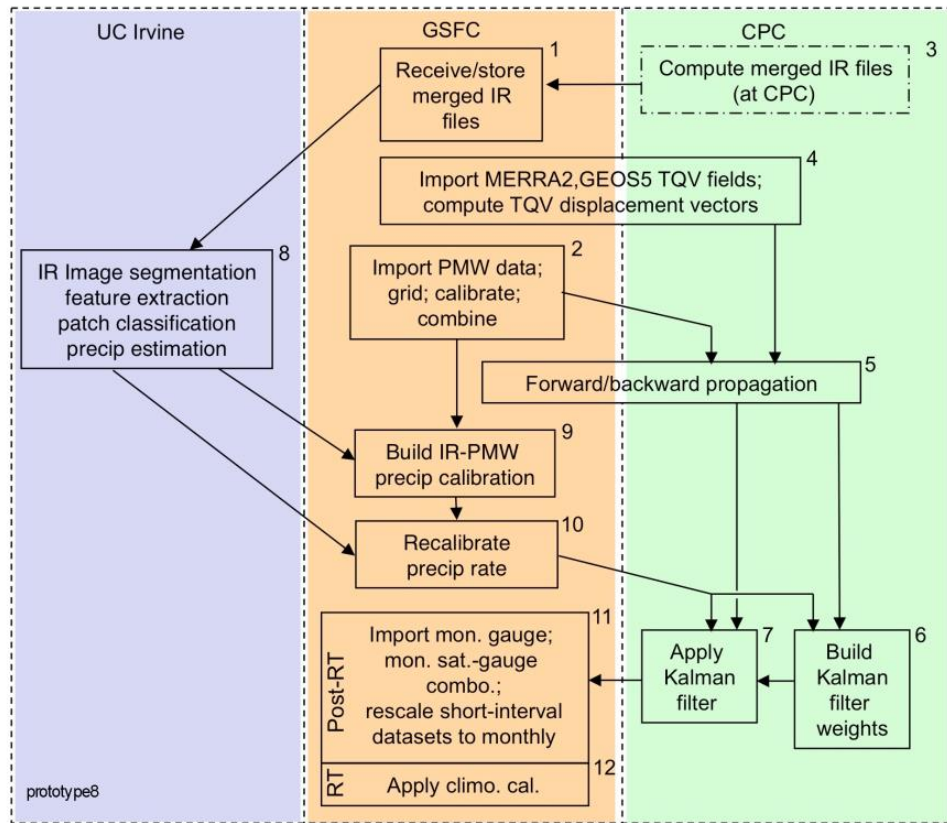


Figure 2-5. IMERG Algorithm Flowchart (Huffman et al., 2015)

## 2.2. Satellite Precipitation Estimates Evaluation

SPEs are evaluated against ground truths with regards to the error through quantitative statistics and detection skill by forecast verification through categorical statistics. The quantitative statistics for the evaluation of SPEs are the mean error or bias (BIAS), relative bias (RBIAS), mean absolute error (MAE), root-mean-squared error (RMSE), and the correlation coefficient (CORR) of the SPE product with respect to the rain gauge measurements at the same point location. On the other hand, the accuracy of a products can be verified by categorical statistics the determination of the number of correct (hits) and incorrect (miss) prediction produced by the SPE. If both of the SPE product and rain gauge measurement show occurrence of rainfall, it would be considered to be a hit. In the same way, should both datasets show no sign of rainfall,

it is simply regarded as a true negative. Otherwise, when the SPE product shows occurrence of rainfall while the gauge measurement does not, the prediction is considered to be a false alarm. Conversely, when the SPE product does not show occurrence of rainfall while the gauge measurement does, the SPE product has missing data. This concept is illustrated in Figure 2-6, where a, b, c, and d are the number of hits, false alarms, misses, and true negatives respectively. It also relates how the contingency table show conditional probability for forecast-event pairs.

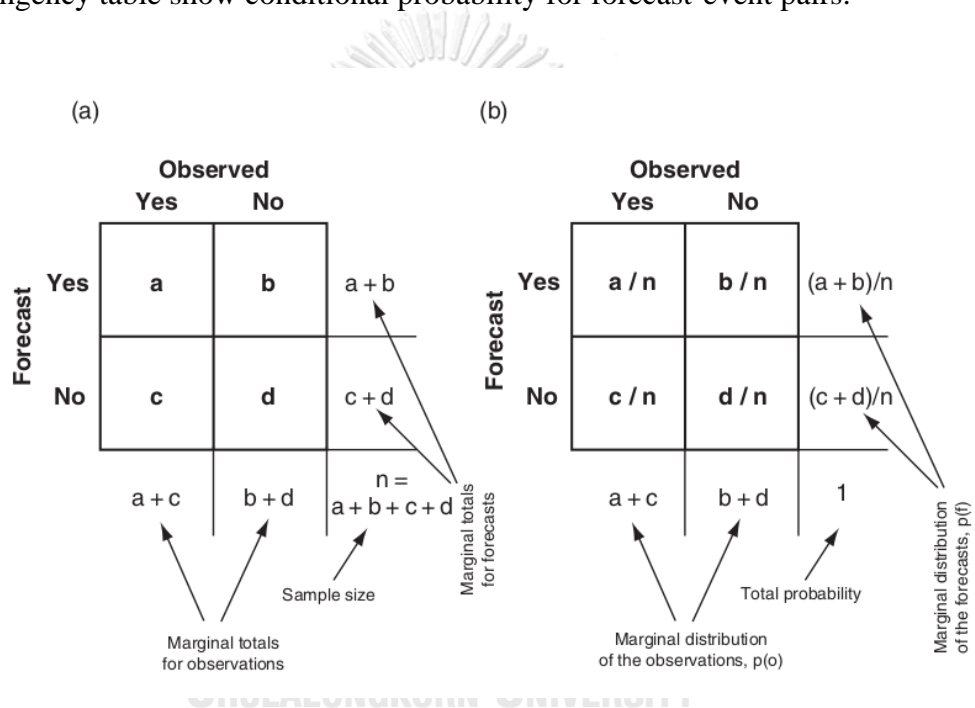


Figure 2-6. 2x2 Contingency Table for Forecast-Event Pairs (Wilks, 2011)

With the hits, false alarms, missing data, and true negatives, the SPEs products can be further analyzed by calculating the probability of detection (POD), false alarm ratio (FAR), and skill scores depending on the purpose of the analysis. Each skill score uses varying equations as shown in Table 2.2, which provide a different representation of the data (Wilks, 2011). Heidke Skill Score (HSS) measures accuracy of the prediction or estimate with respect to random chances. Peirce Skill Score (PSS) evaluates the true

skill of the prediction by separating the correct and false prediction. Critical Success Index (CSI), sometimes known as the threat score (TS), determines the performance of the correct prediction. On the other hand, Gilbert Skill Score (GSS), usually referred to as Equitable Threat Score (ETS), relies on the number of true negatives unlike TS.

Table 2-2. Equations for Evaluation of SPEs

QUANTITATIVE STATISTICS		CATEGORICAL STATISTICS	
<i>BIAS</i>	$\frac{1}{n} \sum_{i=1}^n (S_i - G_i)$	<i>POD</i>	$\frac{a}{a + c}$
<i>RBIAS</i>	$\frac{\sum_{i=1}^n (S_i - G_i)}{\sum_{i=1}^n (G_i)} \times 100\%$	<i>FAR</i>	$\frac{b}{b + d}$
		<i>HSS</i>	$\frac{2(ad - bc)}{(a + c)(c + d) + (a + b)(b + d)}$
<i>MAE</i>	$\frac{1}{n} \sum_{i=1}^n  S_i - G_i $	<i>PSS</i>	$\frac{ad - bc}{(a + c)(b + d)}$
<i>RMSE</i>	$\sqrt{\frac{1}{n} \sum_{i=1}^n (S_i - G_i)^2}$	<i>CSI</i>	$\frac{a}{a + b + c}$
<i>CORR</i>	$\frac{\sum_{i=1}^n (S_i - \hat{S})(G_i - \hat{G})}{\sqrt{\sum_{i=1}^n (G_i - \hat{G})^2} \times \sqrt{\sum_{i=1}^n (S_i - \hat{S})^2}}$	<i>ETS</i>	$\frac{a - a_{ref}}{a - a_{ref} + b + c}$ $a_{ref} = \frac{(a + b)(a + c)}{n}$

In the evaluation of SPEs, products have similarities and differences to the results of the analysis, especially when compared to other agencies. For example, Climate Hazards Group InfraRed Precipitation with Station (CHIRPS) monthly rainfall data from NOAA prove to be similar to gauge data during the rainy season in Ethiopia (Musie, Sen, & Srivastava, 2019). On the other hand, Famine Early Warning Systems



Network Rain Fall Estimation (FEWS-Net RFE) data overestimates number of rainy days but underestimates precipitation rate when compared to rain gauges (Lekula, Lubczynski, Shemang, & Verhoef, 2018).

During its era, TRMM products showed the best performance among other SPEs (Musie et al., 2019; Trinh-Tuan, Matsumoto, Ngo-Duc, Nodzu, & Inoue, 2019; Y. Yang & Luo, 2014). Moreover, the post real-time product TMPA 3B42 provided better correlation and detection than its NRT (Behrangi et al., 2011; Z. Wang, Zhong, Lai, & Chen, 2017). In addition, a consistent feature of TRMM is its ability to capture precipitation patterns whether it is annual (Tan & Santo, 2018), monthly (Hur, Raghavan, Nguyen, & Liang, 2016; Musie et al., 2019), or daily (Yuan et al., 2018). However, its products still had some issues when it came to the estimation of rainfall. Musie et al. (2019) noted that TRMM has a tendency to overestimate daily rainfall in dry seasons. In some cases, the overestimation is more prevalent with higher rainfall intensity (Tan & Santo, 2018; Y. Yang & Luo, 2014). Moreover, although different study areas have different conditions, there are some consistent results. A number of studies show that TRMM products have high POD but its FAR also show high values (Hur et al., 2016; Kenabatho, Parida, & Moalafhi, 2017; Musie et al., 2019; Y. Yang & Luo, 2014). This scenario leads to lower skill scores, especially with CSI. Some authors noted that the gauge adjusted 3B42V7 product performed better than the NRT product of IMERG (X. Wang, Ding, Zhao, & Wang, 2019; Z. Wang et al., 2017). Even though these datasets cannot be directly compared because of their differences in spatial resolution, latencies, and post-processes, it shows that gauge-adjusted products have a clear advantage to non-adjusted counterparts.

In the case of CMORPH, most studies reported underestimation of rainfall in both monthly (Habib, Haile, Sazib, Zhang, & Rientjes, 2014) and daily scales (Jamandre & Narisma, 2013; Lekula et al., 2018). However, in Northwest China, it seems that overestimation of both rainfall occurrence and rate is more evident (Y. Yang & Luo, 2014). Trinh-Tuan et al. (2019) noted that the CMORPH product performs better in areas with higher station density, which suggests that the density of gauge networks may influence the performance of SPEs.

With GSMaP having various products, each one has a different result when compared to ground truths. The GSMaP\_NRT product showed that it has trouble capturing daily rainfall patterns when compared to gauges (Deng et al., 2018). On the other hand, the post-processed GSMaP\_MVK is able to compensate in improving rainfall as it can capture monthly variations (Bui, Ishidaira, & Shaowei, 2019). However, this product still has a problem with underestimation of rainfall accumulation. Underestimation is more evident during the winter months (Hur et al., 2016; Tian, Peters-Lidard, Adler, Kubota, & Ushio, 2010) which may stem from the PMW estimates that tend to also underestimate winter precipitation (Nguyen et al., 2018). Conversely, the MVK product show different results during summer. In Continental United States (CONUS), precipitation is overestimated while underestimation is observed in Singapore and Vietnam (Bui et al., 2019; Hur et al., 2016). The precipitation estimation is improved with the gauge-adjusted GSMaP\_Gauge which showed less underestimation during dry season compared to its unadjusted version which may be attributed to the propagation algorithm that cannot capture small-scale storm events. It is worth noting that even with the improvements brought by the adjustment, the SPE still underestimates rainfall in areas with complex terrain (Deng et

al., 2018). Bui et al. (2019) mentioned that some areas have sparse gauge networks that ultimately affect the performance of blended SPE in areas with varying elevations. A sufficient number of gauge stations would be needed to produce better satellite-gauge data.

For PERSIANN, there is a consistent pattern of overestimation (Alharbi, Hsu, & Sorooshian, 2018; Behrangi et al., 2011; Y. Yang & Luo, 2014). However, with higher precipitation, the products more often underestimate daily rainfall rate (Katiraie-Boroujerdy, Asanjan, Hsu, & Sorooshian, 2017; Z. Yang et al., 2016). Inversely, in Ethiopia and Malaysia, PERSIANN-CDR tend to underestimate light rain and overestimate moderate to heavy rain (Musie et al., 2019; Tan & Santo, 2018). All three product tend to show higher POD and also higher FAR than other SPEs (Nguyen et al., 2018; Tan & Santo, 2018). In CONUS, the bias-adjusted PERSIANN-CDR also performed better in capturing rainfall pattern and precipitation rate estimation (Nguyen et al., 2018). However, similar to GSMaP, PERSIANN products also show underestimation during winter.

As the successor of TRMM, IMERG has shown its capability to build on its predecessor. When compared to TRMM, IMERG has shown significant improvement in terms of estimation and detection (X. Wang et al., 2019). Although the post real-time product TMPA 3B42 shows better performance than the IMERG NRT products as previously mentioned, the IMERG Final still show superiority with less bias, better correlation, and good overall skill score (Tan & Santo, 2018; Z. Wang et al., 2017; Yuan et al., 2018). In a study in UAE, the Early product showed high POD and correlation with respect to an event-based analysis (Mahmoud, Hamouda, & Mohamed,

2019). In the case of Southeastern Austria and Upper Huaihe River Basin, all products overestimate light rain and underestimate moderate to heavy intensities (Su, Lü, Zhu, Cui, & Wang, 2019; Sungmin et al., 2017). This similarity may stem from both study area are located in the mid-latitudes. However, the opposite is true in the low latitudes of Malaysia which shows underestimation of no and light intensity but overestimation of moderate to heavy rain (Tan & Santo, 2018). Overall, IMERG shows significant improvement from TMPA products and that gauge-adjusted products provide superior benefits compared to NRT.

In general, POD lowers and FAR increases with higher intensity as shown in Figure 2-7 (Behrangi et al., 2011). These false alarms may also contribute to overestimation of rainfall (X. Wang et al., 2019). Adjustment of SPEs is needed because bias-adjusted products (TMPA 3B42, IMERG Final, PERSIANN-CDR, etc.) provided better performance which enhances their applicability in practical (Behrangi et al., 2011; Nguyen et al., 2018; Z. Wang et al., 2017). However, blending with gauge data does not always lead to better precipitation estimation (Bui et al., 2019). Sufficient gauge stations are needed to produce better blended satellite-gauge data. Similar to the case in Malaysia, global gauge datasets sometimes do not have enough coverage in some countries as is depicted in Figure 2-8 (Tan & Santo, 2018). This suggests that correction using local gauge may have a better effect. Furthermore, performance of SPEs (BIAS, POD, FAR, etc.) significantly vary depending on elevation and location of the study area (Deng et al, 2018; Trinh-Tuan et al, 2019). These conditions must be considered also in the adjustment of the datasets. Analysis by using precipitation indexes helped in decomposition of errors and categorizing climate patterns (Hur et al., 2016; Katiraie-Boroujerdy et al., 2017; Nguyen et al., 2018).

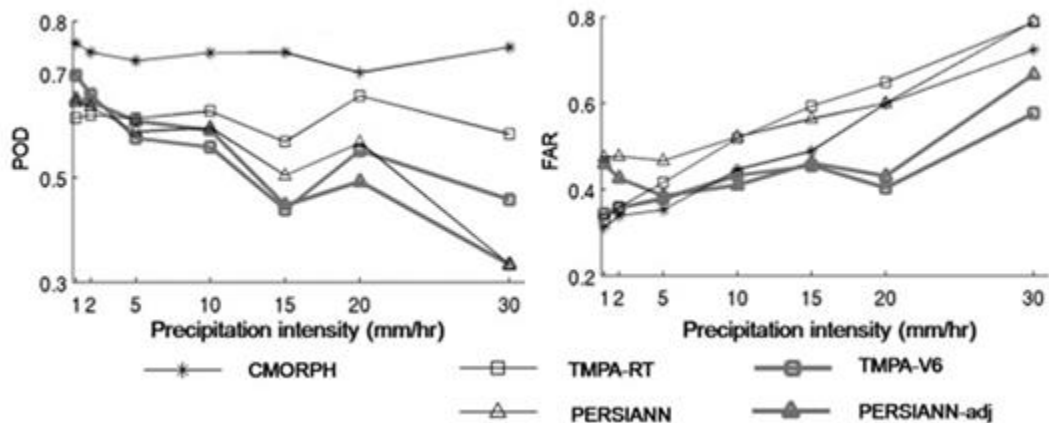


Figure 2-7. POD and FAR over increasing rainfall intensity (Behrangi et al., 2011)

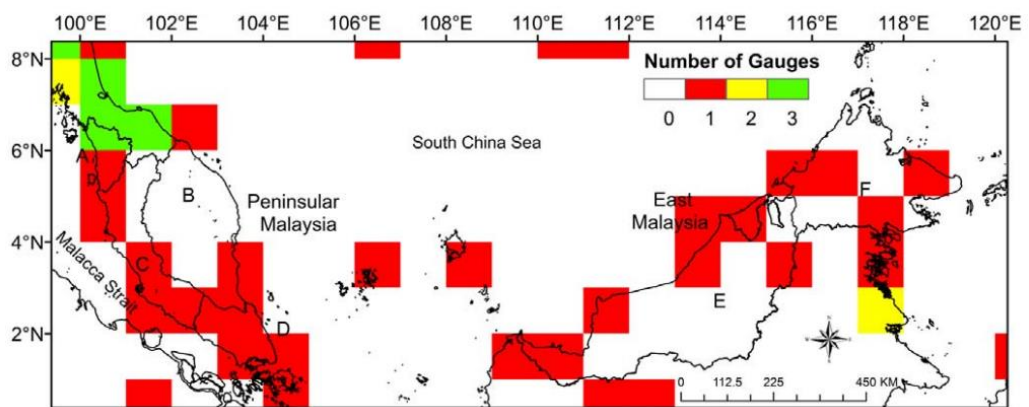


Figure 2-8. GPCP Gauges over the whole country of Malaysia (Tan & Santo, 2018)

### 2.3. Satellite Precipitation Estimates Bias Correction

As shown in the previous section, systematic errors are present in SPE products, especially in NRT products. Bias correction is required to remove these errors and fully utilize the SPEs. This process may require ancillary data (e.g. wind, temperature, cloud movement, etc) and ground truths (e.g. gauge measurements, multi-sensor data, radar estimates, etc) to adjust each rainfall estimate at specified time scales. The common bias correction methods are bias factor scaling, curve fitting and regression, and

quantile mapping (QM) (Deng et al., 2018; Gumindoga, Rientjes, Haile, Makurira, & Reggiani, 2016; Z. Yang et al., 2016).

Bias correction methods were initially used for correction of radar rainfall data and climate models (Gumindoga et al., 2016). Corrections are applied to climate model prediction such as precipitation and temperature to accurately represent the possible actual scenario in the future (Amengual, Homar, Romero, Alonso, & Ramis, 2012; Jakob Themeßl, Gobiet, & Leuprecht, 2011). From the study of Jakob Themeßl et al. (2011), direct methods, such as local intensity scaling or QM, are more effective in bias correction of climate model data than indirect methods, such as linear regression and resampling. This claim holds true in another study where distribution mapping is the best correction method among five other processes (Teutschbein & Seibert, 2012).

### 2.3.1. Scaling Correction

In scaling correction, the method applies a bias factor (BF) to the SPE dataset through either multiplication or addition (Gumindoga et al., 2016; Habib et al., 2014). The BF may be computed in various ways depending on the spatiotemporal analysis involved. However, the most common form of the BF equation is shown in Equation 1 as

$$BF = \frac{\sum_{i=1}^n G_i}{\sum_{i=1}^n S_i} \quad (1)$$

where n is the total number of gauge stations, i is the observed gauge stations, G is the gauge measurement, and S is the satellite estimate (Lekula et al., 2018). Allowing the influence of spatio-temporal variability in the bias correction of SPEs would show another form of the BF equation in Equation 2 as Time-Space Variable (TSV),

$$BF_{TSV} = \frac{\sum_{t=d}^{t=d-l} S(i, t)}{\sum_{t=d}^{t=d-l} G(i, t)} \quad (2)$$

where  $d$  is the selected day,  $i$  is the observed gauge station,  $t$  is the Julian day number (Habib et al., 2014). The value of  $l$  in the literature equals to 7 which gives a seven-day time window for the BF factor. Other forms may take on Time-Space Fixed (TSF) and Time Variable (TV) as shown in Equations 3 and 4 respectively

$$BF_{TSF} = \frac{\sum_{t=1}^{t=T} \sum_{i=1}^{i=n} S(i, t)}{\sum_{t=1}^{t=T} \sum_{i=1}^{i=n} G(i, t)} \quad (3)$$

$$BF_{TV} = \frac{\sum_{t=d}^{t=d-l} \sum_{i=1}^{i=n} S(i, t)}{\sum_{t=d}^{t=d-l} \sum_{i=1}^{i=n} G(i, t)} \quad (4)$$

Another scaling method is referred to as Distribution Transformation which is an additive approach (Gumindoga et al., 2016). It first computes a bias factor for monthly mean of gauge and satellite as shown in Equation 5,

$$DT_{\mu} = \frac{G_{\mu}}{S_{\mu}} \quad (5)$$

where  $G_{\mu}$  and  $S_{\mu}$  are the monthly mean of the gauge measurements and satellite estimates respectively for all gauge stations. In addition, the methodology also computes for a bias factor for the variation which is shown by Equation 6,

$$DT_{\tau} = \frac{G_{\tau}}{S_{\tau}} \quad (6)$$

Finally, the corrected satellite value would be computed by Equation 7,

$$S_{DT} = (S_o - S_{\mu})DT_{\mu} + DT_{\tau}S_{\tau} \quad (7)$$

where SDT is the corrected SPE and SO is the original SPE value. The advantage of this method is that it adjusts the satellite with respect to standard deviation and percentile values.

### 2.3.2. Regression and Curve Fitting

With regression and curve fitting, SPEs are corrected by using a certain function that relates the satellite data with ground truths. In some cases, it could be as simple fitting the precipitation estimate with gauge measurements through simple or multiple linear regression as with climate model downscaling and bias correction (Jakob Themeßl et al., 2011; Teutschbein & Seibert, 2012). However, it is also possible to use other equations such as polynomial and power functions to determine the corrected value of SPEs (Deng et al., 2018; Gumindoga et al., 2016). In the study of Deng et al. (2018), the Mean Error (ME) is plotted against the Precipitation Intensity (PI) to fit a quadratic function for correcting the SPE product. Figure 2-9 shows the plot and functions used in the said study.

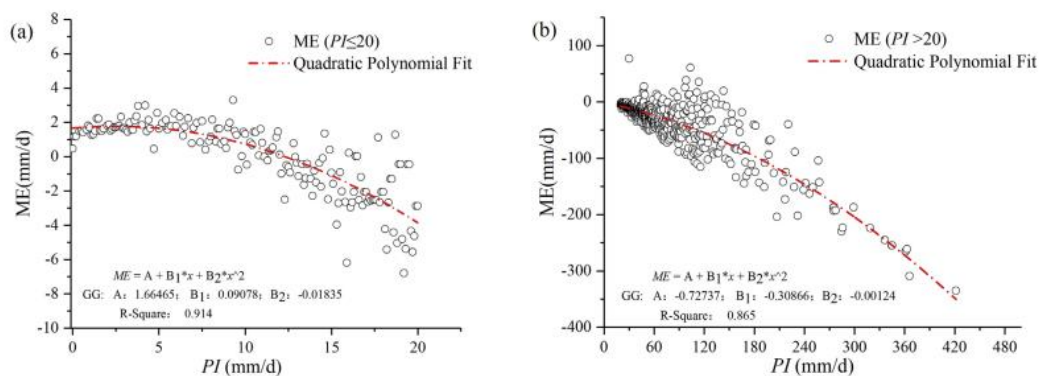


Figure 2-9. Curve fitting PI vs ME for a)  $0 < PI \leq 20$  and b)  $20 \text{ mm/day} < PI$

(Deng et al., 2018)

On the other hand, Gumindoga et al. (2016) shows a power transform function for correcting SPE as shown in Equation 8,



$$P^* = aP^b \quad (8)$$

where  $P^*$  is the corrected SPE value,  $P$  is the monthly rainfall from gauge,  $a$  is the factor that represent the corrected SPE to be equal to the gauge mean, and  $b$  is the coefficient of variation (CV) of the satellite to the gauge measurements. The variables  $a$  and  $b$  are coefficients for the power function which are then optimized using a generalized reduced gradient algorithm.

### 2.3.3. Quantile Mapping

In the QM methodology, the cumulative distribution functions (CDF) of both gauge and SPEs are used for bias correction. As with climate model downscaling, the CDFs may be fitted into a specific distribution (Teutschbein & Seibert, 2012). However, empirical or non-parametric distributions have been considered to produce better results as the curve fitting is not required (Z. Yang et al., 2016). The basic equation of QM is shown by Equation 9,

$$S_{adj} = CDF_G^{-1}(CDF_S(S_{ori})) \quad (9)$$

where  $CDF_G^{-1}$  is the inverse CDF of the gauge measurements,  $CDF_S$  is the CDF of the SPE at the same gauge location, and  $S_{adj}$  and  $S_{ori}$  are the adjusted and original SPE values respectively. This concept is represented in Figure 2-10 where PMW estimates are used instead of gauge measurements to correct PERSIANN-CCS (Karbalae, Hsu, Sorooshian, & Braithwaite, 2017).

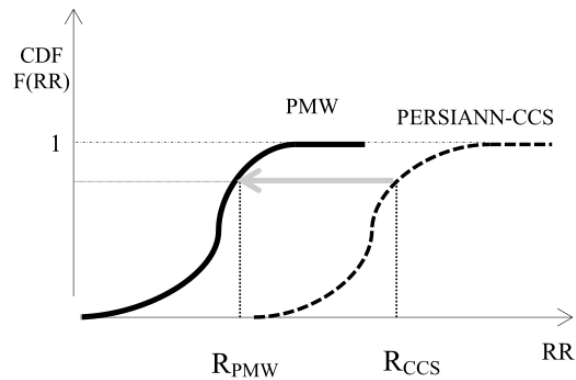


Figure 2-10. Quantile Mapping Algorithm (Karbalaee et al., 2017)

Scaling correction of SPEs show that the processed data have improved correlation, reduced biases, and less false alarms (Lekula et al., 2018; Saber & Yilmaz, 2018). When comparing between scaling methods in Zambezi River Basin, the multiplicative method STB and additive method DT were the most effective in correcting the mean values (Gumindoga et al., 2016). However, multiplicative methods are considered to be better than additive method in some areas (Saber & Yilmaz, 2018). Moreover, in an area where spatio-temporal variations are significant, the TSF method barely adjusted the data (Habib et al., 2014).

With the Quadratic fitting method used by Deng et al. (2018), the RMSE decreased and correlation increased after correction. Moreover, the precipitation intensity patterns by gauges were captured by the corrected data. However, in the study, the product chosen for correction was GSMaP\_Gauge which was already adjusted. Furthermore, the corrected data resulted in higher standard deviation which may be rooted from bias that the curve fitting may not be able to adjust.

In the study of Gumindoga et al. (2016), the Empirical QM method was the least performing correction method. However, it showed that QM is more effective in terms

of rainfall accumulation such as in monthly and annual time scales. It is stated that the QM method does not fully adjust daily events as it loses effectiveness with time scales less than a month (Alharbi et al., 2018; Z. Yang et al., 2016). It is also worth noting that the effectiveness of QM correction depends on the data used for adjustment. Corrected SPE data using with PMW-based rainfall estimates, which are less effective during winter, show improvement only during the summer season when compared to radar data (Karbalaee et al., 2017).

QM methodologies were coupled with other processes to improve correction. Common methodologies were to apply separation by zones and interpolation. Corrected SPE using QM coupled with separation by climate zones showed better performance compared to without separation (Alharbi et al., 2018). It is also able to capture daily rainfall pattern in a time series as shown in Figure 2-11.

Interpolation methods provide spatial variability in QM bias correction (Habib et al., 2014). Inverse Distance Weighing (IDW) and Gaussian Weighing (GW) are some of the interpolation methods used with QM (Alharbi et al., 2018; Z. Yang et al., 2016). In the study of Z. Yang et al. (2016), the 1° x 1° box grids were used in Chile to consolidate gauge data for one CDF per season. Figure 2-12 illustrates the location of the box grids, gauges, CDFs, and Gaussian function. The SPE adjusted by the coupled QM-GW is computed by Equation 10,

$$R_i = \sum_{j \in \Omega} w_{ij} \cdot CDF_{G-j_s}^{-1} \left( CDF_{S-j_s}(r_i(t)) \right) = \sum_{j \in \Omega} w_{ij} \cdot r'_i(t) \quad (10)$$

where  $R_i$  is the adjusted rainfall,  $r_i(t)$  is the satellite rainfall at pixel  $i$  at time  $t$ ,  $w_{ij}$  is the gaussian weight,  $CDF_{G-j_s}^{-1}$  is the inverse CDF of the gauge rainfall

measurement for season  $s$  at box  $j$ ,  $CDFs_j$  is the CDF of the SPE for season  $s$  at box  $j$ . The Gaussian weights are computed by Equation 11 and 12,

$$w_{ij} = \frac{\exp\left(-\left(\frac{d_{ij}}{C}\right)^2\right)}{\sum_{j=1}^4 \exp\left(-\left(\frac{d_{ij}}{C}\right)^2\right)} \quad (11)$$

$$d'_{ij} = \frac{d_{ij}}{D} \quad (12)$$

where  $d_{ij}$  is the normalized distance of pixel  $i$  to the center of the nearby box  $j$ ,  $d_{ij}$  is the actual distance of pixel  $i$  to nearby box  $j$ ,  $D$  is the farthest distance between two box centers, and  $C$  is the Gaussian shape parameter with a value of 0.33 in the study. All statistical metrics were consistently improved in the annual and monthly scale. Although random errors still exist in local daily time steps, the adjusted data captures the daily pattern of the rain gauges.

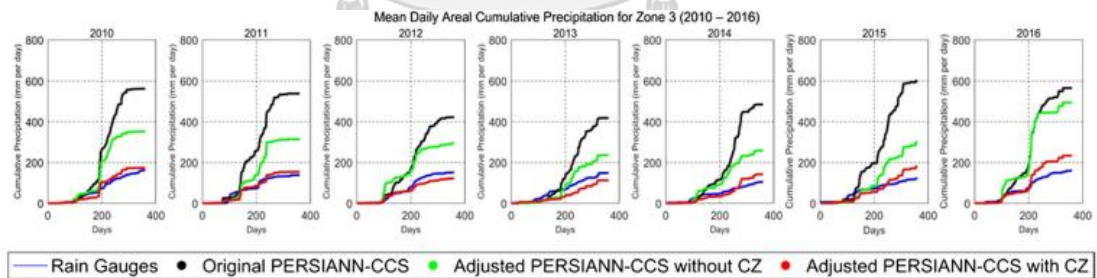


Figure 2-11. Mean Daily Accumulated Rainfall (Alharbi et al., 2018)

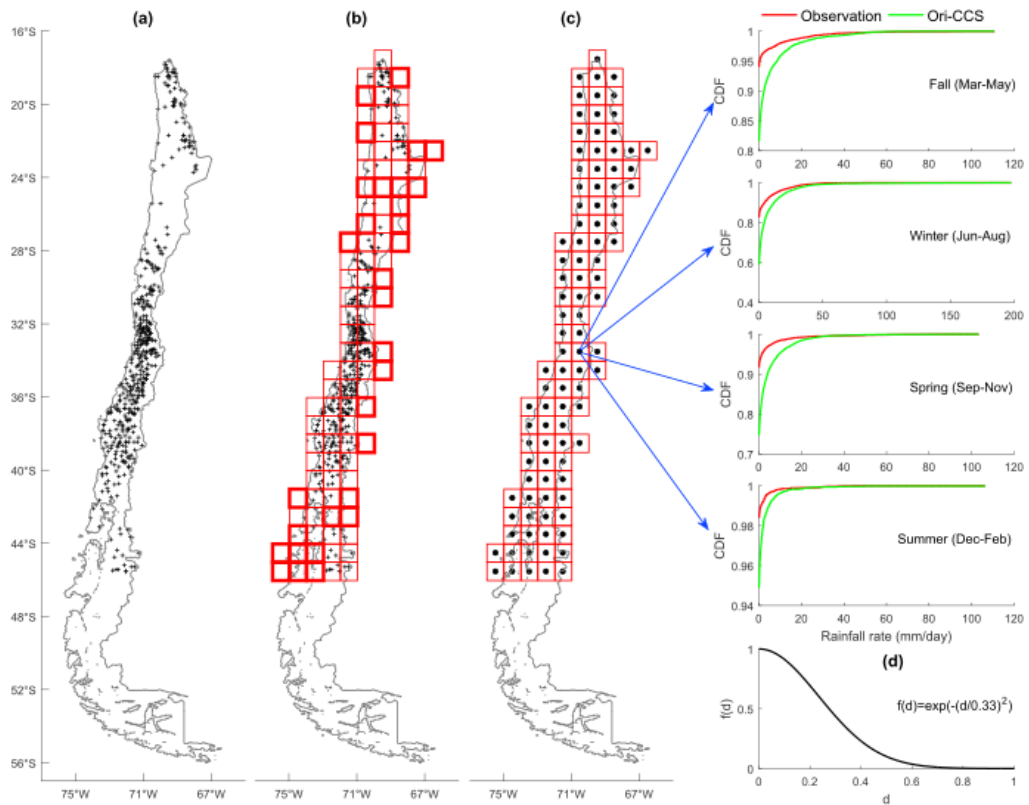


Figure 2-12. CDF Calculation Procedure (Z. Yang et al., 2016)

#### 2.4. Bias Correction using Machine Learning

With the increase in availability of large datasets in recent years, machine learning algorithms have gained popularity for its advanced capability in data analytics and processing which could be straining for traditional programs (Rebala, Ravi, & Churiwala, 2019). Contrary to conventional programming which inputs data into a program, machine learning algorithms produces the programs using both input and output data as shown in Figure 2-13. Due to this structure, challenging problems are solved indirectly without requiring detailed description of the models. However, the algorithms would need huge amounts of data to produce accurate results.

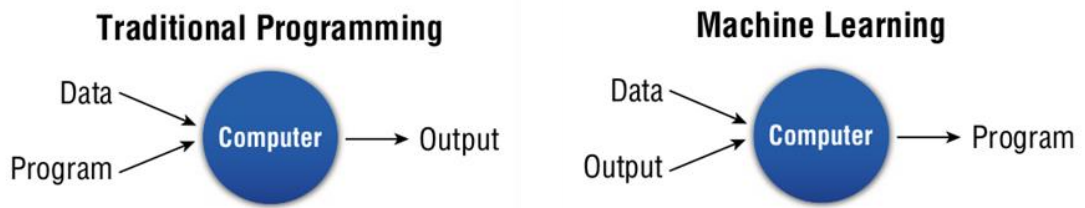


Figure 2-13. Difference between traditional programming and machine learning

(Lee, 2019)

Problems that machine learning algorithms can solve can be differentiated into three types; regression (prediction), classification, and clustering (Lee, 2019; Swamynathan, 2019). Regression or prediction refers to producing models which estimates and predicts continuous values using the relationships between the labelled data and variables. Classification seeks to identify the discrete values, groups or categories of the data. Clustering groups the data points with similar characteristics. Examples of each type is depicted in Figure 2-14.

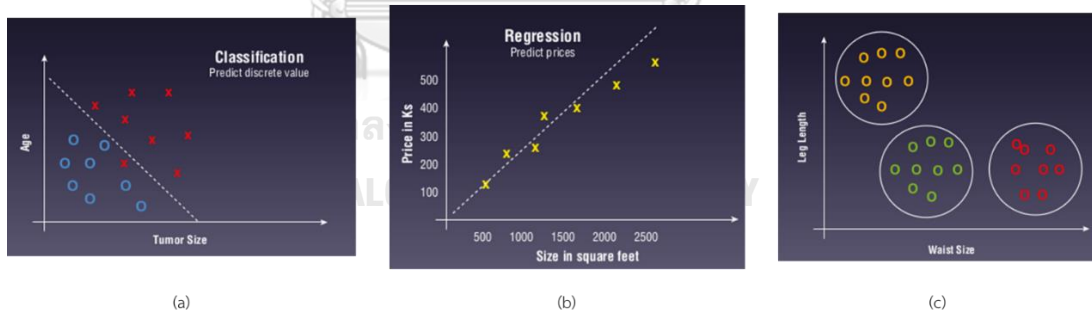


Figure 2-14. Examples of Machine Learning Problem Types; (a) regression, (b) classification, and (c) clustering (Lee, 2019)

Some more advanced machine learning algorithms are the combination and improvement of the mentioned problem types. Artificial neural networks (ANNs) are extension of the logistic regression model which is also useful in classification (Rebala et al., 2019). Simple classification algorithms such as polynomial classifiers have a

tendency to overfit noisy data whereas ANN algorithms provide better performance (Kubat, 2017). This algorithm, also known as a Multilayer Perceptron (MLP), is called a neural network because it imitates the functions of an oversimplified brain. Each node or perceptron (neuron) of the ANN (brain) is connected to another by a transfer function (synapse) which transmits the data (electric pulse or stimuli) as shown in Figure 2-15. In the feed-forward propagation scheme, a neuron sums its weighted inputs then subjects it to a transfer function where it passes the information to the next neuron. The weighted sum of the inputs or the net input can be solved using Equation 18

$$net = \sum_{i=1}^n w_{ji}x_i - \theta \quad (18)$$

where net is the net input vector,  $x_i$  is the input value,  $w_{ji}$  is its corresponding weight, and  $\theta$  is the bias of the neuron or perceptron (Du & Swamy, 2013). On the other hand, the most common transfer function is a sigmoid which is shown in equation 19

$$\phi(net) = \frac{1}{1 + e^{-net}} \quad (19)$$

where  $\phi$  is the transfer function. These steps are repeated until it reaches the nodes of the output layer. The key algorithm in using ANN is its backpropagation algorithm. This approach simply propagates back the difference between the actual predicted value and the output of the ANN model. The algorithm utilizes a gradient-descent based approach to adjust the weights. This adjustment is simply done by Equation 20 to 22

$$w_{ji}^{t+1} = w_{ji}^t + \Delta W_{ji}^t \quad (20)$$

$$\Delta W_{ji}^t = \eta \delta_i^t h_j + \alpha \Delta W_{ji}^{t-1} \quad (21)$$

$$\delta_i^n = \begin{cases} y_i(1 - y_i)(t_i - y_i) ; & \text{at output layer} \quad (22a) \\ h_i(1 - h_i) \sum \delta_i^{n-1} w_{ji} ; & \text{at hidden layer} \quad (22b) \end{cases}$$

where  $w_{ji}$  is the weight from node  $j$  to node  $i$  at iteration  $t$ ,  $\Delta W$  is the weight change,  $\eta$  is the learning rate of the gradient descent,  $\delta_i^n$  is the gradient descent factor of node  $i$  at layer  $n$ , and  $\alpha$  is the momentum rate (Kubat, 2017). The learning rate dictates how fast the adjusted weight would reach convergence while the momentum rate controls how much the adjusted weight oscillates per iteration (Rebala et al., 2019). The typical values for learning rate and momentum rate used in practice are 0.1 and 0.9 respectively (Du & Swamy, 2013). The forward-backward propagation continues until the computation reaches the convergence or when it reaches a predesignated number of iterations. The ANN schematic is shown in Figure 2-15.

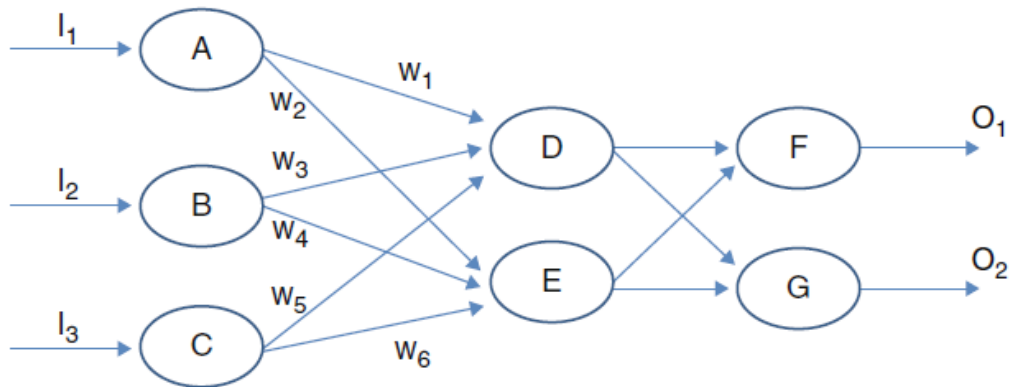


Figure 2-15. Scheme of a sample neural network (Rebala et al., 2019)

Although the sigmoid and tanh functions have been widely used in most neural networks, these activation function exhibits some limitations in terms of its reliability (LeCun, Bottou, Orr, & Muller, 1998; Nwankpa, Ijomah, Gachagan, & Marshall, 2018). There would be cases where once the net input vector reaches a significantly high value, the output of the sigmoid function becomes saturated and very close to the value of 0



and 1 for sigmoid and 1 and -1 for the tanh function. This result would make the slope of the function needed for the gradient descent method become extremely low to the point that it would not have much changes in the node affected. This problem is commonly known as the Vanishing Gradient (Roodschild, Sardiñas, & Will, 2020). Therefore, in recent years, the Rectified Linear Unit (ReLU) transfer function has gained popularity in neural networks as it overcomes the limitation of the sigmoid function. As shown in Figure 2-16, the ReLU function would not have the same problem encountered with the sigmoid function as there are no presence of saturation at high values. Moreover, because of the simplicity of the function, it allows for faster computations that which benefits deep learning models (Nwankpa et al., 2018; Oostwal, Straat, & Biehl, 2020; Roodschild et al., 2020).

However, the ReLU still poses some problems. In some cases that the learning rate is not adjusted properly, a ReLU node can potentially stop working in the training phase due to having a lower boundary situated at the zero value (Nwankpa et al., 2018). This state is known as the “dying ReLU” problem. Literature has shown that this problem can be circumvented by properly adjusting the learning rate or adapting a variation of the transfer function which is the Leaky ReLU (Oostwal et al., 2020). This activation function adjusts the ordinate negative values in proportion to a constant instead of simply replacing them as zeroes.

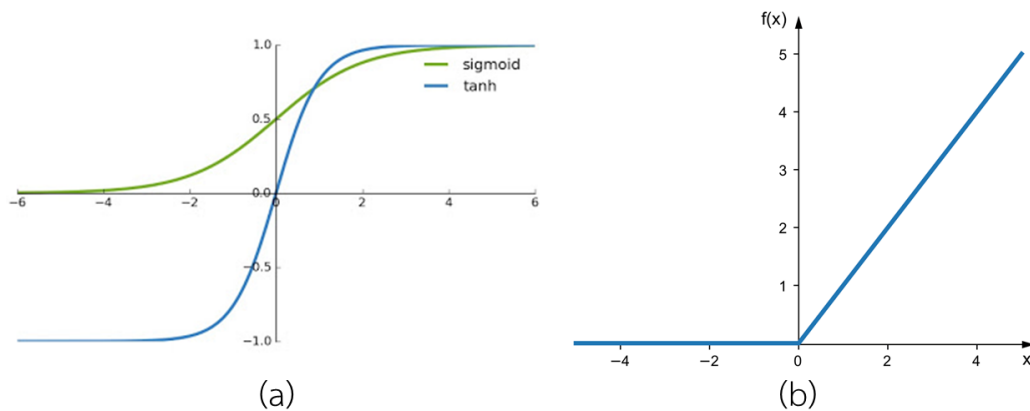


Figure 2-16. (a) Sigmoid and Hyperbolic Tangent vs (b) ReLU Activation Functions

ANNs can be further improved to provide better results for specific purposes. Recurrent neural networks (RNNs) are used for sequential data such as time series and repetitive datasets. In addition, convolutional neural networks (CNNs) may be more useful for image and feature processing as it uses convolution to measure the overlap between figures. On the other hand, another advanced machine learning method is by applying Support Vector Machine (SVM). SVM is a classification type algorithm. However, by adapting regression algorithms in the methodology, it is possible to predict continues values.

Machine learning algorithms may also be utilized in hydrology and water resources engineering. Although the most popular machine learning method is ANN, the common machine learning algorithm in statistical downscaling and bias correction is SVM (Kumar, Ramsankaran, Brocca, & Munoz-Arriola, 2019; Kundu, Khare, & Mondal, 2017; Lary, Remer, MacNeill, Roscoe, & Paradise, 2009; Najafi, Moradkhani, & Wherry, 2011; Sachindra, Ahmed, Rashid, Shahid, & Perera, 2018; Vandal, Kodra, & Ganguly, 2019). One of the reasons why SVM is popular is because SVMs evolved from actual theory while ANN considers the heuristics within the data (Lary et al.,

2009). However, aside from selection of predictors, SVM-type of algorithms require the selection of the kernel algorithm for the its process which may not be a one-for-all-situations case (Sachindra et al., 2018). In the case of SPE correction, neural network-based algorithms are still more commonly employed than SVM-based (Kumar et al., 2019; Ngo-Duc, Matsumoto, Kamimera, & Bui, 2013; Tao, Gao, Hsu, Sorooshian, & Ihler, 2016). However, the predictor data for their correction usually comes from gridded data and/or satellite data such interpolated rainfall dataset (Ngo-Duc et al., 2013), IR imagery (Nasrollahi, Hsu, & Sorooshian, 2013), and soil moisture (Kumar et al., 2019). On the other hand, ground data used as neural network predictors for the purpose of rainfall prediction are usually meteorological parameters such as temperature, relative humidity, wind speed, atmospheric pressures, and the like (Abbot & Marohasy, 2012; Coulibaly & Evora, 2007; Devi, Arulmozhivarman, Venkatesh, & Agarwal, 2016; Kashiwao et al., 2017; Velasco, Serquiña, Zamad, Juanico, & Lomocso, 2019).

## CHAPTER 3

### METHODOLOGY

#### 3.1. Study Area

The study area covers the whole Thailand. The country is situated in the mainland of South East Asia. As shown by Figure 3-1, It shares its border with Cambodia on the east, Laos on the north east, Myanmar on the west, and Malaysia on the south. the country has a tropical climate which is influenced by seasonal monsoons and tropical storms. Southwest monsoon season occurs during May to October bringing large amount of rainfall. This is followed by the northeast monsoon on October to February which is the cooler period, especially in December and January. Afterwards, the dry period occurs from February to May, with April typically being the hottest month.

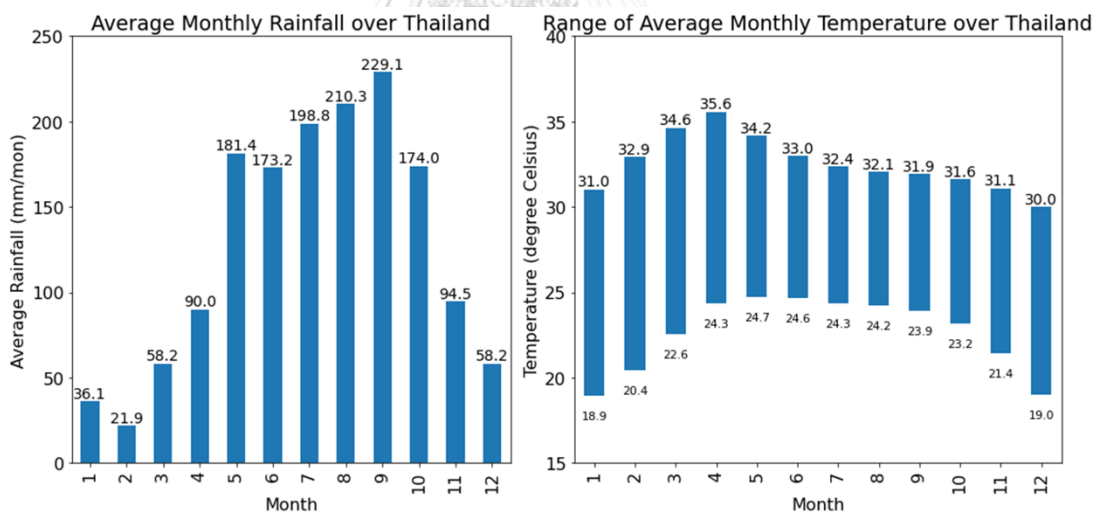


*Figure 3-1. Averaged Monthly Rainfall and Temperature Over Thailand*

There are 22 major river basins as defined by the Office of Natural Water Resources (ONWR) in Thailand. However, because the Sakae Krang river basin does not contain a TMD gauge stations in its vicinity, it would be merged with the Lower Chao Phraya river basin as the rainfall patterns in the area is similar to each other. Thus, the river

basins used in this study would amount to a total of 21 major watersheds as shown in as shown in Figure 3-2.

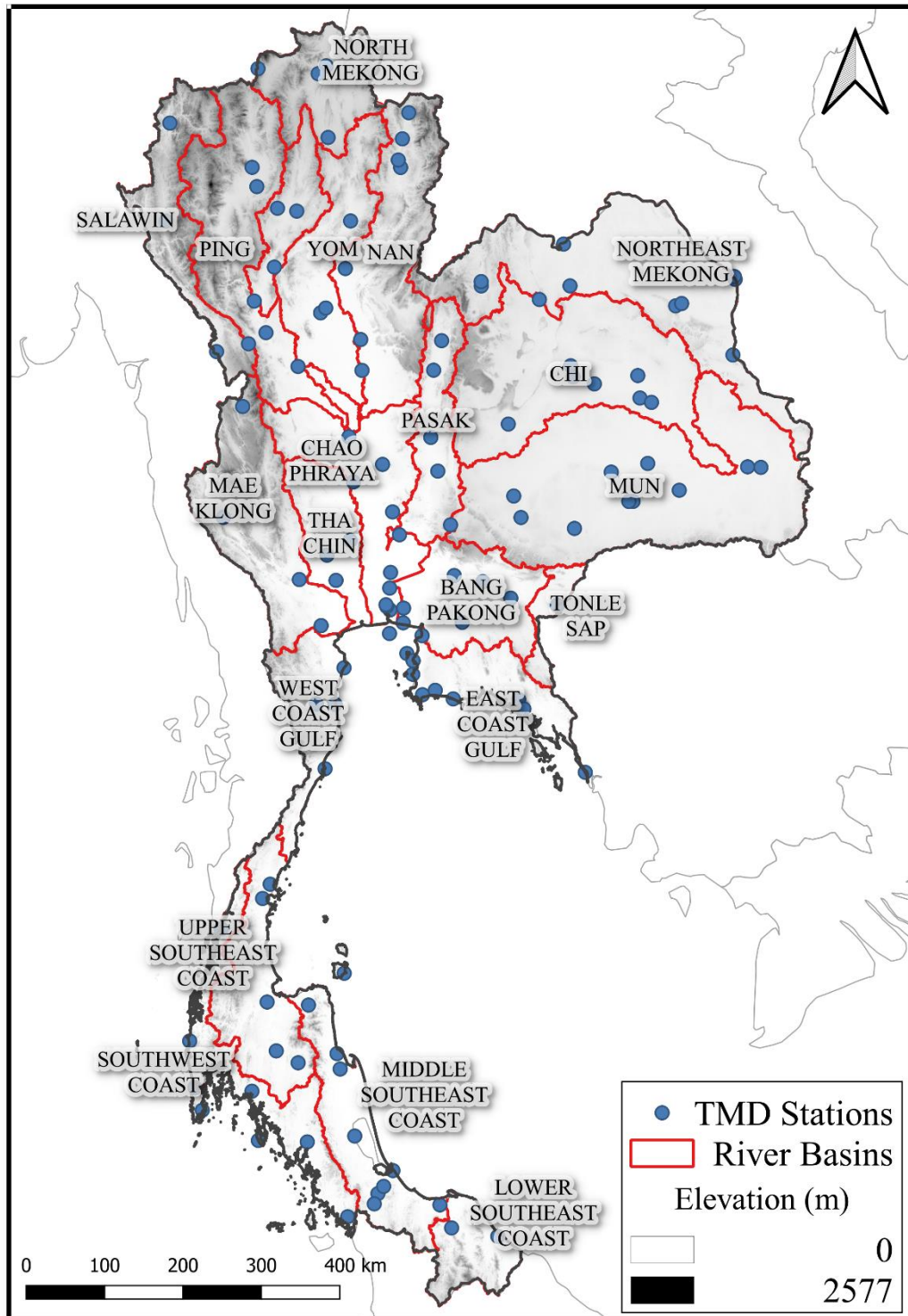


Figure 3-2. Thailand River Basin and TMD Station Locations

### 3.2. Data Sources

Rain gauge measurements were used for the evaluation and bias correction of the SPE products. The 123 TMD synoptic stations from would be used for the evaluation of the study. The locations of these are also shown previously in Figure 3-2. However, only the data from year 2003 and above would be used in the study to account for the consistency of data coinciding with the SPE products. Furthermore, although the synoptic stations have better data quality, it contains some missing data during some years as well as in some stations. In addition to the rainfall data from the TMD stations, the minimum and maximum daily temperature records would be used as supplementary predictors in the ANN bias correction approach that would be discussed later. The temperature records cover years as early as 1975 to present; however, in this study, both datasets only have measurements until early 2017. Thus, the validation period of the ANN bias correction would be until the end of 2016.

A Double Mass Curve analysis was performed to determine the consistency of the rain gauge observations with each other. It would compare the cumulative annual values of a station with the average cumulative annual values of reference stations (Searcy and Hardison, 1960). In the case of this study, the consistency of each TMD gauges within a river basin would be analyzed with the average rainfall data of other TMD synoptic stations therein. Should a basin have less than 3 gauges within it, the consistency analysis would not be conducted.

As for the satellite data, the NRT SPE products for the study are PERSIANN-CCS, GSMAP\_NRT, and IMERG Early. The satellite data are retrieved at an hourly time scale from 2003 coverage to 2018. The coverage of the data is selected in order for all

products would have consistency in the temporal scale. Moreover, since the SPE products are in UTC format, the sub-daily data would be aggregated to daily starting from the time of collection in local time, UTC+7. The time coverage of the datasets is shown in Figure 3-3. The specific product details are presented in Table 3-1.

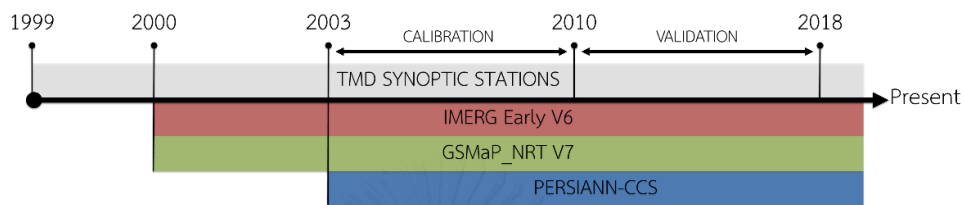


Figure 3-3. Temporal Coverage of Rain Gauge Data and SPE Products

Table 3-1. SPE Product Spatiotemporal Resolutions and Latency

SPE Product	Spatial	Temporal	Latency
PERSIANN-CCS	0.04° x 0.04°	1 hour	~ 1 hour
GSMaP_NRT	0.1° x 0.1°	1 hour	4 hours
IMERG Early	0.1° x 0.1°	30 mins	4 hours

### 3.3. Methodology

The methodology of the study is illustrated in Figure 3-4 which depicts the overall procedure to obtain the bias corrected SPE datasets and determine which adjusted product performs the best in each river basin. After the data collection, the original SPE products would be evaluated using the TMD manual stations over Thailand. Afterwards, all SPE product would be subjected to bias correction by Scaling, Quantile Mapping (QM), and Artificial Neural Network (ANN) approaches. The adjusted product that produced the least RMSE in a river basin would be considered as the best performing dataset in that specific basin.

The evaluation of the SPE products would be conducted by determining the following factors; quantitative statistics, categorical statistics, rainfall patterns, monthly performance, precipitation intensity performance, and basin-specific performance. The metrics used for quantitative statistics are the mean bias (BIAS), root-mean-squared error (RMSE), and correlation coefficient (CORR). On the other hand, the categorical statistics considers the probability of detection (POD), false alarm ratio (FAR), and Equitable Threat Score (ETS). The formula and optimal values of the categorical statistics are listed in Table 3-2. Furthermore, ETS was chosen among the other skill score metrics because of its ability to consider true negatives in its computation and its non-linearity which heavily weighs the mistakes over correct prediction (Wilks, 2011).

The rainfall pattern would be evaluated by comparing the average monthly rainfall over Thailand in each year. The monthly performance is evaluated by determining both quantitative and categorical statistics for each month of the year. On the other hand, the performance of the SPE in terms of its precipitation intensity estimation is evaluated by determining the quantitative statistics in specific intervals as provided the TMD guidelines shown in Table 3-3. As for the basin-specific evaluation, the quantitative statistics would be determined in reference to the TMD gauges that are present within a specific basin. Afterwards, the SPE evaluation results would be compared with each other to determine which original SPE dataset produced the best performance over Thailand.



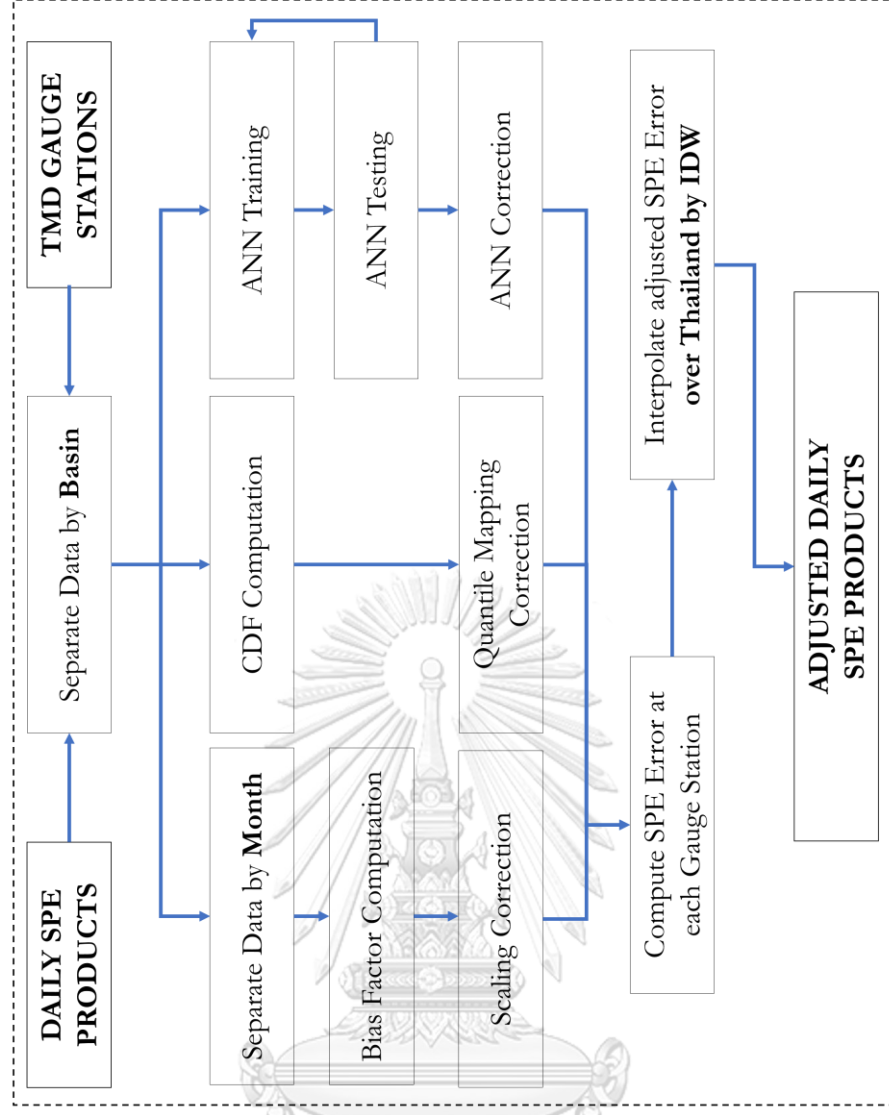
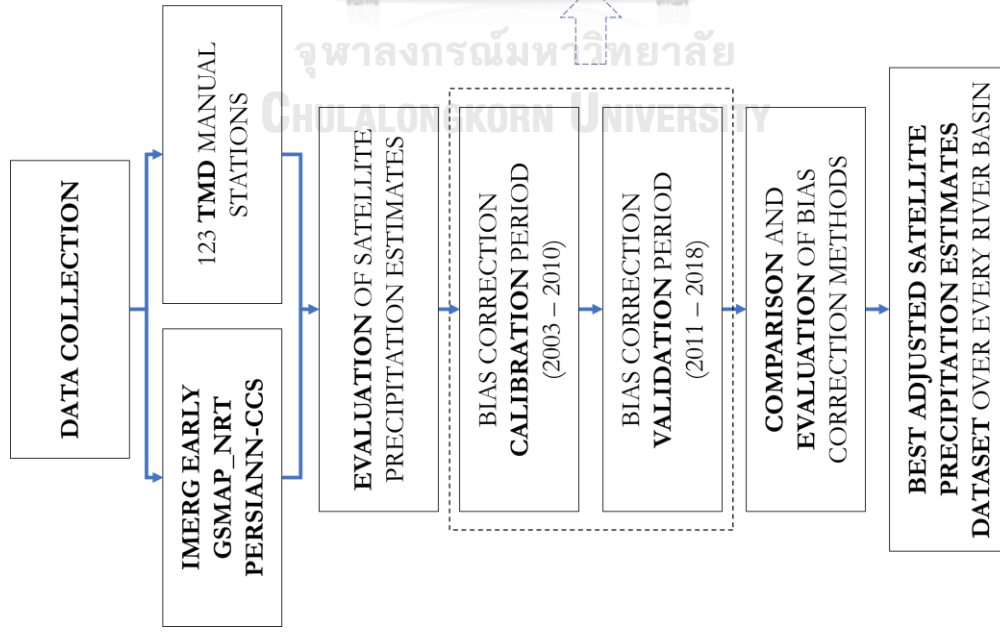


Figure 3-4. Flowchart of the Methodology

After the comparison of the evaluation, three bias correction methodologies would be implemented in this study. As mentioned previously, the adjustments would be carried out to the three SPE products in the study using scaling correction, quantile mapping, and ANN bias correction methods. The calibration period for all methods would be from 2003 to 2010 while the validation period would be from 2011 to 2018, except for the ANN correction that would be shortened to the end of 2016. All corrections are done in only SPE rainfall pixels that contains a TMD stations within it.

*Table 3-2. Categorical Statistics Formula and Optimal Values*

<b>Metric</b>	<b>Formula</b>	<b>Optimal Value</b>
<b>POD</b>	$\frac{a}{a + c}$	1
<b>FAR</b>	$\frac{b}{b + d}$	0
<b>ETS</b>	$\frac{a - a_{ref}}{a - a_{ref} + b + c}$	1

*Table 3-3. TMD Precipitation Intensity Ranges*

<b>Precipitation Intensity</b>	<b>Range</b>
Light Rain	0.1 – 10 mm/day
Moderate Rain	10.1 – 35 mm/day
Heavy Rain	35.1 – 90 mm/day
Extreme Rain	> 90 mm/day

The scaling correction would follow a TSV approach which would vary the bias factor depending on month and basin. Each bias factor would be computed from the data within the calibration period from 2003 to 2010. After obtaining these values, the said bias factors would be applied to the SPE datasets in both calibration and validation

period and compared to the gauge values in order to determine the performance of the adjusted SPE products.

In addition, the Quantile Mapping approach would be utilized to correct the SPE products. In order to apply this method, the cumulative distribution functions (CDF) of both satellite and gauge daily rainfall data needs to be constructed. In this study, the CDFs would vary within each river basin to account for the spatial variability. Similar to the scaling correction, only the data from the calibration period would be used for building the CDFs to be used in this correction.

As for the ANN bias correction method, the study would utilize the Scikit-Learn library of Python to conduct the training and testing of the Multilayer Perceptron neural network for the bias correction. The parameters of the ANN model would be set with regards to values that are recommended for practical use for the stochastic gradient descent method. The learning rate is set at a constant of 0.01 while the momentum rate is at 0.9. In order to prevent the model from running infinitely, the maximum number of iterations would be at 1 million iterations with an error tolerance of  $1 \times 10^{-6}$ . However, unlike the typical methods, the model would employ a Rectified Linear Unit (ReLU) function instead of the commonly used sigmoid function. This change of activation function is done to avoid the vanishing gradient problem that occurs for with the sigmoid and hyperbolic tangent functions.

The input predictor vector would contain the SPE rainfall value, maximum temperature, and minimum temperature while the target value in the output layer would be the adjusted SPE rainfall value. In this study, only one hidden layer would be employed in order to account for simplicity of the model. The number of nodes within

the hidden layer would be selected by through trial and error. The selected number of hidden nodes would be the lowest possible value in which adding more nodes would not cause fluctuations of the RMSE during training phase. Moreover, due to the nature of scaling that is required for the data, some of the outputs may results in negative value which is impossible for rainfall data. Negative values are automatically replaced as zero.

Afterward the correction at each gauged pixel, the deterministic interpolation method IDW would be used to interpolate the error between the original and adjusted SPEs. The interpolation is applied throughout the whole country. The difference between these two values would be used to correct subsequent ungauged pixels as shown in Figure 3-5. Since the interpolated error may be larger than the original daily rainfall value, any negative values would automatically be converted to zero.

After bias correction, the RMSE and normalized RMSE of each adjusted SPE in each basin would be compared in order to determine the best performing adjusted SPE. The normalized RMSE is included in order to objectively compare the bias corrected datasets. The normalized RMSE is computed by applying Equation 23 (Wilks, 2011).

$$\text{Normalized RMSE} = \frac{RMSE}{stdev_{gauge}} \quad (23)$$

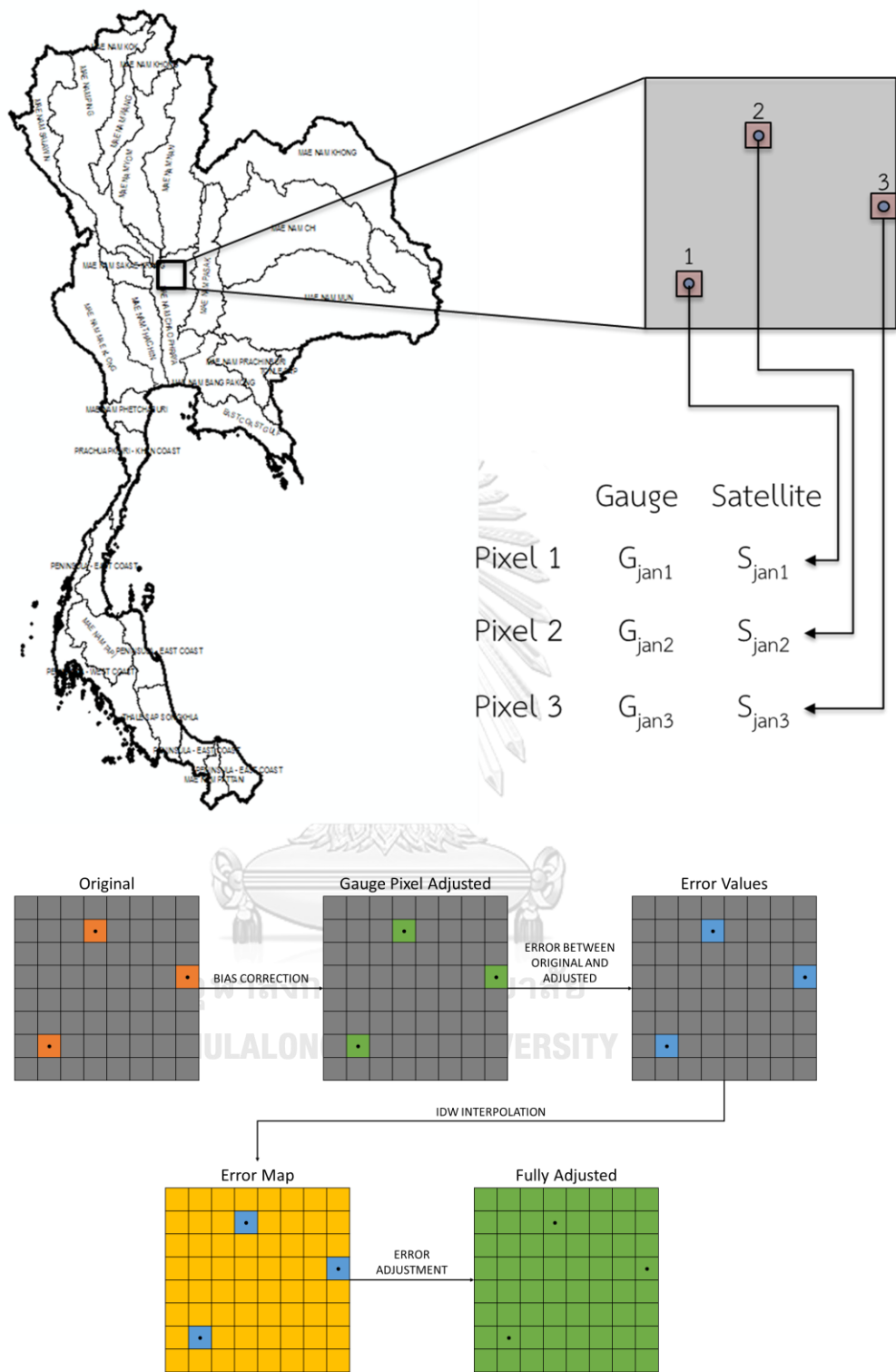


Figure 3-5. Bias Correction – Interpolation Scheme Example

## **CHAPTER 4**

### **EVALUATION OF SATELLITE PRECIPITATION ESTIMATES OVER THAILAND**

The evaluation of the selected SPEs over Thailand shows the varying performances of the three products as well as each of its innate characteristics, such as spatial and temporal accuracy. Each SPE product is compared to surface precipitation measurements using the 123 synoptic rain gauges of TMD located all over Thailand. The time frame observed for the evaluation is set from year 2003 to 2018 to provide consistency in terms of the data availability of all considered products. Every product would be evaluated in terms of quantitative and categorical statistics, annual accumulated time series comparison, monthly rainfall variation, and varying precipitation intensity.

#### 4.1.1. Annual Precipitation

As shown in Figure 4-1, the annual rainfall scatterplots of each satellite product are plotted against the rain gauge measurements. PERSIANN-CCS shows greater spread of data; however, it can be observed that the higher rainfall intensities are underestimated. As for GSMaP\_NRT, the annual satellite rainfall has less spread and the alignment to the 1:1 line is more evident in comparison to PERSIANN-CCS. Among the three SPE products evaluated, the IMERG Early has the least spread based on visual inspection. However, it is evident for all products that the higher rainfall is underestimated.

As for the quantitative statistics of each product, Table 4-1 details the values of their biases, RMSEs, and correlation coefficients. Based on the computed bias, both PERSIANN-CCS and IMERG Early tend to overestimate annual rainfall values. On the

other hand, GSMaP\_NRT shows a tendency of underestimation for the yearly precipitation. As for the RMSE, PERSIANN-CCS has the highest value at 680.0 mm, followed by GSMaP\_NRT at 470.0 mm, then IMERG Early with 451.7 mm. Among the three products, PERSIANN-CCS has the least correlation at 0.55. The correlation coefficient of GSMaP\_NRT and IMERG Early are relatively close to each other at 0.79 and 0.82 respectively. However, it is evident that IMERG Early has the better performance overall in terms of annual precipitation.

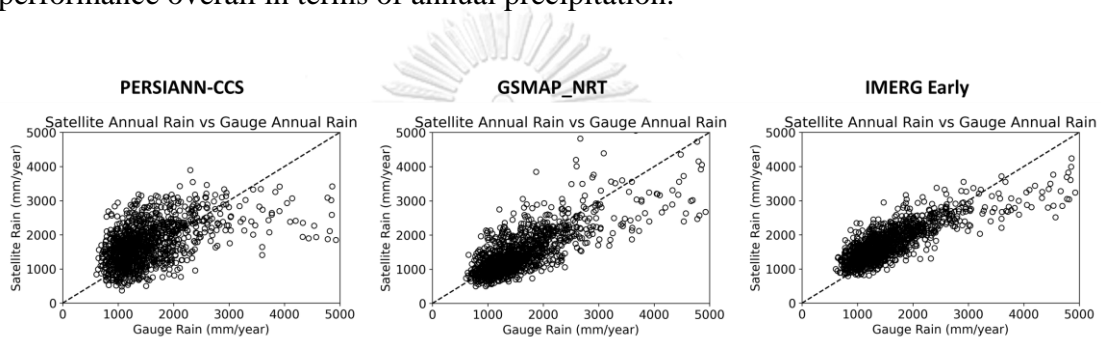


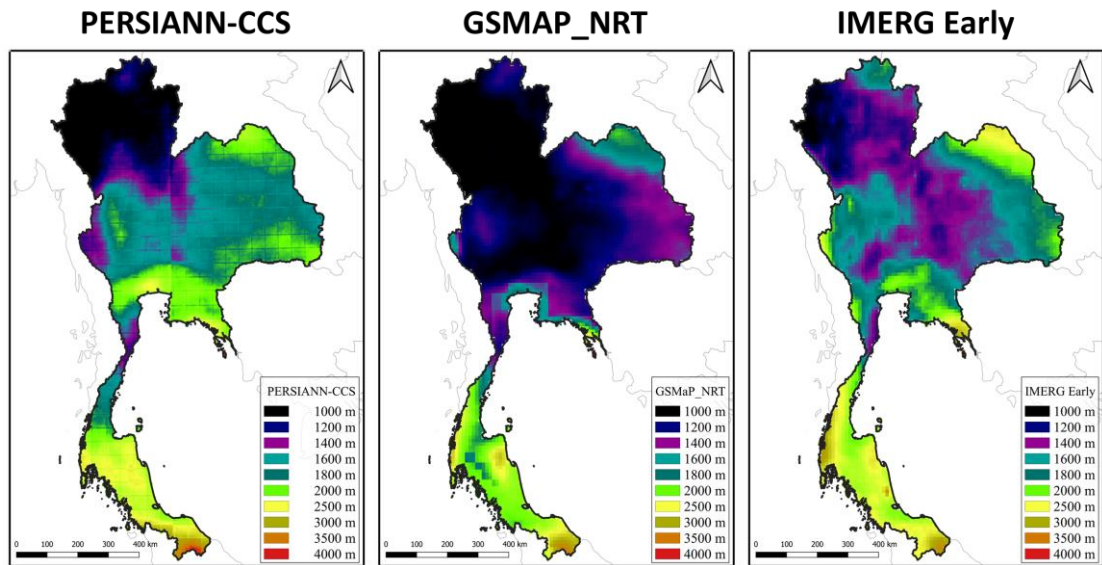
Figure 4-1. Annual Scatterplot of SPE Products

Table 4-1. Annual Precipitation Quantitative Statistics

	PERSIANN-CCS	GSMaP_NRT	IMERG Early
BIAS (mm/yr)	199.5	-120.1	171.5
RMSE (mm/yr)	686.0	470.0	451.7
CORR	0.5	0.8	0.8

In terms of the annual satellite rainfall averaged over the study period shown in Figure 4-2, all SPE products follow the known patterns over Thailand where lower rainfall is evident in the northern regions and increases in intensity to the southern regions. However, the underestimation of GSMaP\_NRT can be observed as even the central region of Thailand has relatively low annual rainfall. On the other hand, IMERG Early produces higher rainfall in the northern regions and other parts of the country. As

for the southern region, all SPE products show the same patterns with higher rainfall occurring near the shore.



*Figure 4-2. Average Annual Rainfall for PERSIANN-CCS (left), GSMaP\_NRT (center), and IMERG Early (right)*

#### 4.1.2. Monthly Precipitation

In terms of monthly rainfall, Figure 4-3 illustrates the scatterplot of the monthly precipitation of each SPE product versus the gauge observation. Both PERSIANN-CCS and GSMaP have high spread of their data. PERSIANN-CCS clearly shows underestimation of higher rainfall values while there are significantly higher occurrences of overestimation for GSMaP\_NRT. However, majority of the GSMaP\_NRT data is still below the 45° line. As for IMERG Early, it can be observed that the data does not have a large spread unlike the two other SPE. Moreover, the monthly values align well to the 1:1 line, even though the high precipitation intensities are still underestimated.



As listed in Table 4-2, the computed monthly values for the quantitative statistics of each SPE product follow the same pattern as the annual precipitation. Both PERSIANN-CCS and IMERG Early still tend overestimate the rainfall while GSMaP\_NRT shows underestimation of the monthly precipitation. PERSIANN-CCS has the higher RMSE and lowest CORR values. On the other hand, IMERG Early still performs the best among the three SPEs in terms of both RMSE and correlation coefficient.

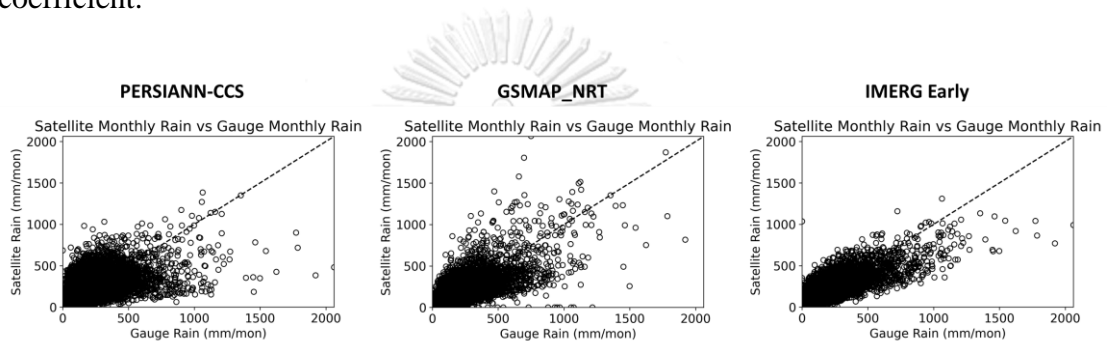


Figure 4-3. Monthly Scatterplot of SPE Products

Table 4-2. Monthly Precipitation Quantitative Statistics

	<b>PERSIANN-CCS</b>	<b>GSMaP_NRT</b>	<b>IMERG Early</b>
BIAS (mm/mon)	15.6	-12.1	12.7
RMSE (mm/mon)	121.4	96.4	86.0
CORR	0.7	0.8	0.8

Each SPE product has been plotted in a monthly timeseries graph as shown in Figure 4-4. PERSIANN-CCS mostly overestimates rainfall by the end of the year; however, it still underestimated rainfall in 2011 and slightly in 2016. As for GSMaP\_NRT, it mostly underestimates in early years but the monthly rainfall estimations have gotten closer in the recent years. Similarly, IMERG Early also improved its performance in recent years in which the overestimation has been lessened

to a degree where the monthly satellite rainfall and gauge measurements are almost the same.

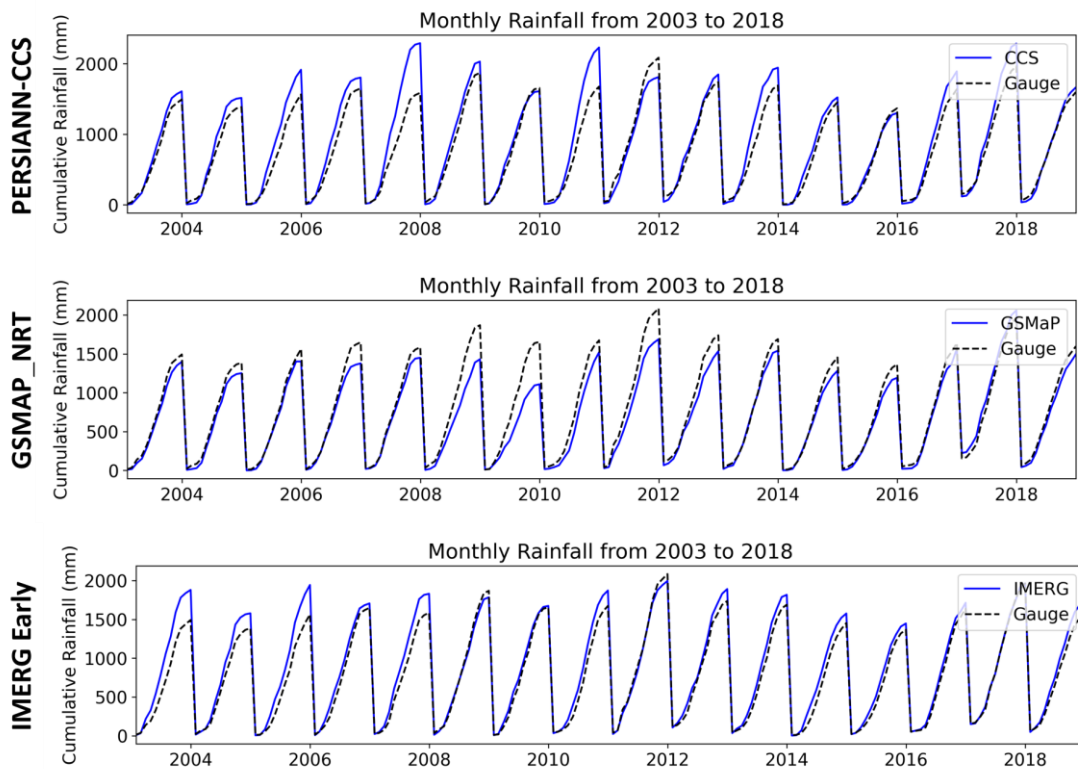


Figure 4-4. Cumulative Average Monthly Rainfall over Thailand

## 4.2. Daily Precipitation Assessment

### 4.2.1. Over Whole Study Period

Figure 4-5 shows the scatterplot of the daily satellite precipitation in comparison to the daily gauge rainfall observations. Due to having a finer temporal resolution, the data points for all SPE products shows higher spread. The larger spread of data is evident in the GSMaP\_NRT dataset. As for the PERSIANN-CCS, its data does not align well to the 1:1 line. A significant portion of its points over estimates low intensity rainfall and also underestimates high intensity rainfall. In addition, although IMERG

Early may visually appear better than the other two SPE products, the dataset still has a noticeable spread as well as clear underestimation of high intensity precipitation.

In terms of their quantitative statistics, all evaluated SPE products still maintain similar pattern as with the annual and monthly rainfall as presented in Table 4-3. However, it is observed that the correlation coefficient has been significantly lowered. This change is expected as daily rainfall proved to be harder to estimate because of various reasons, including sudden pulses of rainfall evident in the tropical region which is difficult to be fully captured by the satellite data.

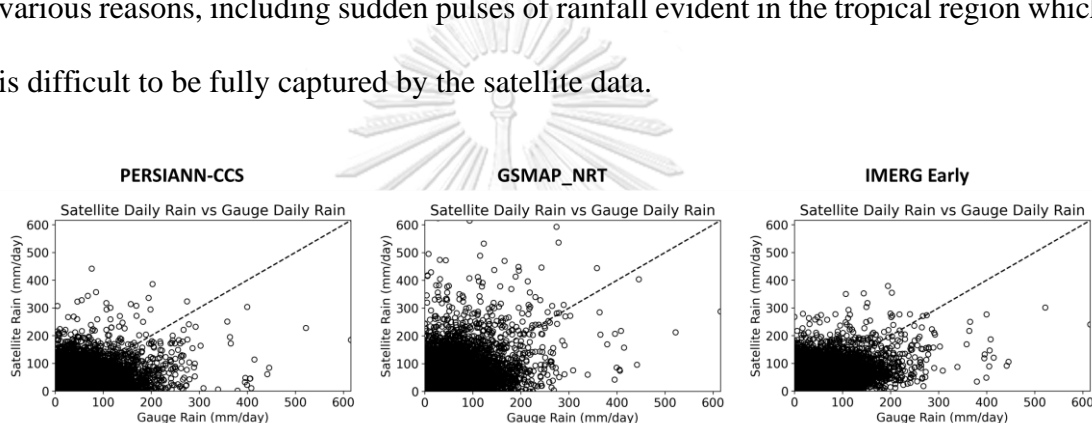


Figure 4-5. Daily Scatterplot of SPE Products

Table 4-3. Daily Precipitation Quantitative Statistics

	<b>PERSIANN-CCS</b>	<b>GSMaP_NRT</b>	<b>IMERG Early</b>
BIAS (mm/day)	0.5	-0.5	0.4
RMSE (mm/day)	13.3	12.3	11.0
CORR	0.4	0.5	0.6

#### 4.2.2. By Month

In order to further evaluate the daily rainfall, the satellite precipitation data has been separated and evaluated by month. Both PERSIANN-CCS and IMERG Early tend to have similar patterns. The only difference is that IMERG Early showed better performance than PERSIANN-CCS. Both datasets show overestimation in wet months and underestimation in dry months as shown in Figure 4-6. Moreover, the RMSE for

both SPE products on Figure 4-7 shows that wet months have higher errors while dry months have lower values. Inversely, Figure 4-8 illustrates that the correlation coefficients for these two SPEs are higher during dry month but lower in wet months. As for GSMaP\_NRT, the observed underestimation from the previous evaluation remains evident, especially in the wet months from May to October. On the other hand, GSMaP\_NRT has lower errors in wet season compared to CCS but have higher errors in colder months from November to January. As for the correlation, the computed values do not vary significantly, but it can still be observed that the correlation coefficients are lower in the wet season similar to the other two SPE products.

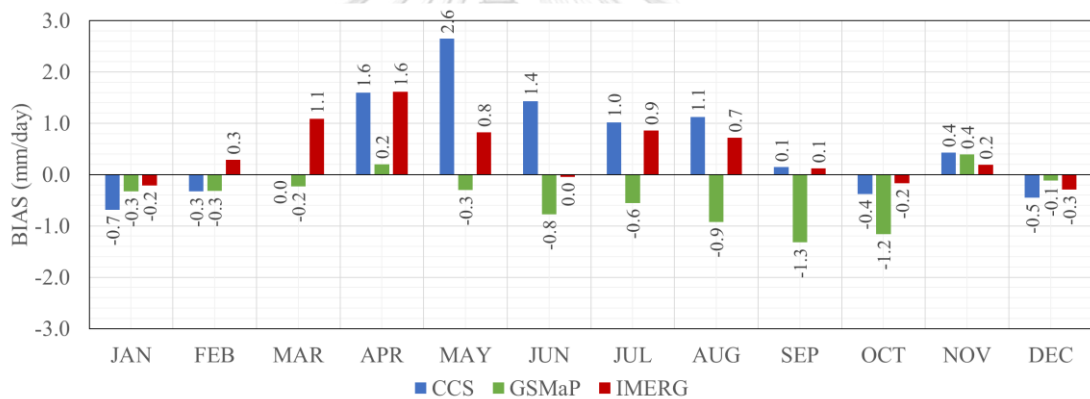


Figure 4-6. BIAS of Daily Rainfall per Month

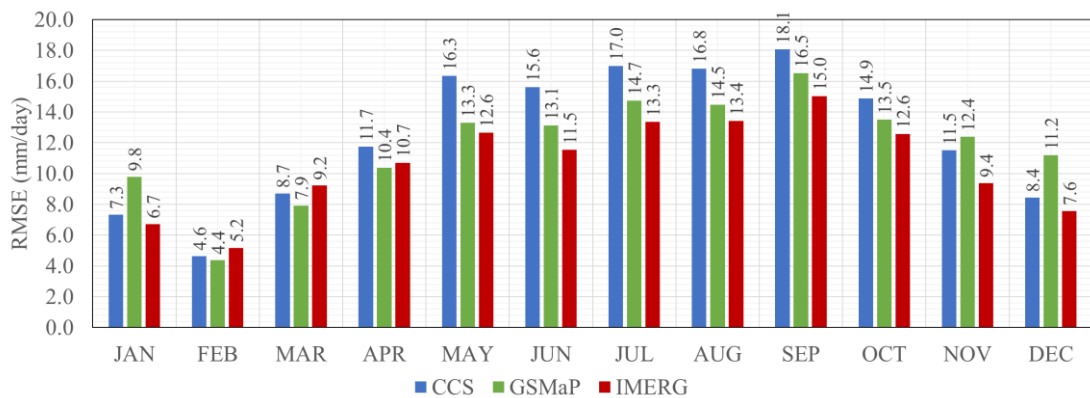


Figure 4-7. RMSE of Daily Rainfall per Month

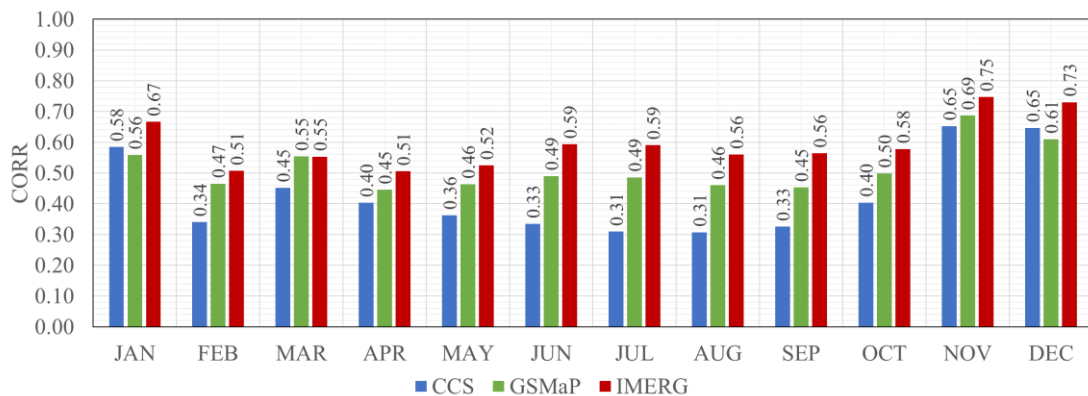


Figure 4-8. CORR of Daily Rainfall per Month

#### 4.2.3. By Precipitation Intensity

Furthermore, separating the satellite data by rainfall intensity gives insight on how well the SPE products performance depending on occurring precipitation. The range for the rainfall intensities are based on the precipitation range prescribed by TMD with light rain at 0.1 – 10 mm, moderate rain at 10.1 – 35 mm, heavy rain at 35.1 – 90 mm, and extreme rain at anything above 90 mm per day. As shown in Figure 4-10, it is evident that all three SPE products follow the same patterns. Light rain is overestimates while everything above said intensity is underestimated. In addition, as the precipitation intensity increases, the underestimation increases. Among the three SPEs, PERSIANN-CCS generally has the largest values except for moderate rainfall. On the other hand, GSMaP\_NRT generally has the lower bias except during moderate and heavy rainfall. IMERG Early produced the least bias in moderate and heavy rainfall. In terms of RMSE, Figure 4-11 illustrates that IMERG Early has least error for moderate to extreme rainfall while GSMaP\_NRT has least error for no rain and light rain. As for correlation, all three SPEs still show the same pattern in which the correlation values increase with higher intensities as depicted in Figure 4-12. All evaluated satellite products resulted in poor correlation coefficient values. Even though the extreme rainfall has slightly better

correlation, it is still relatively small in comparison to the overall daily precipitation.

Overall, IMERG Early shows the best performance among the three SPE products.

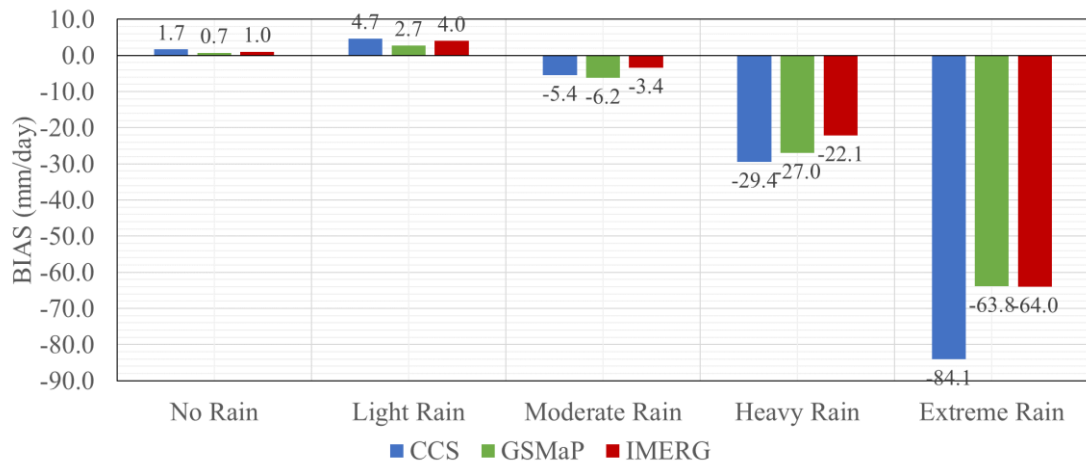


Figure 4-9. BIAS of Daily Rainfall by Intensity

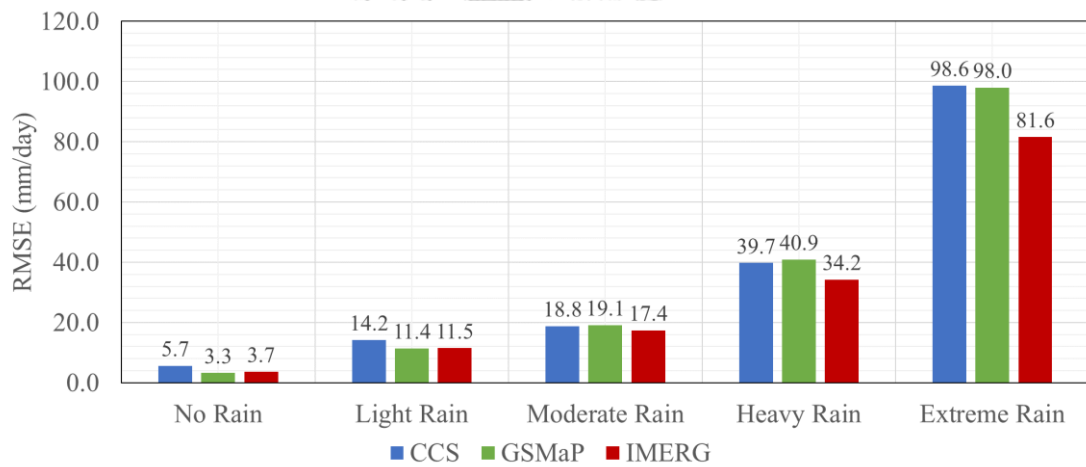
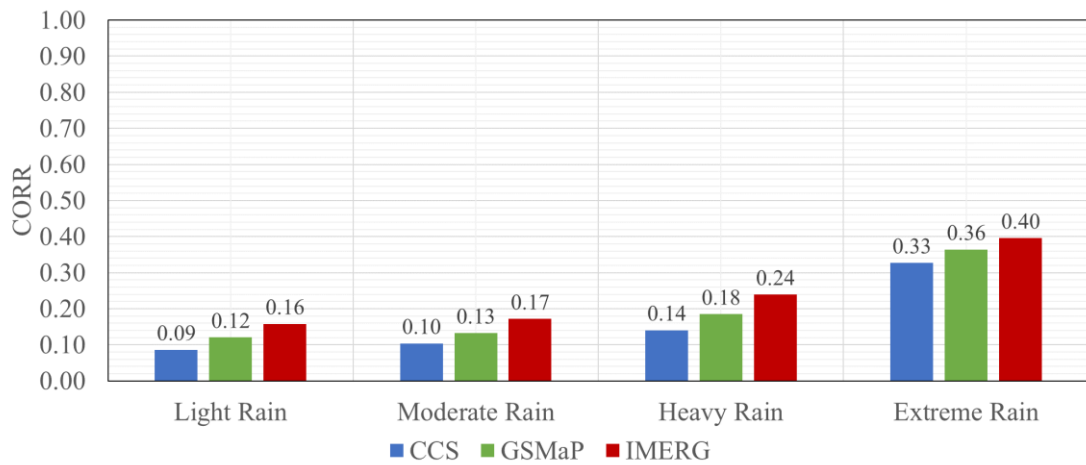


Figure 4-10. RMSE of Daily Rainfall by Intensity



*Figure 4-11. CORR of Daily Rainfall by Intensity*

#### 4.2.4. By Basin

Taking into account the spatial variability of rainfall over the country, the datasets have been separated and evaluated by basin. As shown in Figure 4-13, PERSIANN-CCS and IMERG Early show similar patterns; however, PERSIANN-CCS showed greater overestimation in the central and eastern region of the country. On the other hand, GSMaP\_NRT showed general underestimation in the northern, central, and eastern region of Thailand. However, the southern regions near the Gulf of Thailand showed overestimation as more rainfall occur in these areas. It is worth noting that the basin on the southwestern region of the country has generally been underestimated by all SPE products. Figure 4-14 show that all SPE product show lower RMSE in the northern half of the country but increases in value in the southern regions, especially near the oceans. Among the three SPEs, IMERG Early still show better performance as the colors of each basin tend to be lighter and greener which indicates lower errors. The similar pattern is observed in Figure 4-15 where CCS has worst performance in most basins IMERG Early showed better correlation in the northeast and southern basins.

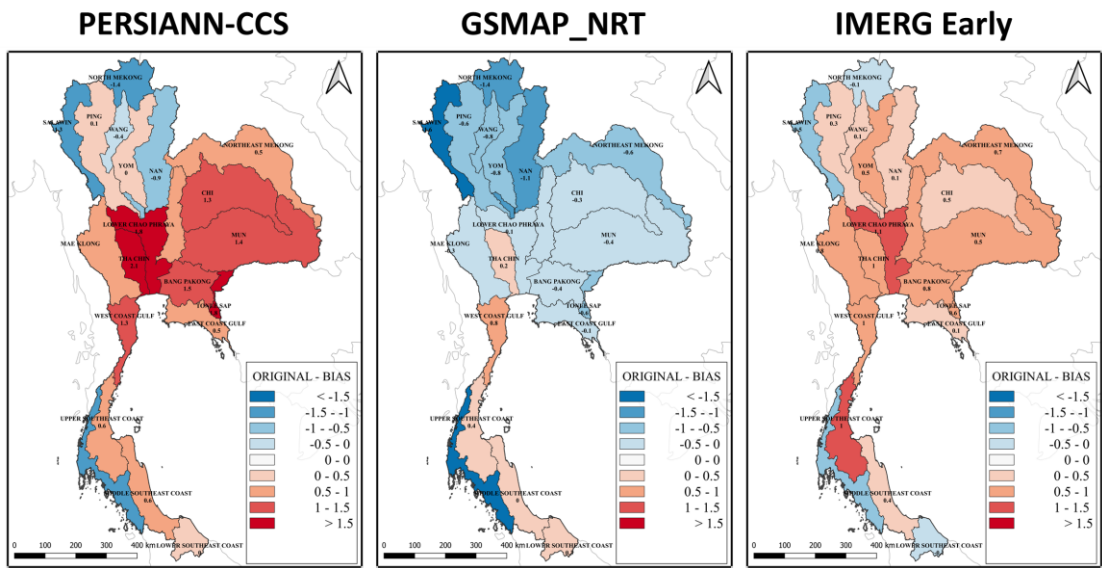


Figure 4-12. BIAS of Daily Rainfall by Basin

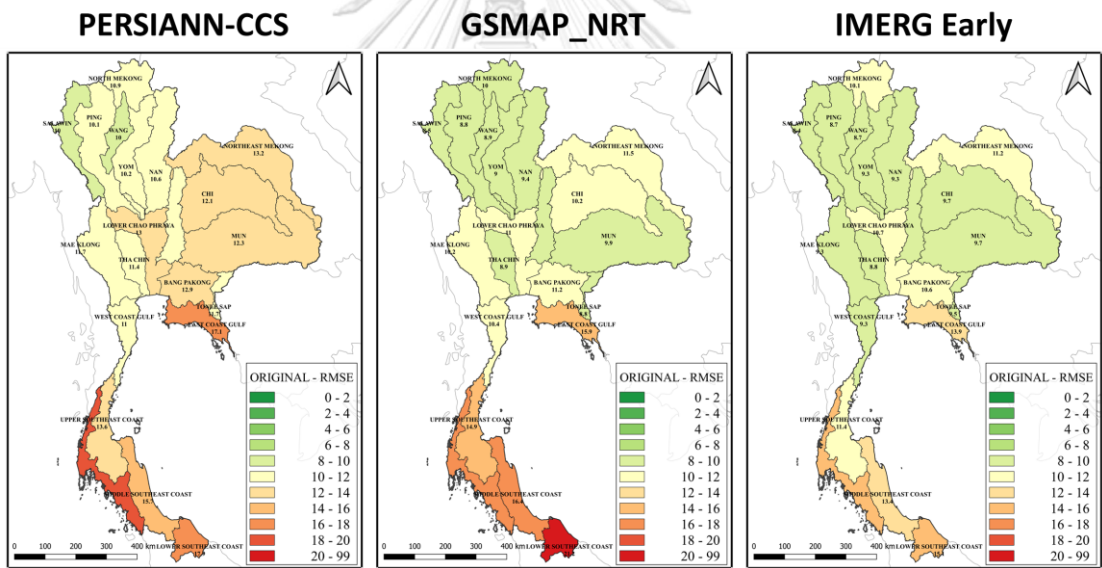


Figure 4-13. RMSE of Daily Rainfall by Basin



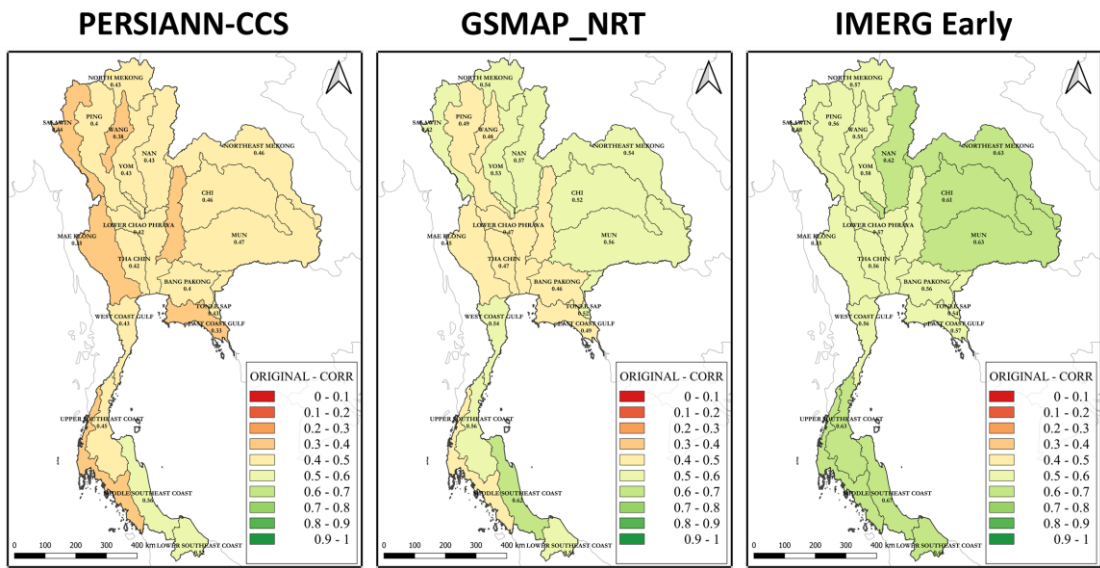


Figure 4-14. CORR of Daily Rainfall by Basin

### 4.3. Precipitation Detection Assessment

#### 4.3.1. Over Whole Study Area

Aside from quantitative statistics, categorical statistics have been applied to evaluate the detection skill of the satellite precipitation products. Table 4-1 lists the percentage of detections and the skill scores. Figure 4-16 shows the differences between the POD, FAR, and ETS of the three SPE datasets. PERSIANN-CCS produced the lowest POD among the three SPEs. This dataset is followed by GSMaP\_NRT and then by IMERG Early. IMERG Early shows an impressive score which is almost close to the optimal POD value of 1. However, this incredible score is pulled down by the relatively high FAR of IMERG Early. This result means that IMERG Early has a lot of false alarms which partially explains why it has a very high POD. Due to the SPE product predicting numerous counts of false alarms, there are only few values that would count as missing data which ultimately leads to higher POD scores. This can be confirmed with the ETS score of IMERG Early in which it resulted lower than

PERSIANN-CCS which had the smallest POD score among the three. In terms of daily precipitation detection, GSMaP\_NRT showed the best performance while the IMERG Early resulted as the worst.

*Table 4-4. Precipitation Categorical Statistics*

	<b>PERSIANN-CCS</b>	<b>GSMaP_NRT</b>	<b>IMERG Early</b>
Hits	26.4%	29.7%	34.4%
False Alarms	14.5%	14.9%	28.9%
Misses	9.6%	6.3%	1.6%
True Negative	49.5%	49.1%	35.1%
POD	0.73	0.82	0.95
FAR	0.35	0.33	0.46
ETS	0.33	0.39	0.28

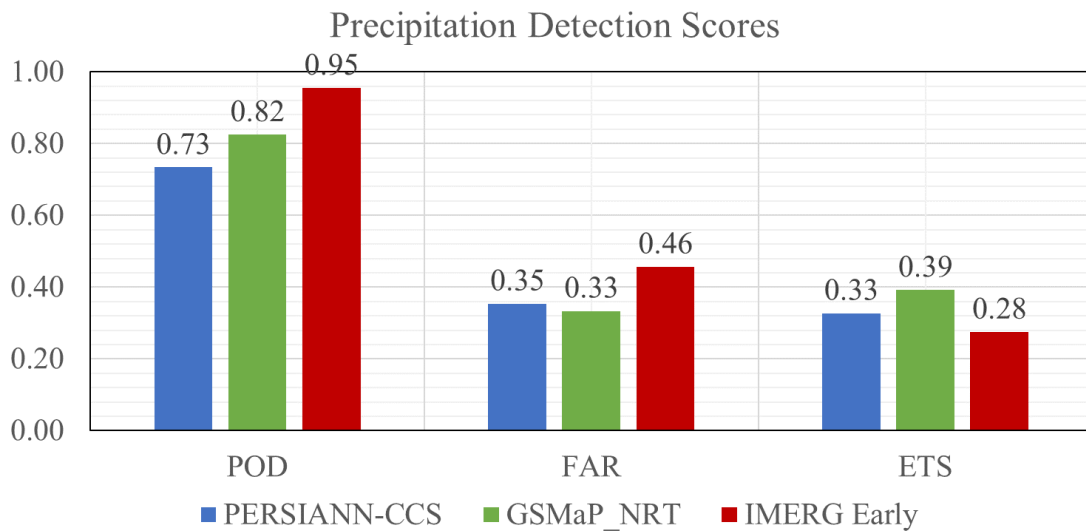


*Figure 4-15. Precipitation Detection Skill of SPE Products*

#### 4.3.2. By Month

When separated by month, all of the evaluated SPE product show the similar pattern of their detection skill scores. As shown in Figure 4-17, it is evident that the POD is lower during December to February but higher during March to November. Inversely, the FAR is higher from November to April and lower from May to October as observed in Figure 4-18. Moreover, similar to the overall daily detection skill,

IMERG Early still does not perform well as shown in the ETS values illustrated in

Figure 4-19. GSMaP\_NRT still showed the best detection skill among the three SPEs.

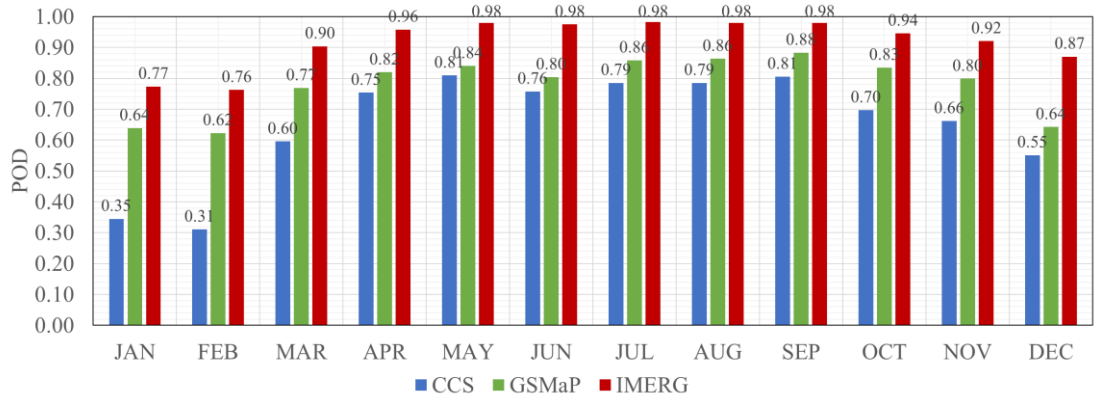


Figure 4-16. POD of Daily Rainfall per Month

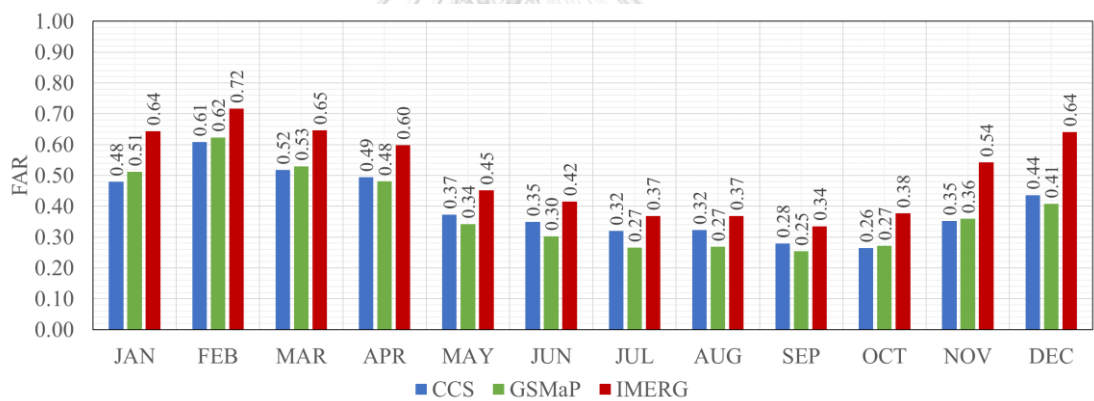


Figure 4-17. FAR of Daily Rainfall per Month

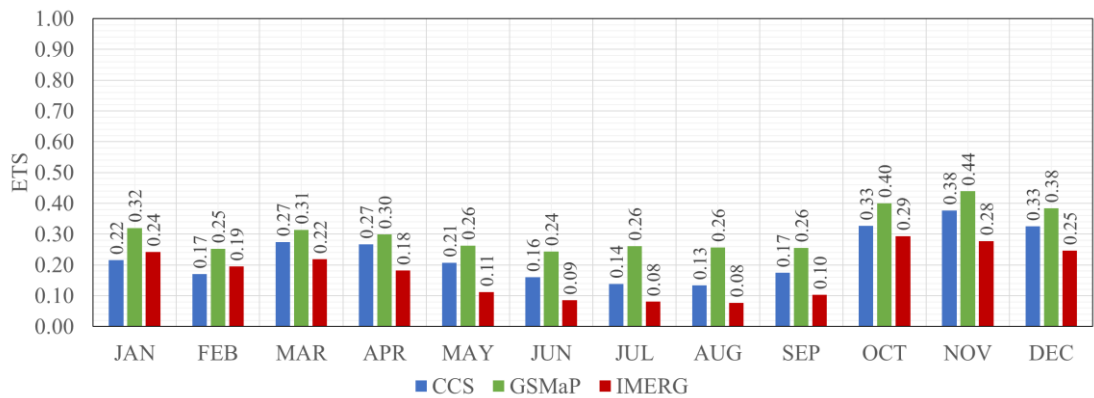


Figure 4-18. ETS of Daily Rainfall per Month

### 4.3.3. By Basin

In terms of spatial variation by basin, the detection skills still show the same pattern. As shown in Figure 4-20, the IMERG Early has high POD among the three, while GSMaP\_NRT has lower POD in the southern region of the country. The FAR of PERSIANN-CCS and GSMaP\_NRT is slightly similar to each other as illustrated in Figure 4-21. However, it is very evident that IMERG Early has worse FAR in most areas. Although all SPE product does not have a high detection skill score, GSMaP\_NRT still showed better results overall in ETS as shown in Figure 4-22.

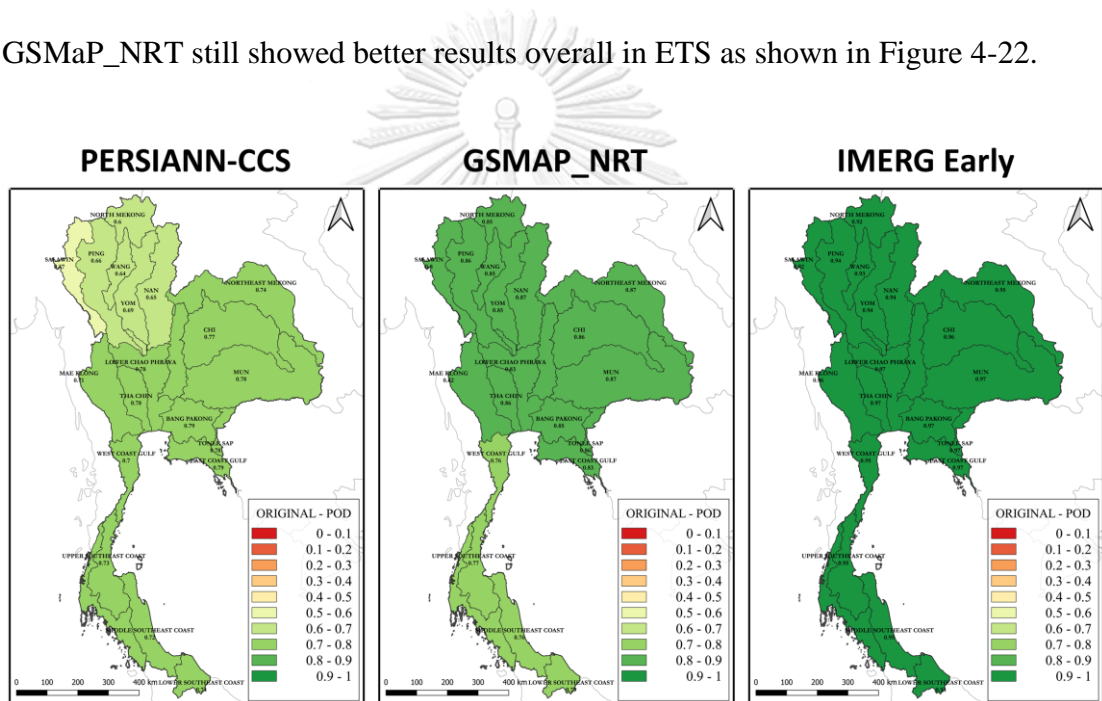


Figure 4-19. POD of Daily Rainfall per Basin

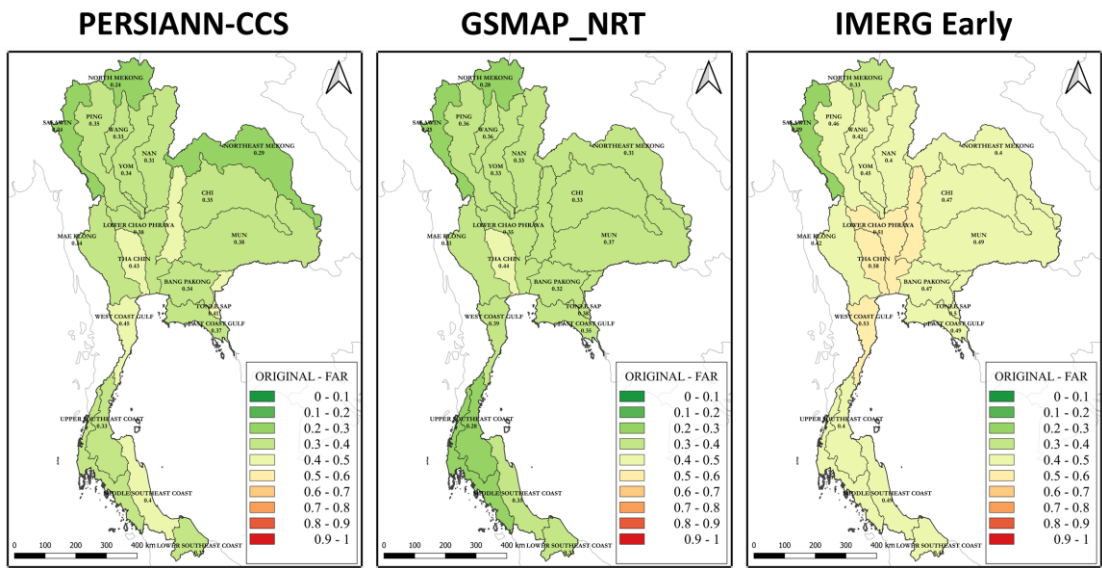


Figure 4-20. FAR of Daily Rainfall per Basin

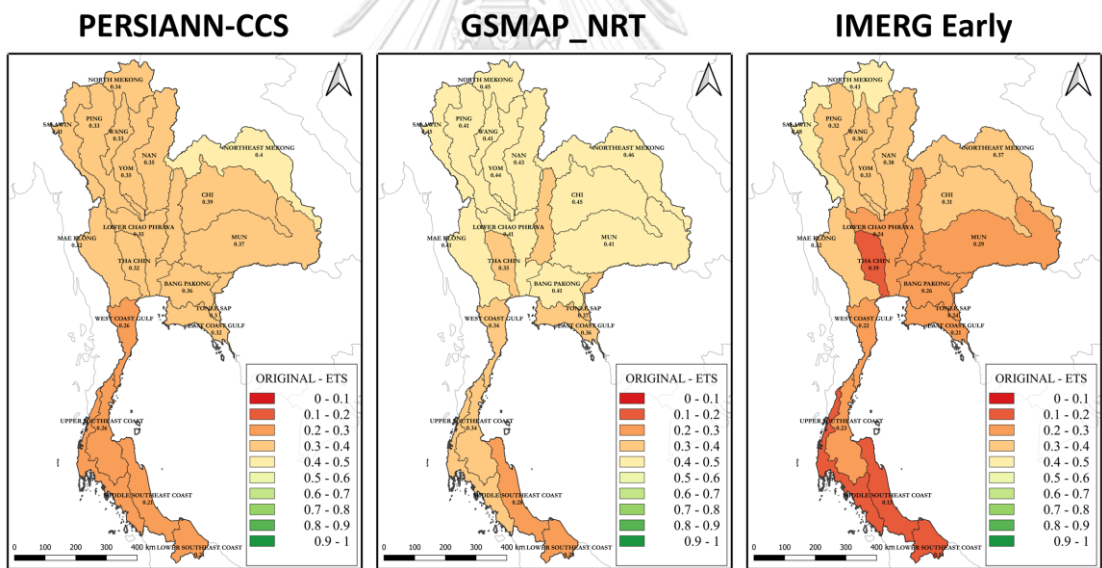


Figure 4-21. ETS of Daily Rainfall per Basin

#### 4.4. Summary of Evaluation

Each one of the three SPE products has its advantages and disadvantages. In addition, there are also some characteristics in the satellite data that are common to all. In all temporal scale, the precipitation at higher intensities are heavily underestimated as confirmed by separating the data by intensity. Furthermore, the satellite data shows

higher errors and lower correlations in the wet months. In terms of spatial variability, higher errors are located in areas near the shore. The similarity among these conditions is that higher rainfall occurs in these situations. However, it is worth noting that for the southern region of Thailand, the correlation coefficient values are higher even though stronger rainfall occurs in those areas. In terms of detection, both the POD and FAR is better during wet months. However, the ETS does not seem to improve during the wet season.

On the other hand, the differences between each SPE product are more noticeable. Both PERSIAN-CCS and IMERG Early tend to overestimate rainfall in any time scale while GSMaP\_NRT has a tendency to underestimate precipitation. The difference between PERSIANN-CCS and IMERG Early is that the latter shows the best performance in terms of quantitative statistics. IMERG Early fall short in its daily precipitation detection where there are large amounts of false alarms. This result shows that IMERG Early has the worst detection skill in terms of ETS. In considering the best performing unadjusted SPE dataset, the purpose of selection should be carefully considered in order to properly utilize the best dataset for the situation. In terms of RMSE, IMERG Early is the best performing satellite precipitation product. If detection skill is considered, GSMaP\_NRT has the best skill score among the three. In any case, the evaluated SPE products still contain errors that should be adjusted which would be covered in the next section.

## **CHAPTER 5**

### **BIAS CORRECTION OF SATELLITE PRECIPITATION ESTIMATES**

As explained in the methodology, there are three bias correction methods that would be applied to the three SPE products evaluated in the previous section. These methods are the scaling, quantile mapping (QM), and artificial neural network (ANN) bias correction approaches. The scaling bias correction method utilizes a Time-Space Varied (TSV) scaling factor in consideration of the spatiotemporal variability present in SPE products. In the case of the QM and ANN bias correction, the observed precipitation gauge measurements would be corrected according to within each of the 21 river basins considered in the study area to account for spatial variations.

#### **5.1. Calibration**

Each bias correction method has its own way in calibrating its model. The scaling bias correction uses the ratio of the mean of the satellite and gauge rainfall values as the bias factor. The QM approach creates a cumulative distribution function (CDF) from both the satellite and gauge data. The values of the bias factors and the produced CDF are included in the appendix. The ANN method uses the calibration dataset to train the neural network. From initial trials using IMERG Early, it was shown that the value of the RMSE does not change significantly with additional nodes in this setup. However, it is noticeable that the time of computation increases further with more nodes as shown in Figure 5-1. In the case of this study, the total number of nodes within the hidden layer would be set at 8 nodes.

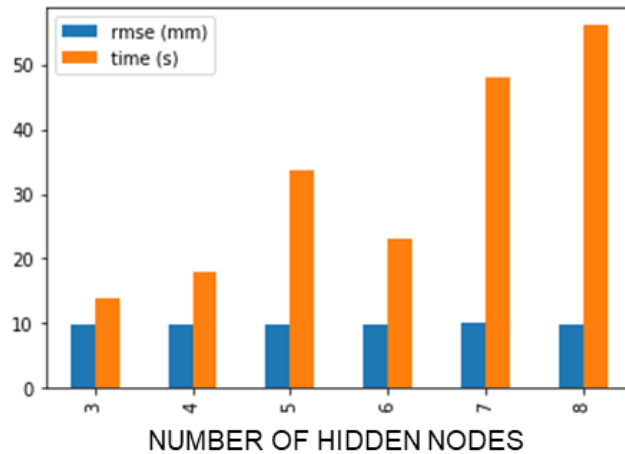


Figure 5-1. Results of Initial ANN trials using varying number of hidden nodes

However, all of these methods aim to reduce the bias of the target dataset to a value almost or equal to zero as shown in Figure 5-2. In order to determine the performance of each bias correction, the main parameter to be used would be the resulting RMSE.

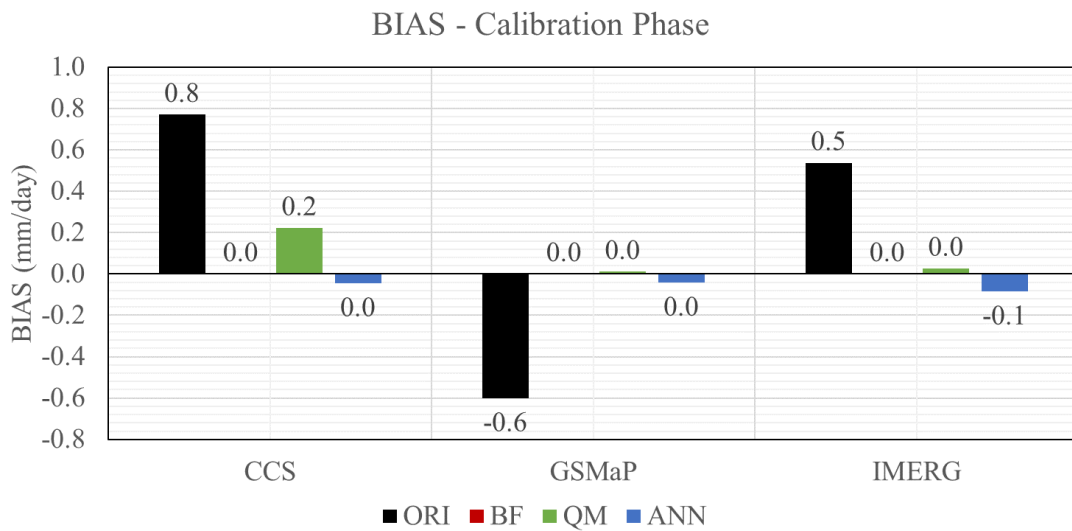


Figure 5-2. BIAS of Original and Adjusted SPE Products - Calibration

As shown in Figure 5-3, the resulting RMSE for each method and each SPE product varies from each other. Both PERSIANN-CCS and IMERG Early show that their RMSE is reduced after applying the scaling and ANN corrections while their



RMSE slightly increases after the QM bias correction was utilized. On the other hand, the RMSE of GSMaP\_NRT slightly increased after being adjusted through the scaling and QM approaches. Only the ANN bias correction effectively lowered the RMSE of all three SPE products.

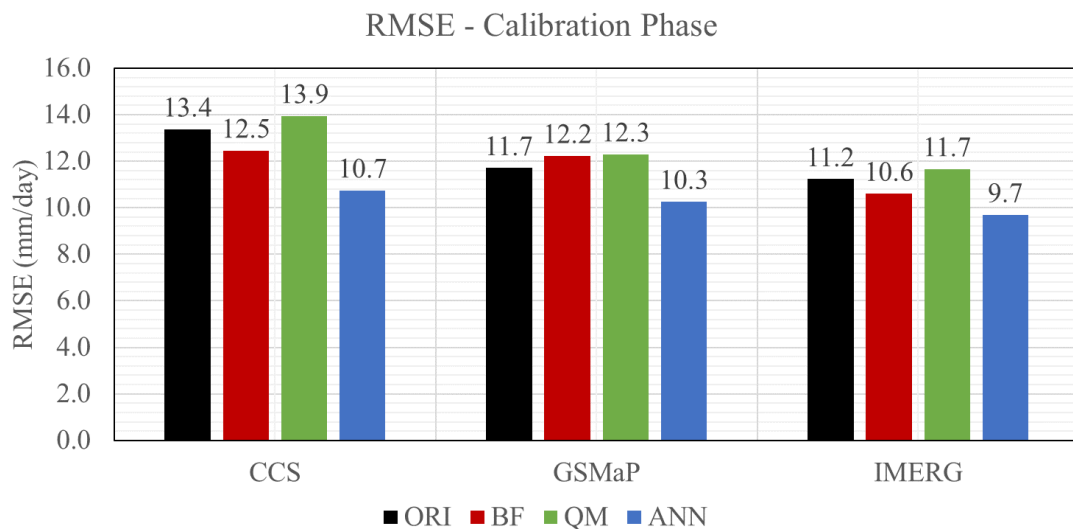
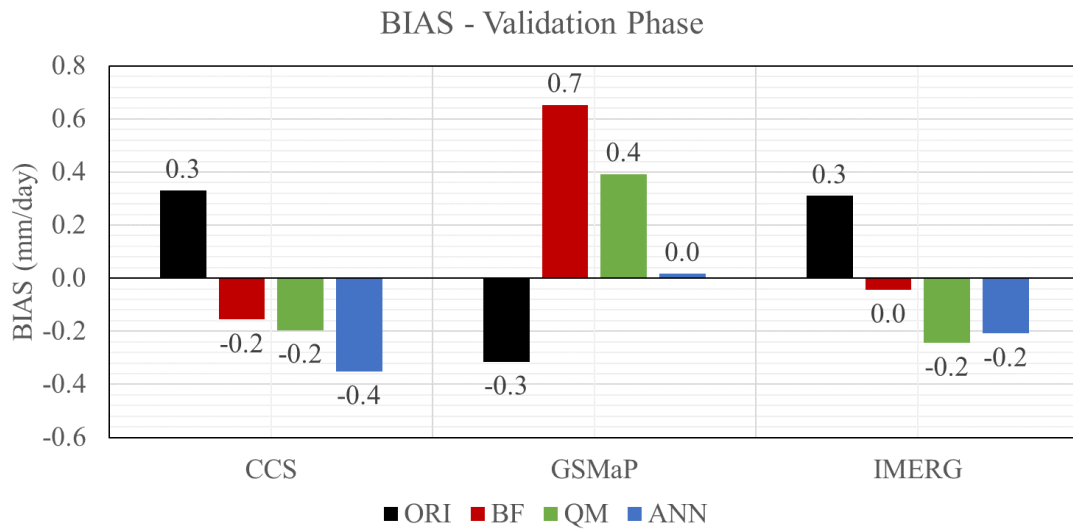


Figure 5-3. RMSE of Original and Adjusted SPE Products - Calibration

## 5.2. Validation

As for the validation phase, the resulting BIAS values for each adjusted SPE are no longer close to or equal to the value of zero as shown in Figure 5-4. In addition, the PERSIANN-CCS and IMERG Early, which are originally overestimated, resulted in slight underestimation after bias correction. Conversely, the GSMaP\_NRT, which originally underestimated the gauge observations, showed overestimation after correction. However, it is worth noting that the bias of GSMaP\_NRT after applying the ANN bias correction is almost equal to zero which indicates good performance.



*Figure 5-4. BIAS of Original and Adjusted SPE Products - Validation*

In terms of RMSE, it is evident in Figure 5-5 that the results are slightly the same as the calibration phase. The adjusted PERSIANN-CCS shows the same pattern; however, it is evident that the scaling correction only lowers the RMSE slightly. As for the GSMaP\_NRT, the resulting RMSE greatly increased after the scaling adjustment. In addition, the IMERG Early also shows increased RMSE after the scaling correction in the validation phase. For all three SPE products, the scaling correction shows higher errors in the validation phase than the calibration phase. As for the QM scaling, it seems that the method does not significantly improve the resulting RMSE for all SPE products. On the other hand, it is still evident that the ANN bias correction consistently lowered the RMSE of the satellite data.

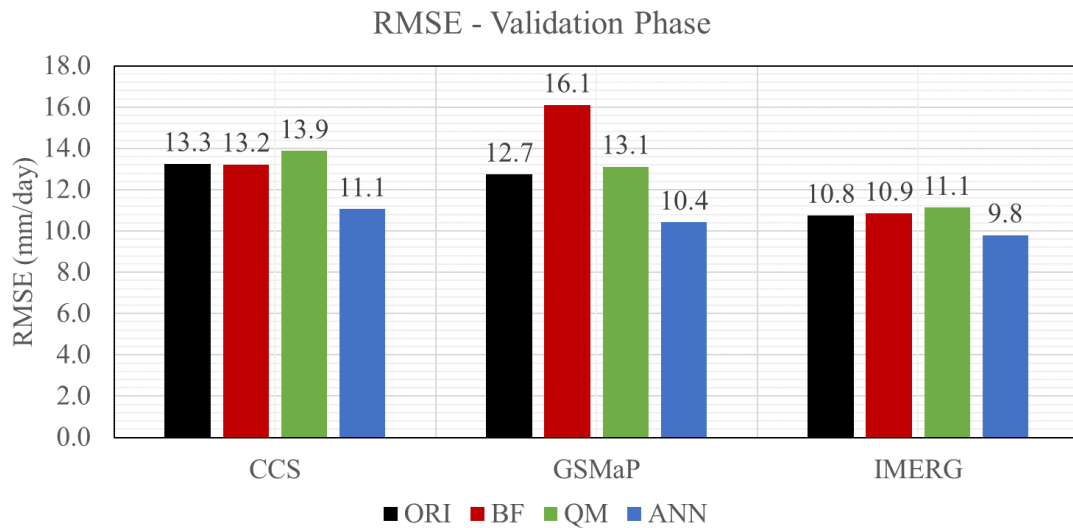


*Figure 5-5. RMSE of Original and Adjusted SPE Products - Validation*

### 5.3. Comparison of Bias Corrected SPE Products

#### 5.3.1. Annual and Monthly Precipitation Patterns

The improvements of bias correction methods can be easily observed in higher timescales. Figure 5-6 illustrates the scatterplot for the both the original and adjusted SPE products in terms of annual timescale. The most noticeable change in pattern for the adjusted annual rainfall of PERSIANN-CCS is that the spread of the data has been reduced in which the cloud of points is closer to the 1:1 line in comparison to the original data. This change is evident in all of the bias correction method; however, the ANN bias correction for PERSIANN-CCS stands out from the other two methods because the annual rainfall of higher intensities is shown to be closer each other even though they are still underestimated. As for the GSMaP\_NRT, the data points have been slightly shifted upwards for all bias correction methods. This result shows that the underestimation of GSMaP\_NRT has been reduced overall. However, after applying the scaling bias correction, the adjusted GSMaP\_NRT appears to have more overestimated values especially in the higher intensities. On the other hand, the ANN

correction still showed underestimation of the stronger annual rainfall. The QM adjustment scheme seem to have the most consistent slope for the data among the three correction methods. Since the IMERG Early already had a better scatterplot than the other two original SPE products, the most notable improvement is that the data has been shifted downwards to address the overestimation of the original dataset. Furthermore, it is worth noting that the scaling and QM bias correction improved the annual rainfall values in the higher intensities in which the ANN still show underestimation of these rainfall values.

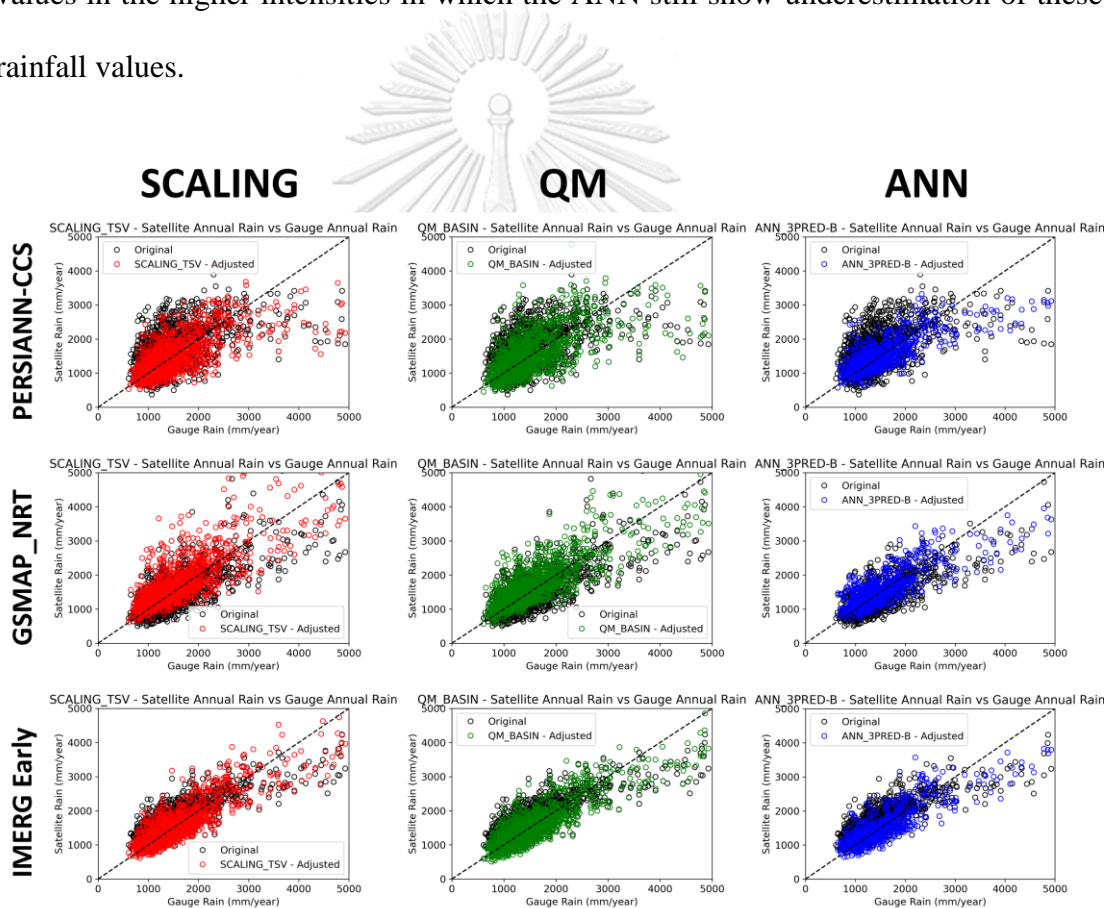


Figure 5-6. Annual Rainfall Scatterplot of Adjusted SPE Products

Furthermore, as shown in Figure 5-7, the biases for the annual rainfall of both PERSIANN-CCS and IMERG Early in all cases shows significant reductions. On the other hand, the bias of the adjusted GSMaP\_NRT only after applying the ANN bias

correction method as the scaling and the QM corrections resulted in great overestimation. However, except for the annual GSMaP\_NRT rainfall adjusted by scaling, all of the cases resulted in reduced errors in the annual timescale as shown in Figure 5-8. The increased error brought by the scaling bias correction to the GSMaP\_NRT could be attributed to the original SPE being underestimated. Since the scaling adjustment scheme would increase rainfall values to reduce the bias, rainfall values that are already high would be transformed into larger numbers. Regardless, the correlation between the annual satellite and gauge rainfall values did not decrease as illustrated in Figure 5-9. Among the three adjusted SPE, the IMERG Early still resulted in the least RMSE for the annual timescale. The RMSE values for the adjusted IMERG Early datasets are close to each other but the scaling adjusted data resulted in the lowest value.

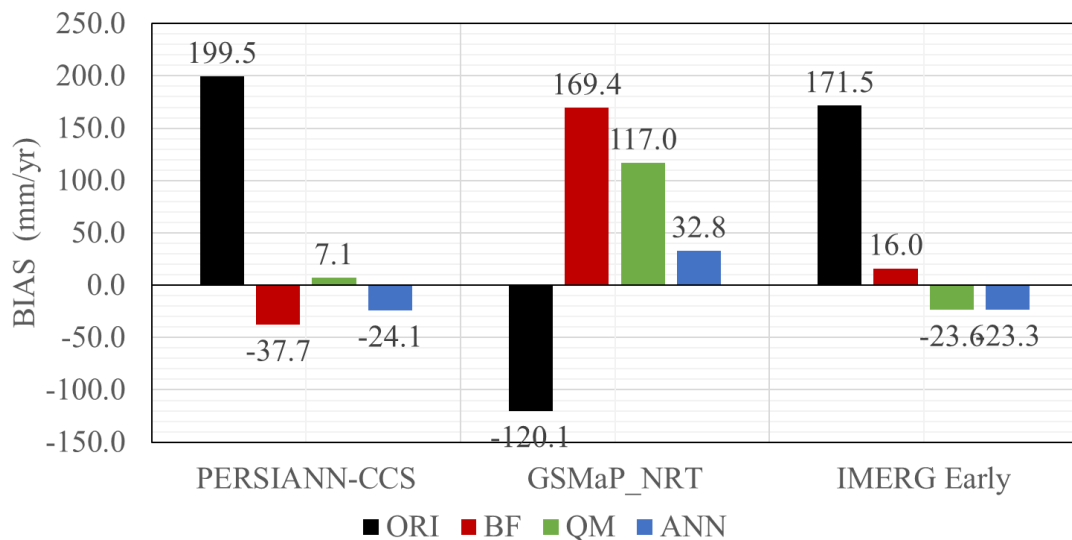


Figure 5-7. BIAS of Adjusted SPE Products Annual Rainfall

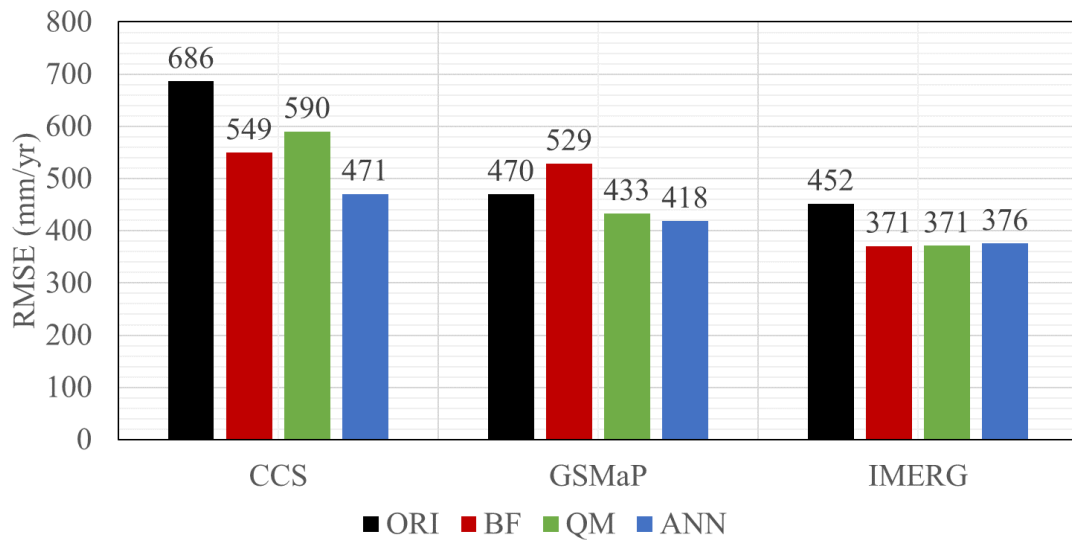


Figure 5-8. RMSE of Adjusted SPE Products Annual Rainfall

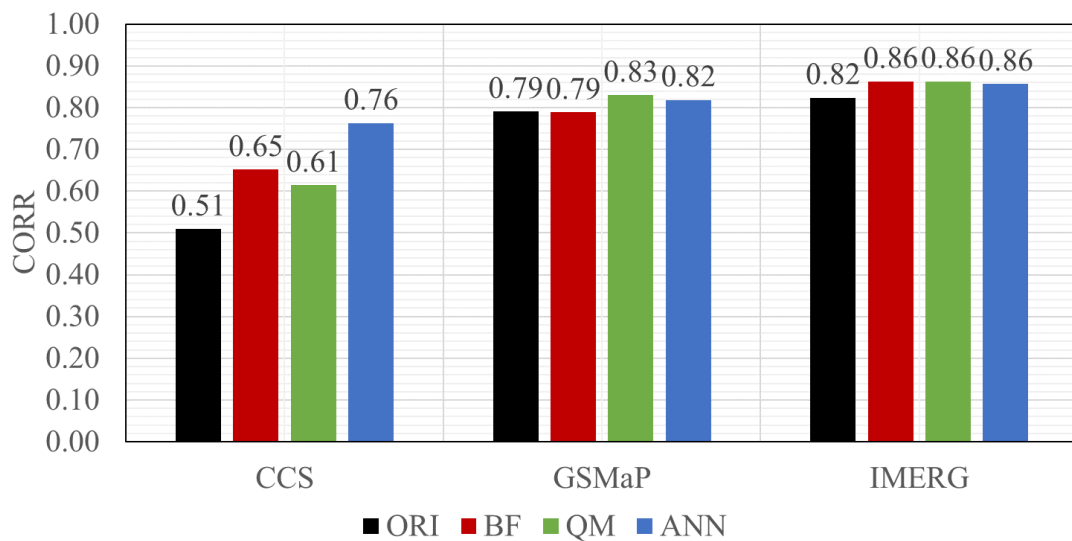


Figure 5-9. CORR of Adjusted SPE Products Annual Rainfall

Proceeding to a finer temporal scale, Figure 5-10 shows the monthly rainfall scatterplot for all three SPE products before and after correction. PERSIANN-CCS shows higher spread of data and higher overestimation in some data points after applying the scaling and QM bias correction. In addition, after the ANN adjustment, the corrected PERSIANN-CCS not only showed less overestimation in lower intensities

but also caused consistent underestimation of higher monthly rainfall values. The pattern after the bias correction seems to be consistent for all SPE products.

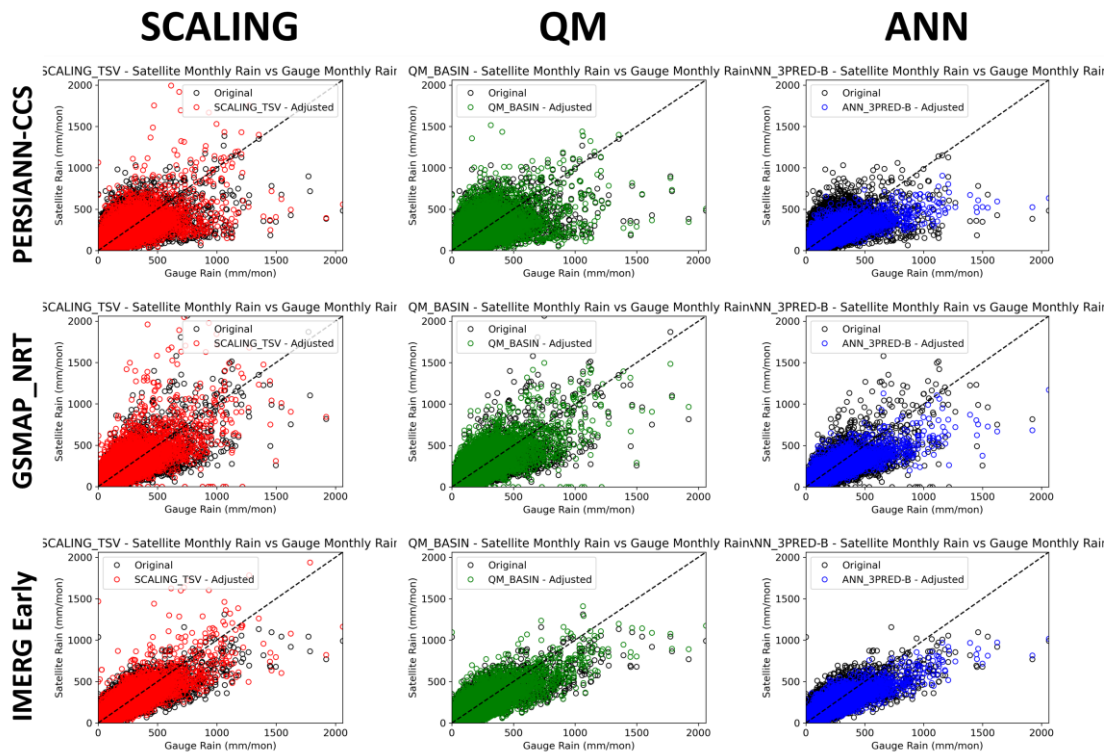


Figure 5-10. Monthly Rainfall Scatterplot of Adjusted SPE Products

As for the quantitative statistics, the pattern of the adjusted bias in the monthly timescale is similar to the annual rainfall cases as shown in Figure 5-11. The main difference is evident in the RMSE as illustrated in Figure 5-12. Unlike in the annual timescale, the RMSE for the QM adjusted datasets is higher as their values are close to the original monthly RMSE. As for the scaling correction, it still increased the resulting error value for the GSMaP\_NRT. On the other hand, the ANN bias correction resulted in the lowest overall error for all three SPE products with adjusted IMERG Early dataset having the least RMSE. However, in Figure 5-13, it is shown that the ANN adjustment

scheme slightly decreased the correlation of the adjusted GSMaP\_NRT and IMERG to the gauge.

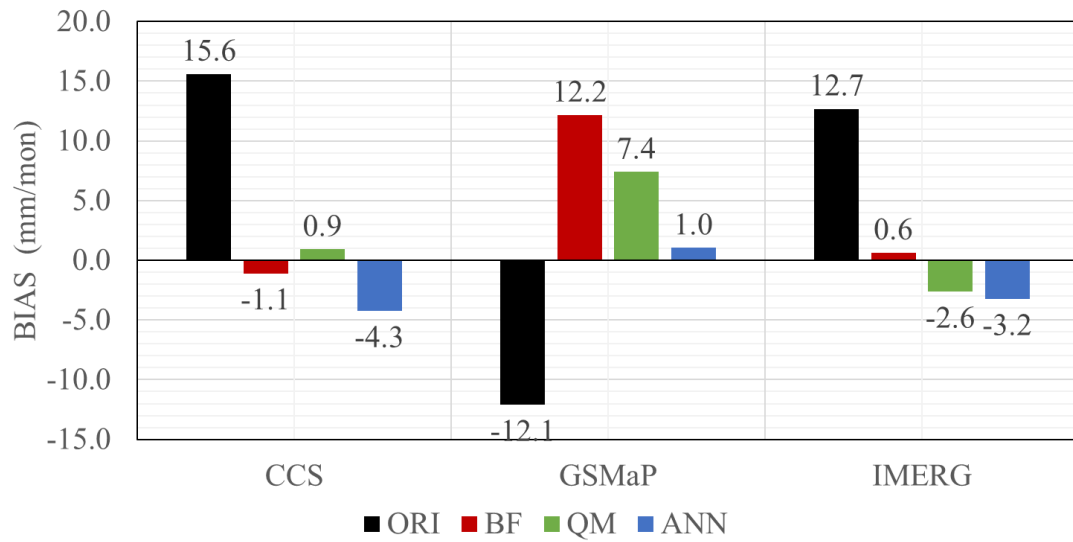


Figure 5-11. BIAS of Adjusted SPE Products Monthly Rainfall

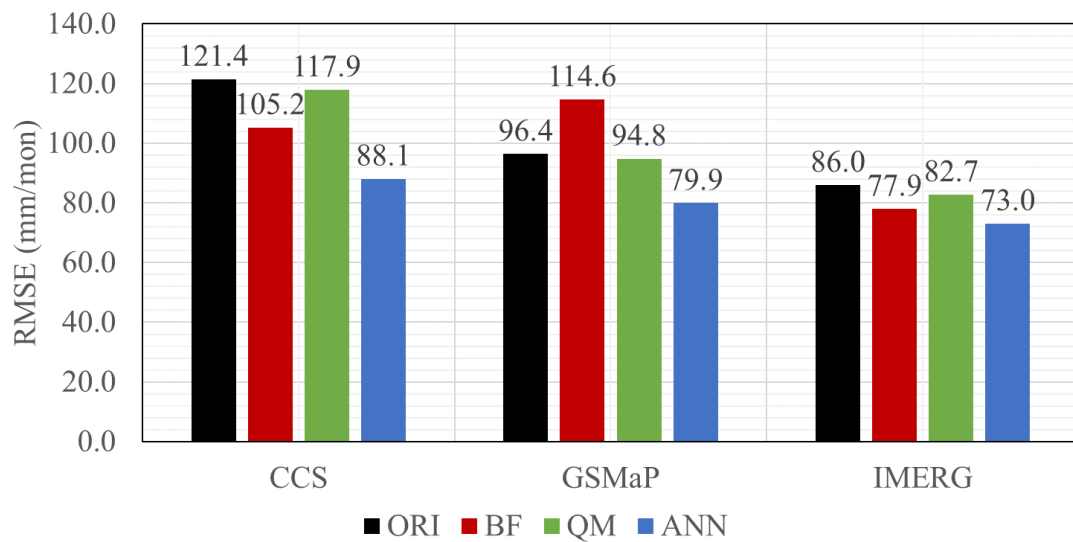
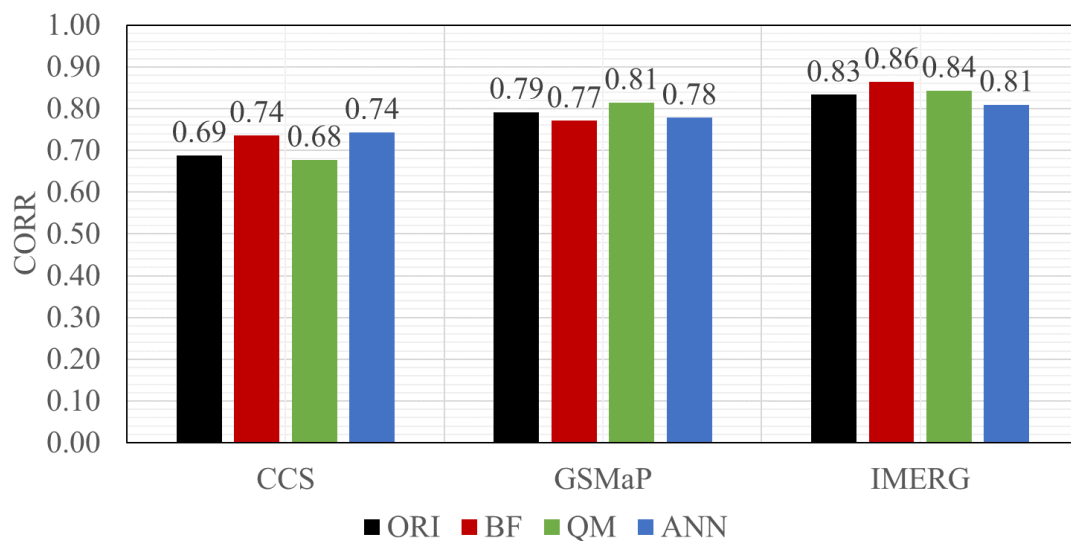


Figure 5-12. RMSE of Adjusted SPE Products Monthly Rainfall





*Figure 5-13. CORR of Adjusted SPE Products Monthly Rainfall*

As for the monthly rainfall pattern in each year, Figure 5-14, Figure 5-15, and Figure 5-16 depicts the yearly accumulated average monthly rainfall for PERSIANN-CCS, GSMaP\_NRT, and IMERG Early respectively. The monthly rainfall for all three SPEs seems to align significantly closer to the gauge observations after applying the ANN correction scheme in years where the differences between the three methods are more noticeable. However, in most cases, the three methods performed almost similarly.

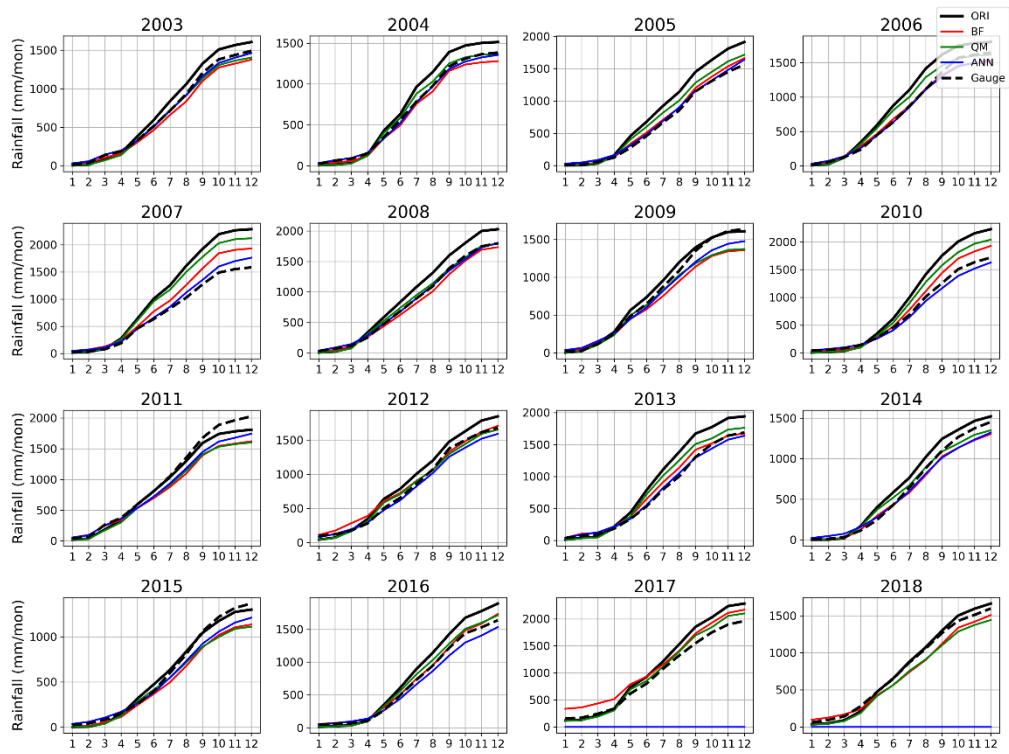


Figure 5-14. Monthly Rainfall Timeseries in each year for Adjusted PERSIANN-CCS

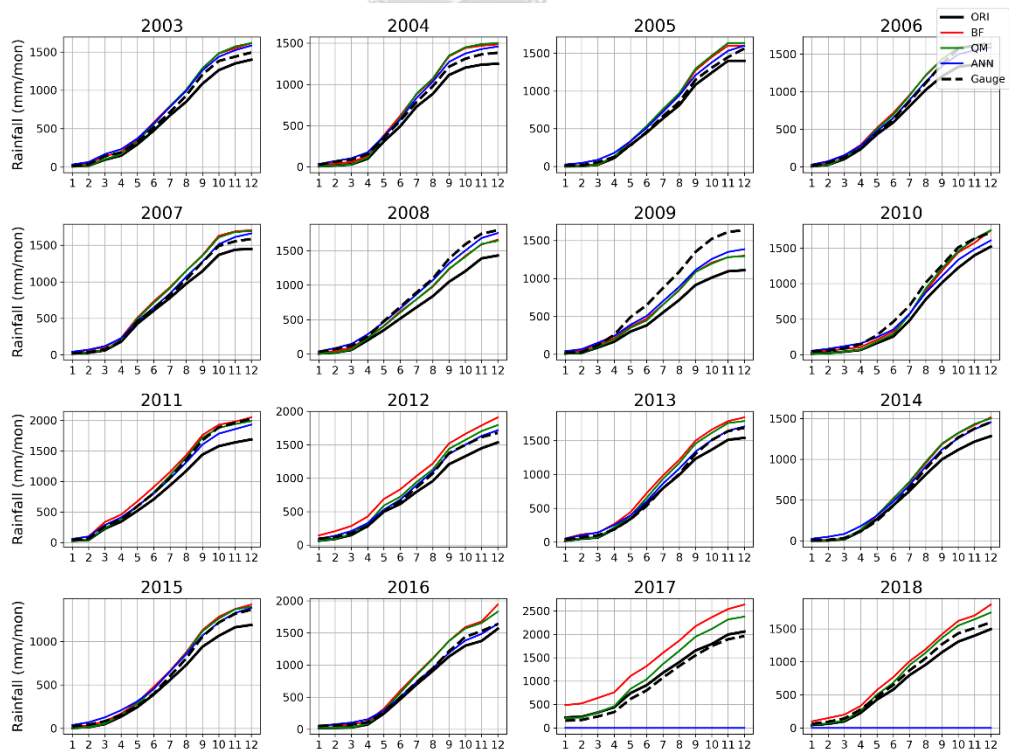


Figure 5-15. Monthly Rainfall Timeseries in each year for Adjusted GSMaP\_NRT

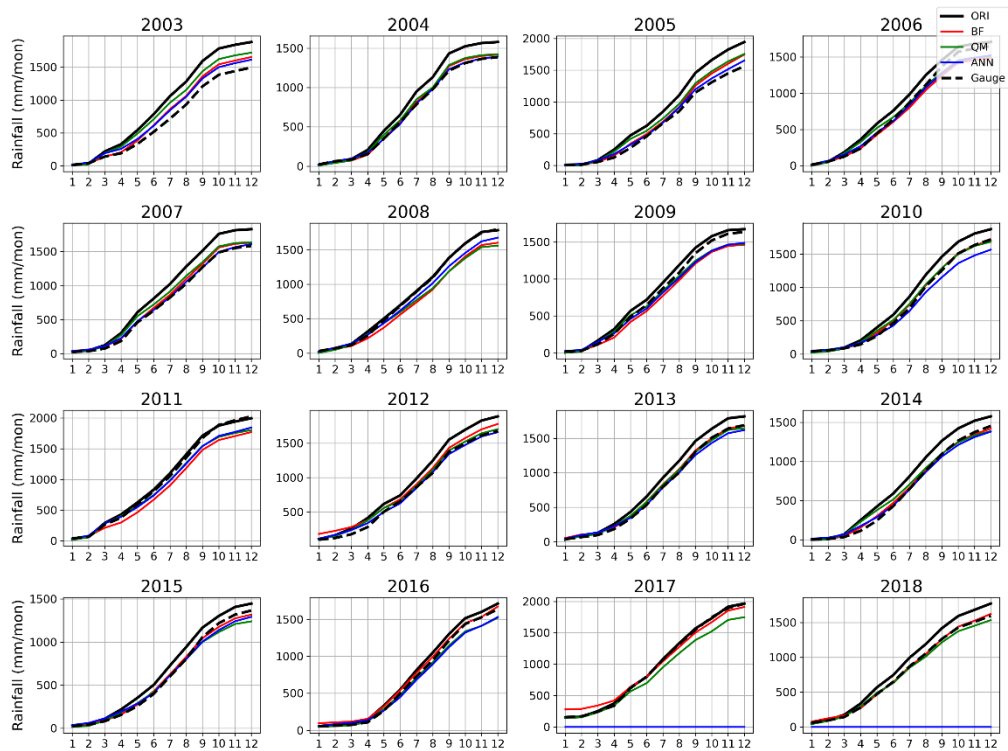


Figure 5-16. Monthly Rainfall Timeseries in each year for Adjusted IMERG Early

### 5.3.2. Daily Precipitation and Detection Skill Analysis

In terms of the daily timescale, Figure 5-17 illustrates the scatterplot of the three SPE products with each bias correction method. The scaling and QM adjusted datasets became slightly more spread out after the correction which resulted in some rainfall values being overestimated further. This pattern is more evident in the case of applying scaling correction to GSMaP\_NRT. Similar to the annual and monthly timescale, this result could be attributed from the original GSMaP\_NRT being generally underestimated which further increased the values for high rainfall estimates. As for the ANN adjusted PERSIANN-CCS, the data points seem to be lowered. This result reduced the overestimation of the lower intensities; however, it increased the underestimation of the rainfall in higher intensities. Furthermore, this pattern after applying ANN bias correction shows similarities with the GSMaP\_NRT and IMERG

Early. In terms of the resulting bias, the pattern for the daily rainfall resembles the one from the annual and monthly timescales as shown in Figure 5-18. Overall, the originally overestimated SPE products become slightly underestimated and originally underestimated become slightly overestimated respectively. However, as shown in Figure 5-19, the adjusted results vary from the higher timescales. Notably, the QM bias correction slightly increased the errors for all three SPE products. However, the scaling adjusted GSMaP\_NRT still has significantly increased RMSE overall which may be attributed to the underestimation of the original SPE product. In addition, all of the ANN adjusted product still showed lower RMSE than their original versions. In terms of the daily rainfall, the ANN adjusted IMERG Early has the least errors among the all cases. Furthermore, among the three SPE products, IMERG Early consistently had the highest correlation values as shown in Figure 5-20.

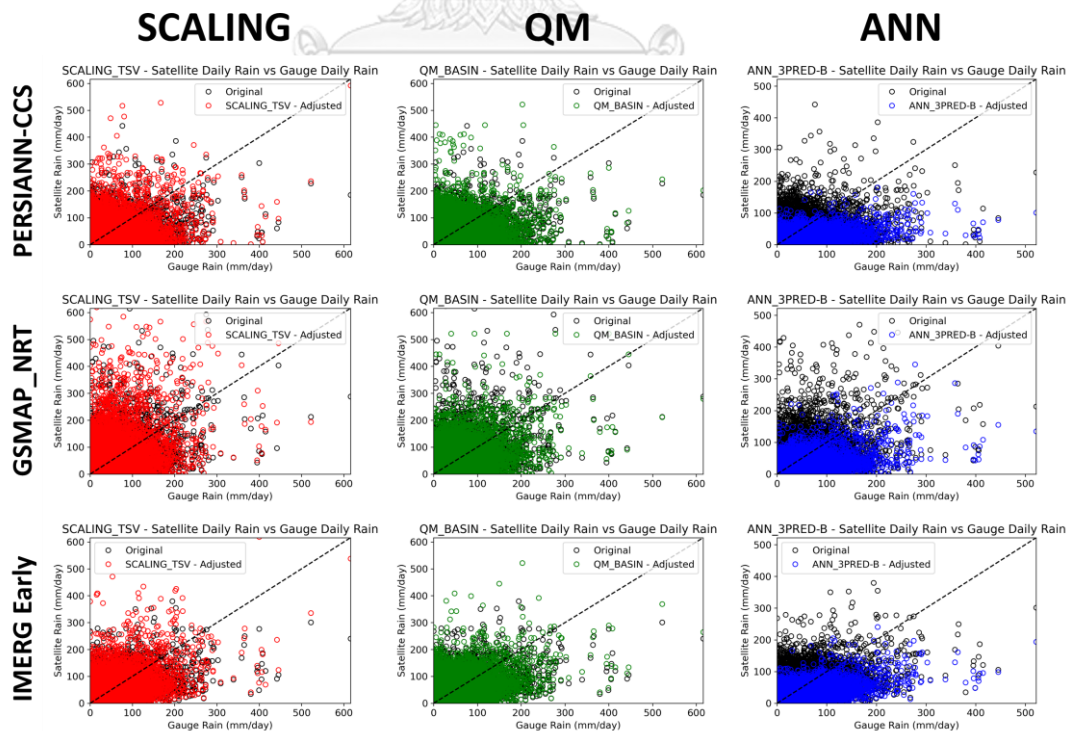


Figure 5-17. Daily Rainfall Scatterplot of Adjusted SPE Products

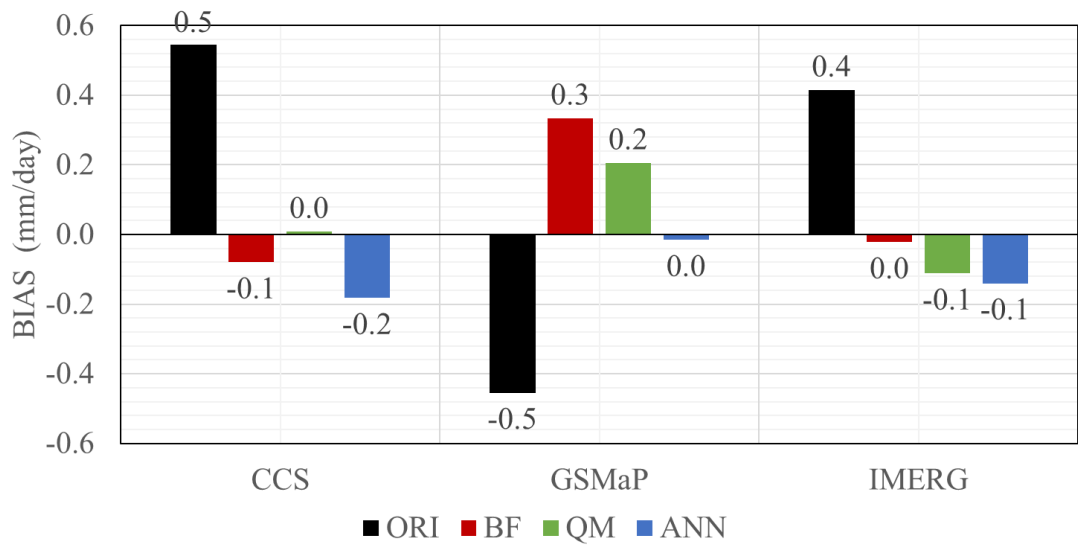


Figure 5-18. BIAS of Adjusted SPE Products Daily Rainfall

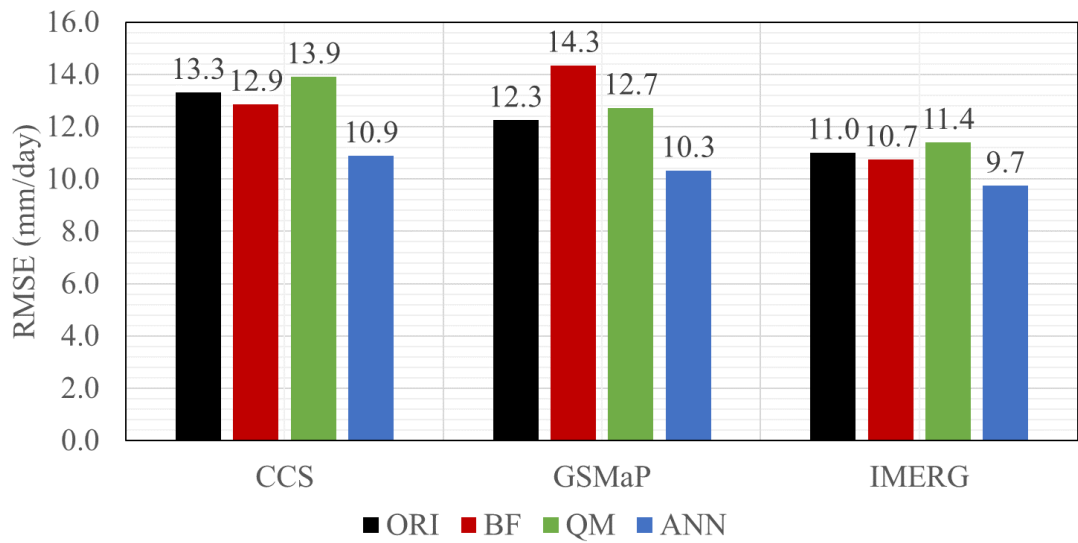
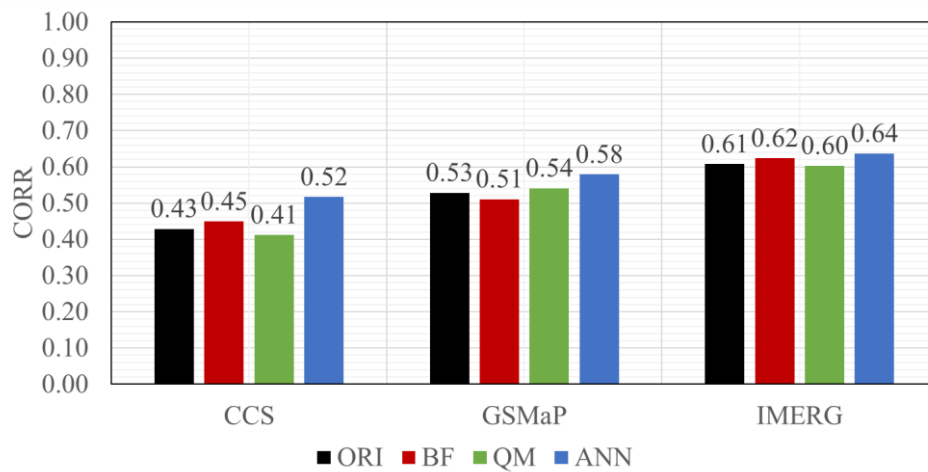


Figure 5-19. RMSE of Adjusted SPE Products Daily Rainfall



*Figure 5-20. CORR of Adjusted SPE Products Daily Rainfall*

As for detection, only QM and ANN bias correction methods can adjust zero to non-zero values and vice-versa. The scaling bias correction cannot adjust the detection skill because of its multiplicative nature. Figure 5-21 and Figure 5-22 shows that the ANN bias correction method increased the POD and FAR of PERSIANN-CCS and GSMaP\_NRT but slightly reduced both for IMERG Early which originally already had higher values. On the other hand, the QM bias correction reduced the POD and FAR for GSMaP\_NRT and IMERG Early. This result can be attributed from the QM method itself where if the satellite CDF may convert the satellite rainfall value to zero if the gauge CDF value of zero is higher than the satellite. Therefore, anything less than that satellite rainfall value would be converted to zero, resulting in decreased POD and/or decreased FAR. Conversely, if the gauge CDF value of zero is lower than the satellite, the adjusted satellite value of zero would be transformed to the corresponding non-zero value. This scenario results in increased FAR and/or POD which is evident with the QM adjusted PERSIANN-CCS. Because mispredictions are weighed more in ETS, it is evident that the skill scores of SPE products that had increased FAR were significantly reduced as shown in Figure 5-23. These results are apparent with both QM

and ANN adjusted PERSIANN-CCS as well as with the ANN adjusted GSMaP\_NRT. On the other hand, the ETS of both QM adjusted GSMaP\_NRT, QM adjusted IMERG Early, and ANN adjusted Early increased due to the reduction of their respective FAR. Among the bias corrections, the QM adjustment scheme has the best potential in improving the detection skill of the SPE products.

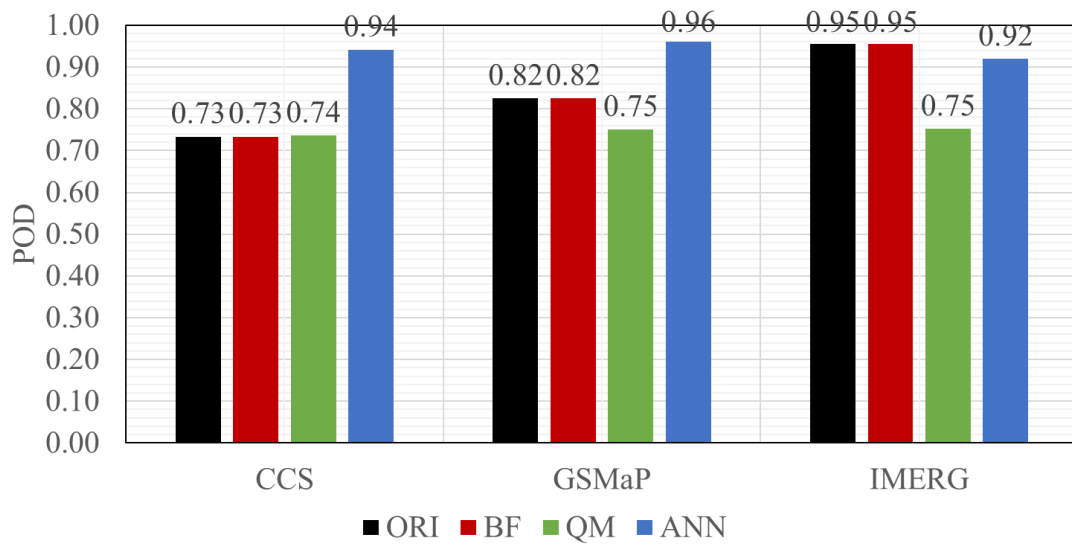


Figure 5-21. POD of Adjusted SPE Products Daily Rainfall

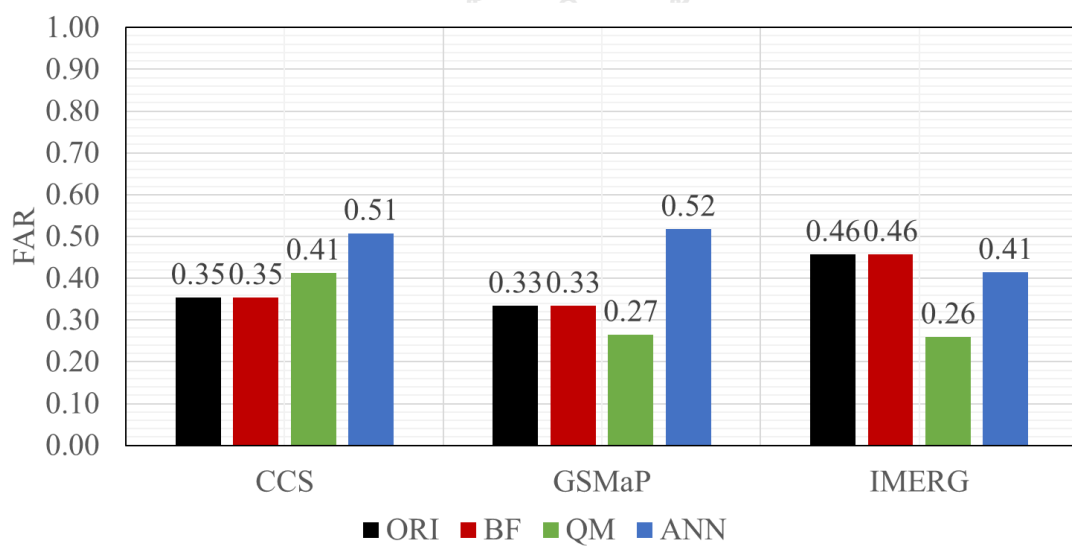


Figure 5-22. FAR of Adjusted SPE Products Daily Rainfall



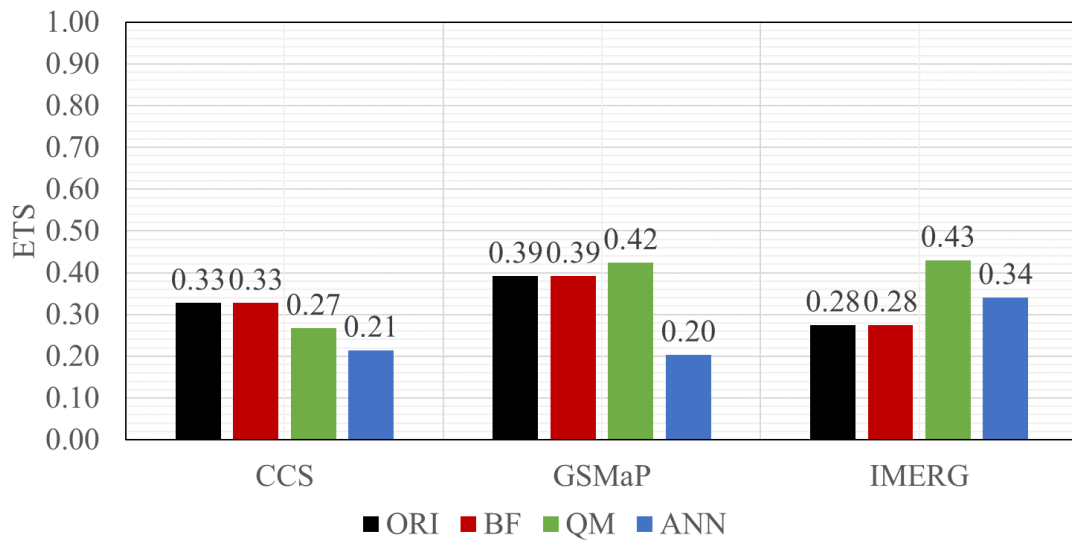


Figure 5-23. ETS of Adjusted SPE Products Daily Rainfall

### 5.3.3. Precipitation and Detection Analysis by Month

Figure 5-24 shows the bias by month of each case of PERSIANN-CCS. The scaling correction of this SPE product significantly reduced the bias by each month and result in slight overestimation in dry months and slight underestimation wet months. This outcome is possible with scaling because monthly variations were considered in the bias correction method. Similarly, the ANN bias correction shows the same pattern; however, the underestimation is noticeably greater especially in the month of September. On the other hand, the QM correction resulted in general underestimation except for April, May, June, and November. Moreover, among the three methods, the ANN bias correction resulted in the least RMSE over all months as shown in Figure 5-25. Similarly, majority of the months have slightly higher correlation after applying the ANN bias correction as illustrated in Figure 5-26. The disadvantage of ANN can be seen again in the detection skill of the adjusted SPE product as shown in Figure 5-27 and Figure 5-28. Although the POD has been increased, the FAR of the adjusted SPE products also increased. This outcome significantly lowers the ETS as observed in



Figure 5-29. Therefore, applying the scaling correction to PERSIANN-CCS could be the option if the main concern for the correction is maintaining an acceptable skill score.

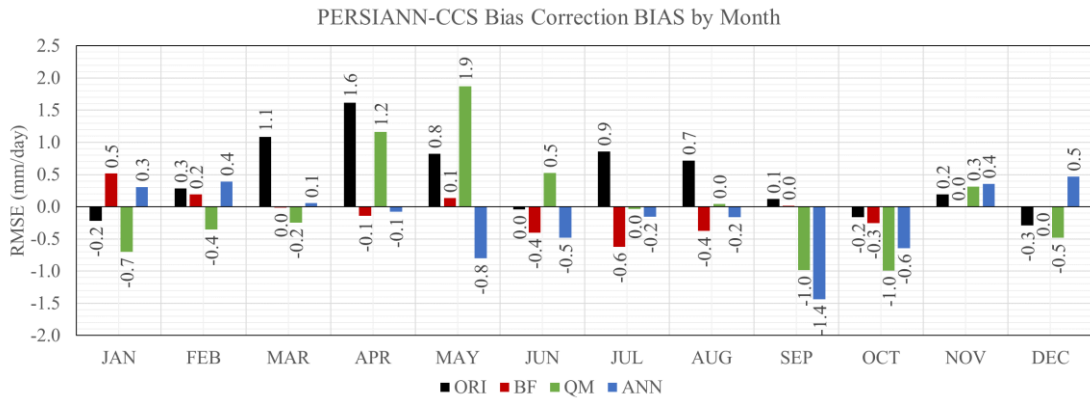


Figure 5-24. BIAS of Adjusted PERSIANN-CCS Daily Rainfall by Month

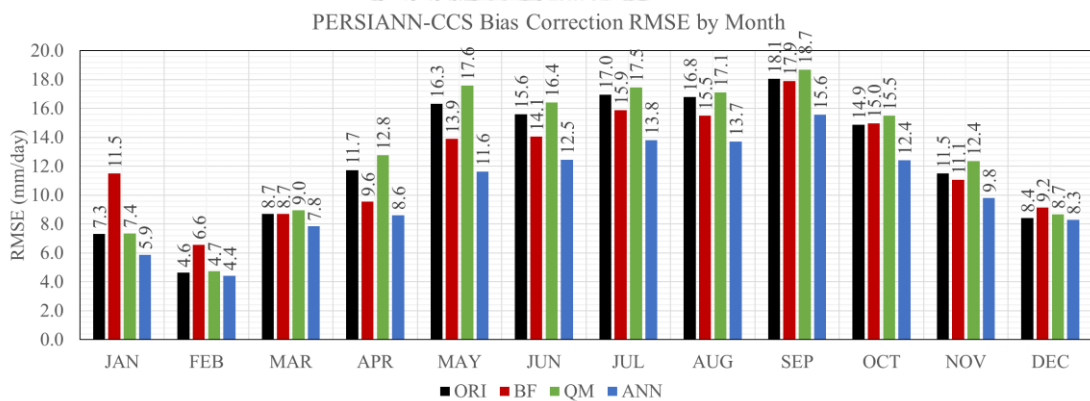


Figure 5-25. RMSE of Adjusted PERSIANN-CCS Daily Rainfall by Month

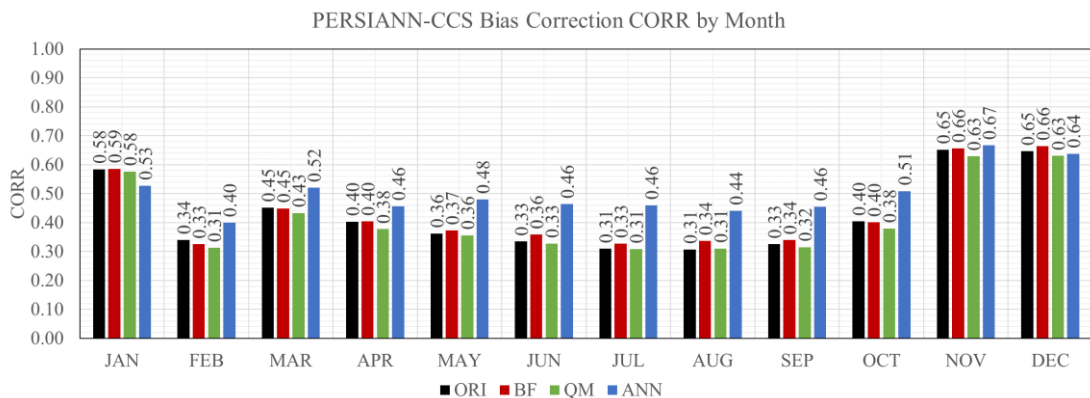


Figure 5-26. CORR of Adjusted PERSIANN-CCS Daily Rainfall by Month

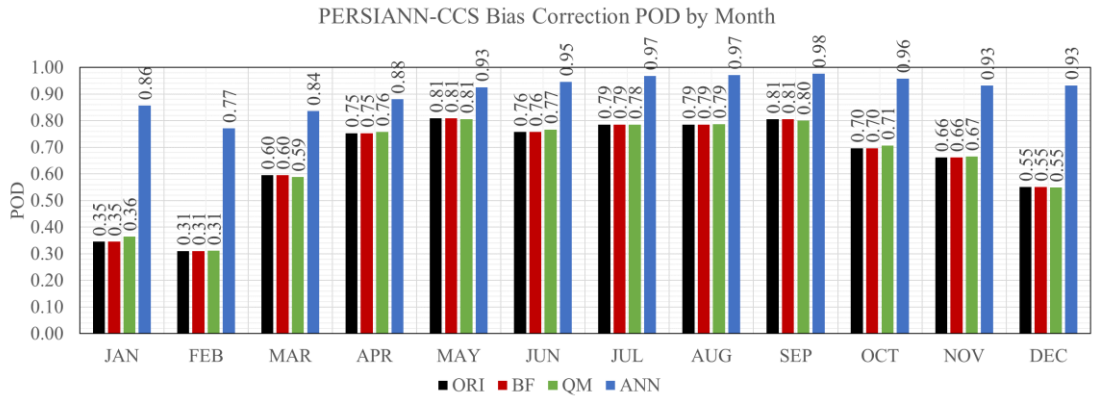


Figure 5-27. POD of Adjusted PERSIANN-CCS Daily Rainfall by Month

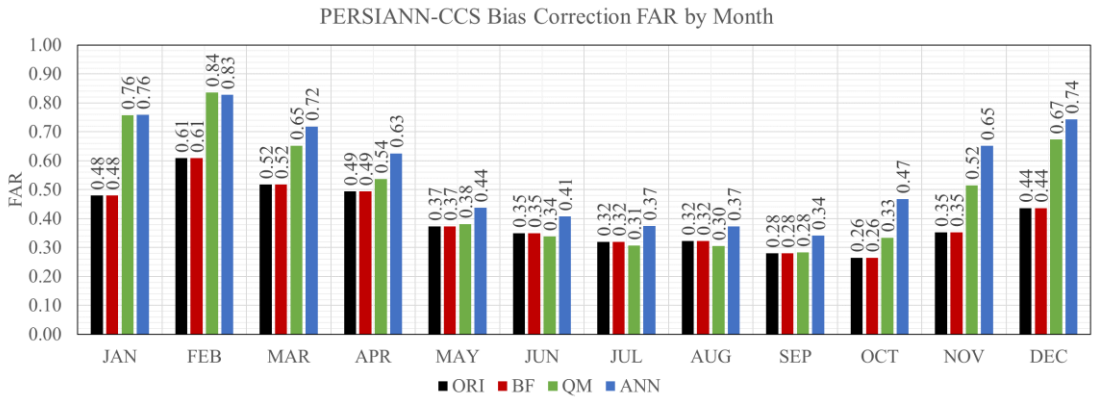


Figure 5-28. FAR of Adjusted PERSIANN-CCS Daily Rainfall by Month

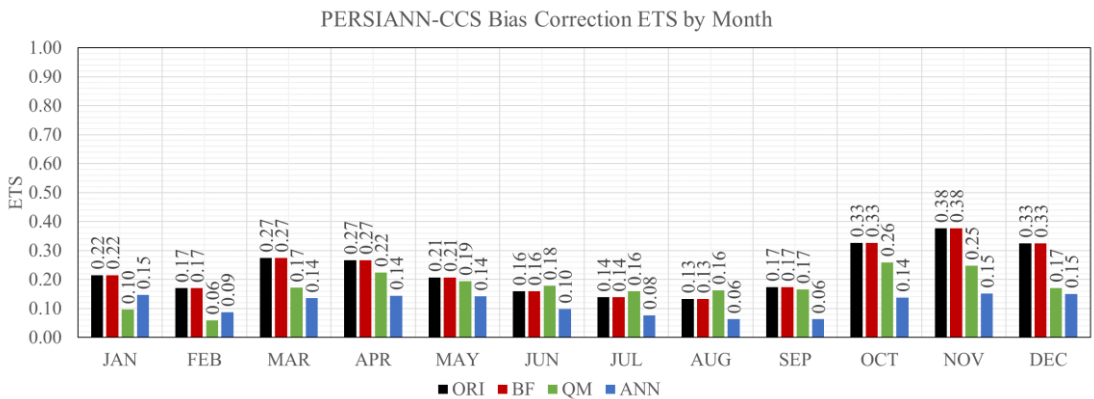


Figure 5-29. ETS of Adjusted PERSIANN-CCS Daily Rainfall by Month

As for the scaling adjusted GSMaP\_NRT, the correction resulted in general overestimation of rainfall throughout the whole year except October as shown in Figure

5-30. This result supports the reason why the GSMaP\_NRT performed poorly after applying scaling correction. The QM adjusted GSMaP\_NRT still shows the same underestimation in dry months; however, the wet months tend to be overestimated. Inversely, the ANN adjusted GSMaP\_NRT follows the same pattern with the PERSIANN-CCS where dry months are overestimated and wet months show underestimation. Because daily rainfall is generally underestimated in the months of December and January, it can be observed from Figure 5-31 that the scaling correction greatly increased the RMSE for these months. Similar to PERSIANN-CCS, the ANN bias correction still produces the least RMSE over all of the months as illustrated in Figure 5-32. Moreover, Figure 5-33 shows increased correlation after applying ANN correction. In terms of detection, the patterns are similar to the overall results of GSMaP\_NRT in which QM reduces while ANN increases both POD and FAR for all months as shown in Figure 5-34 and Figure 5-35. These outcomes are reflected in the ETS as illustrated in Figure where ANN shows lower scores while QM resulted in slightly higher values.

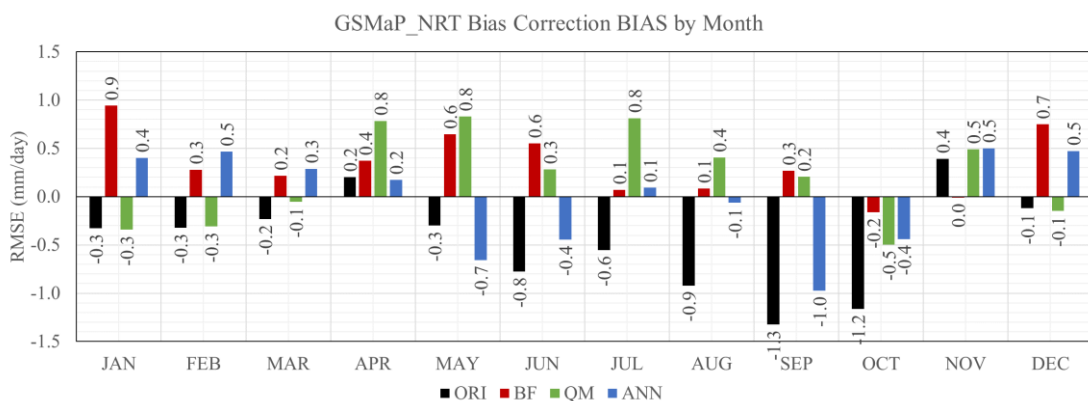


Figure 5-30. BIAS of Adjusted GSMaP\_NRT Daily Rainfall by Month

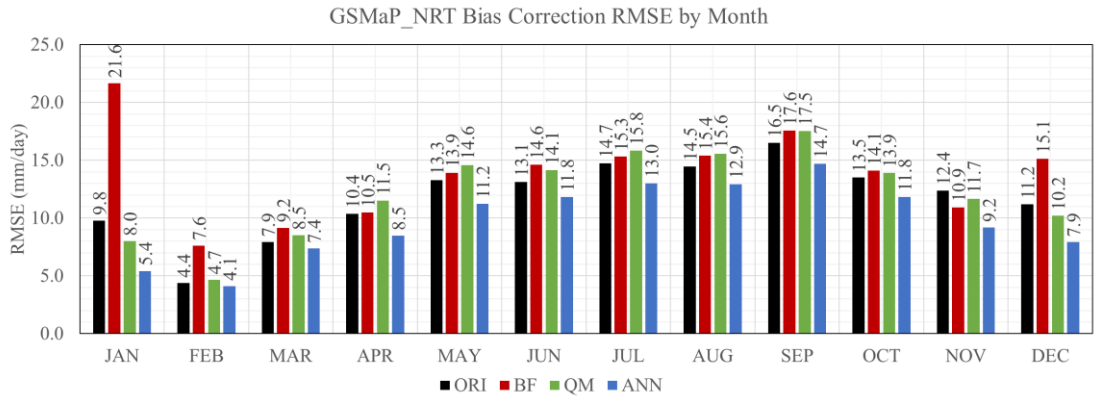


Figure 5-31. RMSE of Adjusted GSMaP\_NRT Daily Rainfall by Month

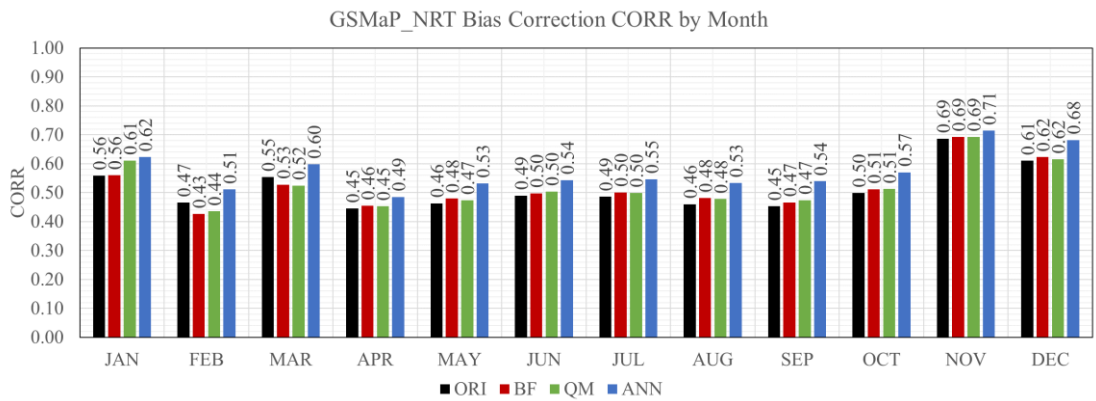


Figure 5-32. CORR of Adjusted GSMaP\_NRT Daily Rainfall by Month

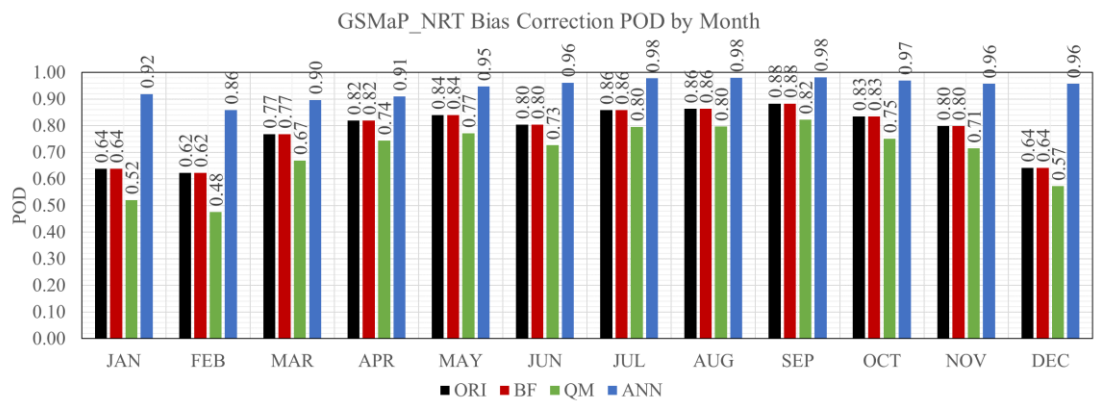


Figure 5-33. POD of Adjusted GSMaP\_NRT Daily Rainfall by Month

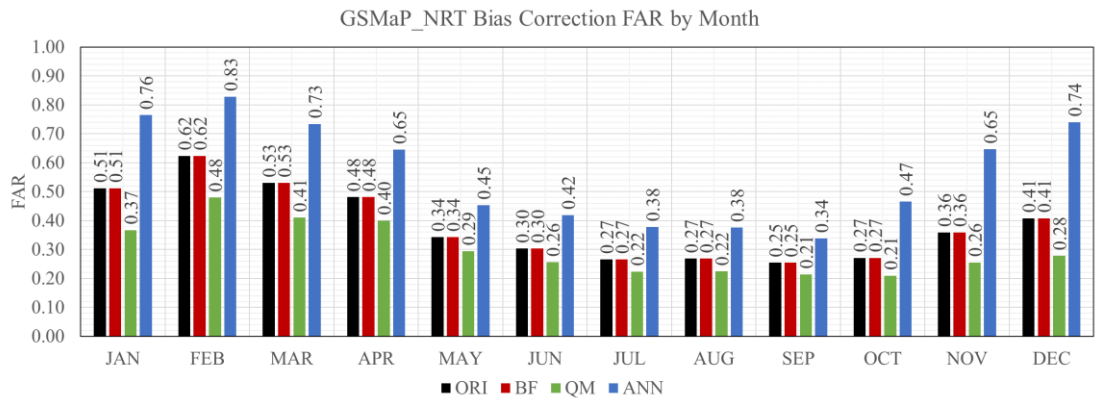


Figure 5-34. FAR of Adjusted GSMaP\_NRT Daily Rainfall by Month

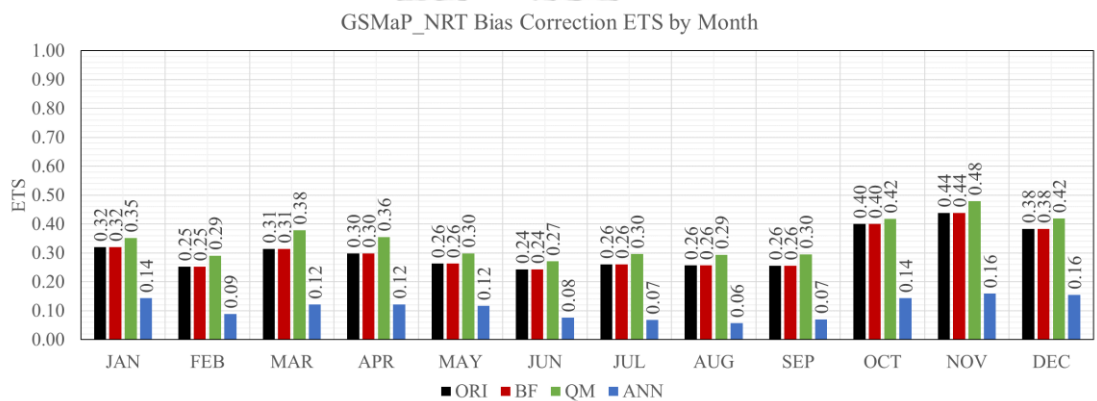


Figure 5-35. ETS of Adjusted GSMaP\_NRT Daily Rainfall by Month

In terms of bias, the results for IMERG Early is slightly similar to PERSIANN-CCS as shown in Figure 5-36. The scaling correction adjusted the bias into slightly overestimating daily rainfall from November to February while having slight underestimation during the rest of the year. The QM bias correction shows underestimation in majority of the months but overestimates in the months of February to April. The ANN bias correction resulted in lower biases but the underestimation is more evident in the months of May, Jun, September, and October. Similar to both PERSIANN-CCS and GSMaP\_NRT, Figure 5-37 illustrates that the ANN bias correction resulted in the least RMSE in each month throughout the year. As for the

correlation, except January, the ANN bias correction has the highest value every month as shown in Figure 5-38. Because IMERG Early already has a high POD and high FAR, the QM and ANN bias correction methods were able to improve the ETS each month by lowering the POD and FAR as illustrated in Figure 5-39, Figure 5-40, and Figure 5-41. Among the three bias correction methods, QM still resulted in the highest ETS in each month.

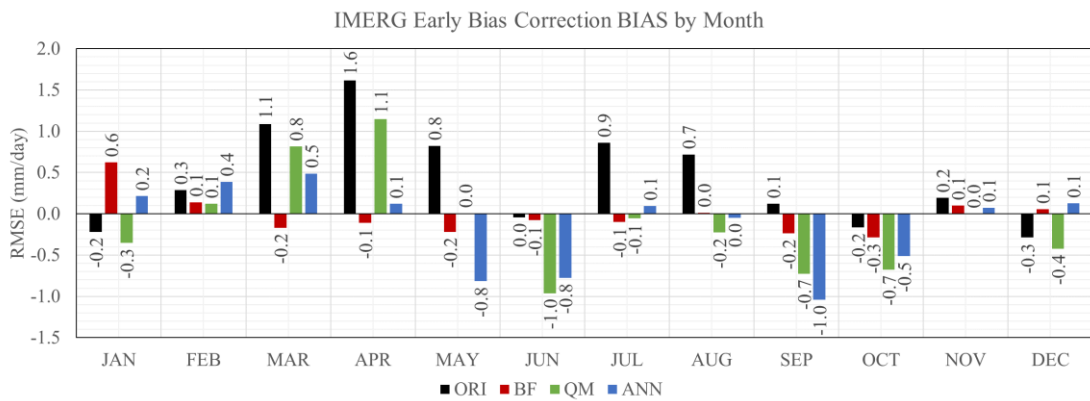


Figure 5-36. BIAS of Adjusted IMERG Early Daily Rainfall by Month

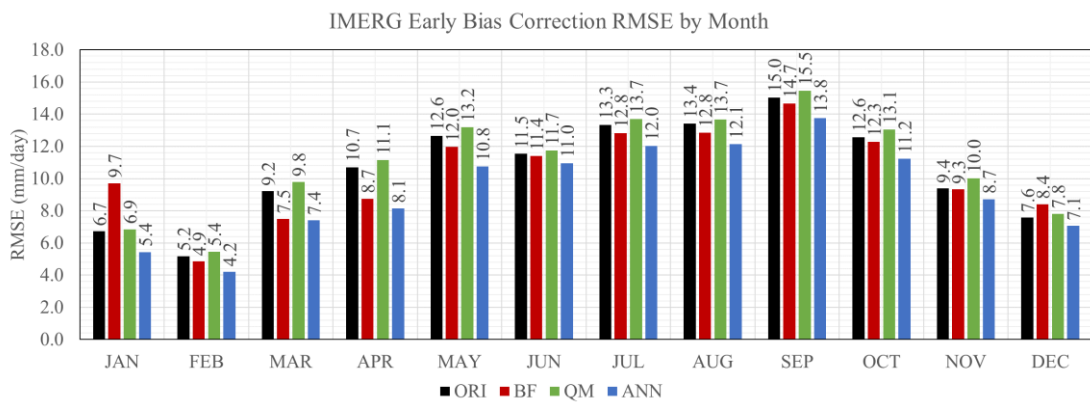


Figure 5-37. RMSE of Adjusted IMERG Early Daily Rainfall by Month

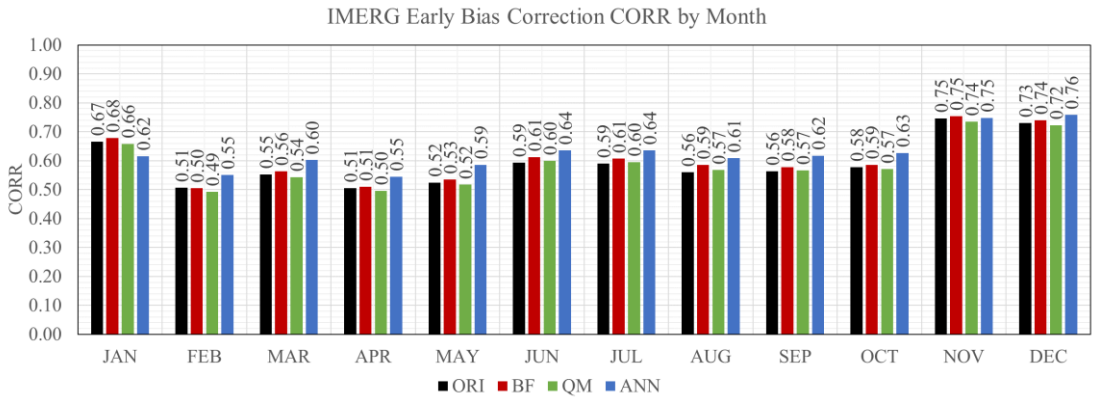


Figure 5-38. CORR of Adjusted IMERG Early Daily Rainfall by Month

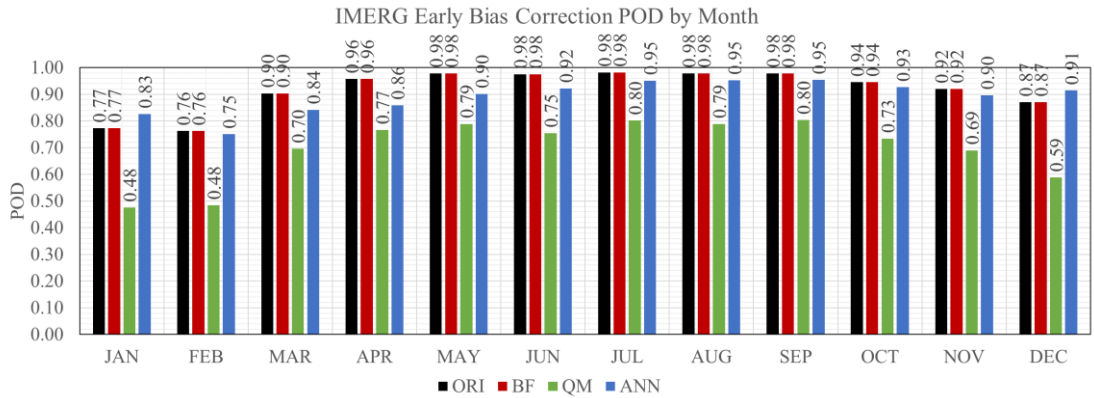


Figure 5-39. POD of Adjusted IMERG Early Daily Rainfall by Month

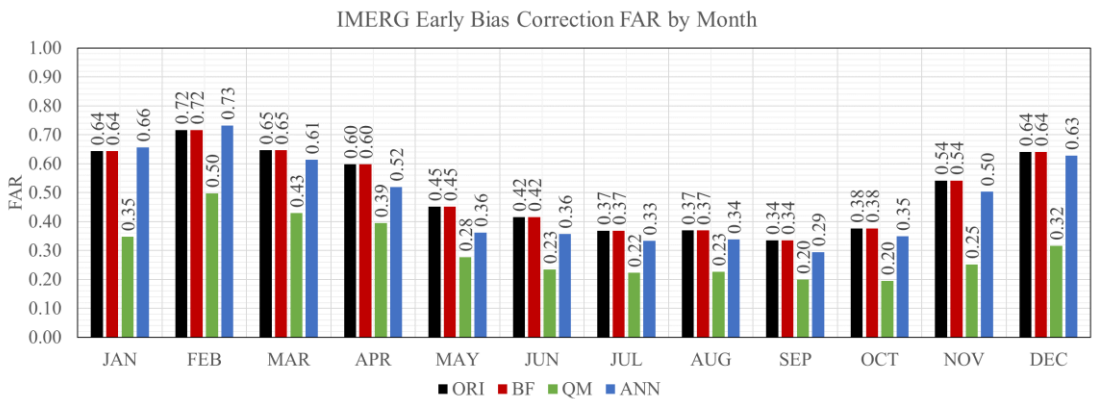


Figure 5-40. FAR of Adjusted IMERG Early Daily Rainfall by Month



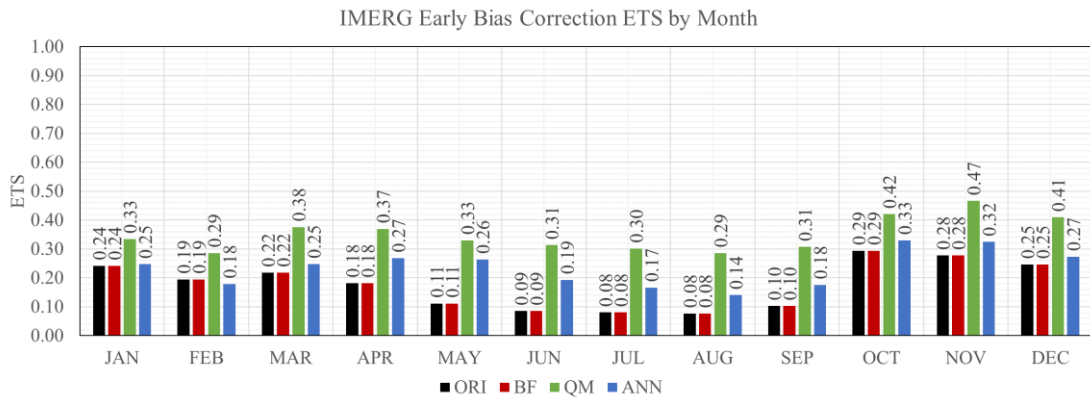


Figure 5-41. ETS of Adjusted IMERG Early Daily Rainfall by Month

#### 5.3.4. Precipitation and Detection Analysis by Basin

Figure 5-42 illustrates the bias of each basin for every case of bias correction method with the three SPE products, including the original dataset. Evidently, the PERSIAN-CCS and IMERG Early which initially overestimate daily rainfall turn to underestimate rainfall in some basins. Inversely, GSMaP\_NRT overestimates daily rainfall in majority of basins in all correction methods. As for the errors, each pair of SPE product and applied bias correction method still follow the overall results as shown in Figure 5-43. The ANN bias correction shows improvement in all basins compared to the original SPE products. Scaling correction improved some basins in the central region for the PERSIANN-CCS and IMERG Early while worsens the errors in some basins for GSMaP\_NRT. The QM method does not significantly improve any basins compared to the other two methods. However, even after correction, it is noticeable that the errors are still higher near the coastal areas where higher intensities of rainfall occur. In addition, the correlation improved in most basins after applying ANN bias correction method to each SPE product as shown in Figure 5-44.



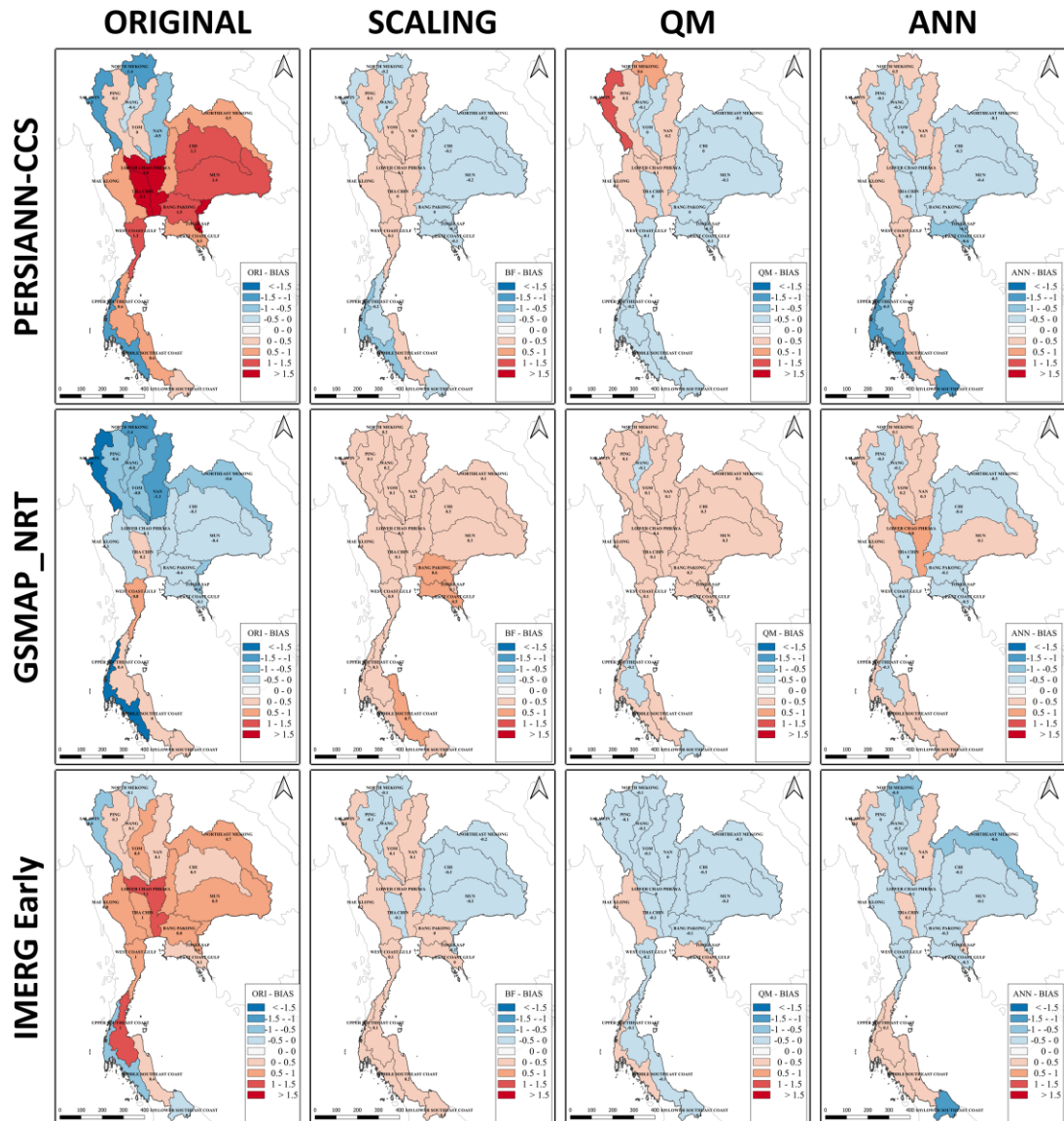


Figure 5-42. BIAS of Adjusted SPE Products Daily Rainfall by Basin

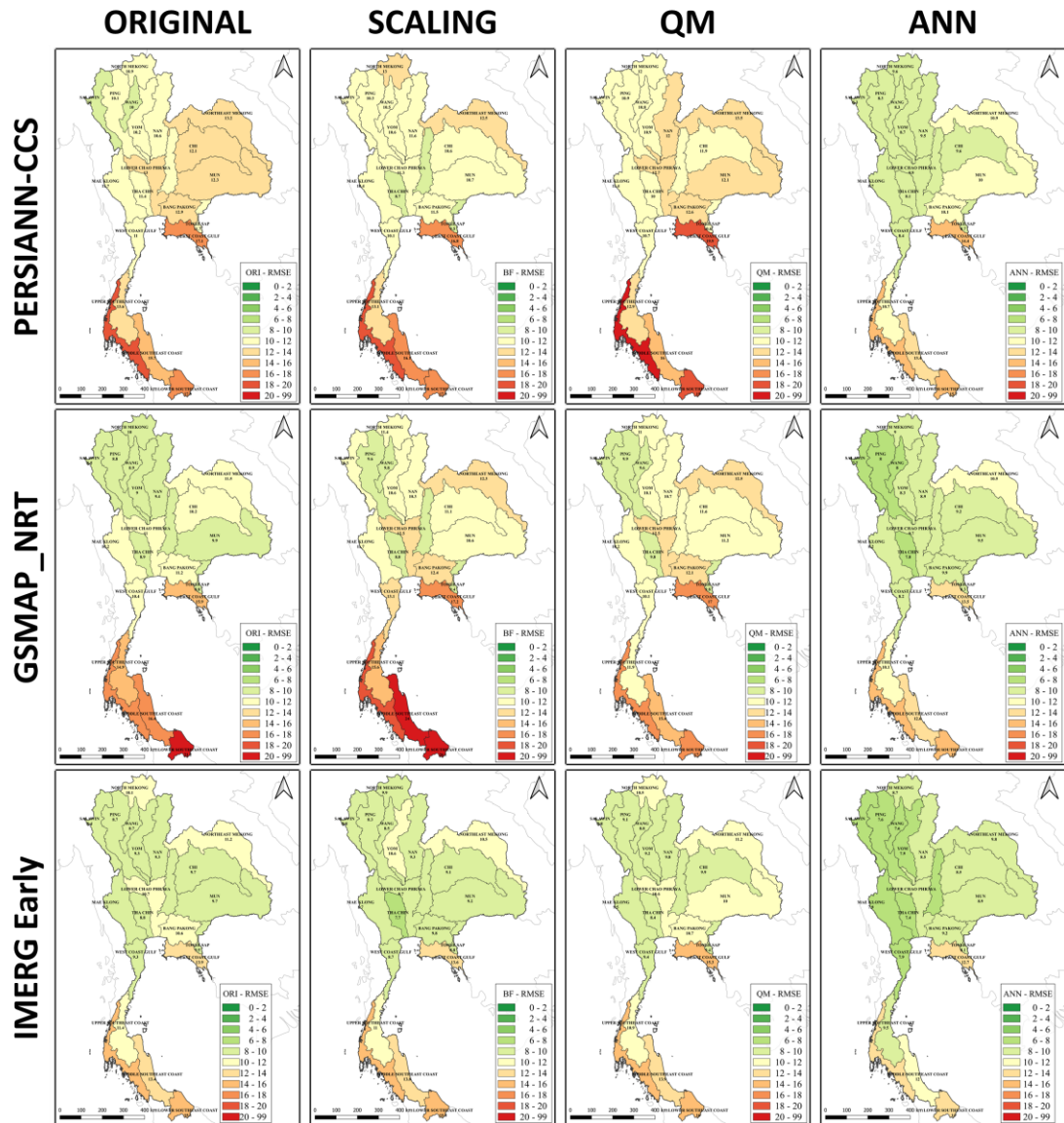


Figure 5-43. RMSE of Adjusted SPE Products Daily Rainfall by Basin

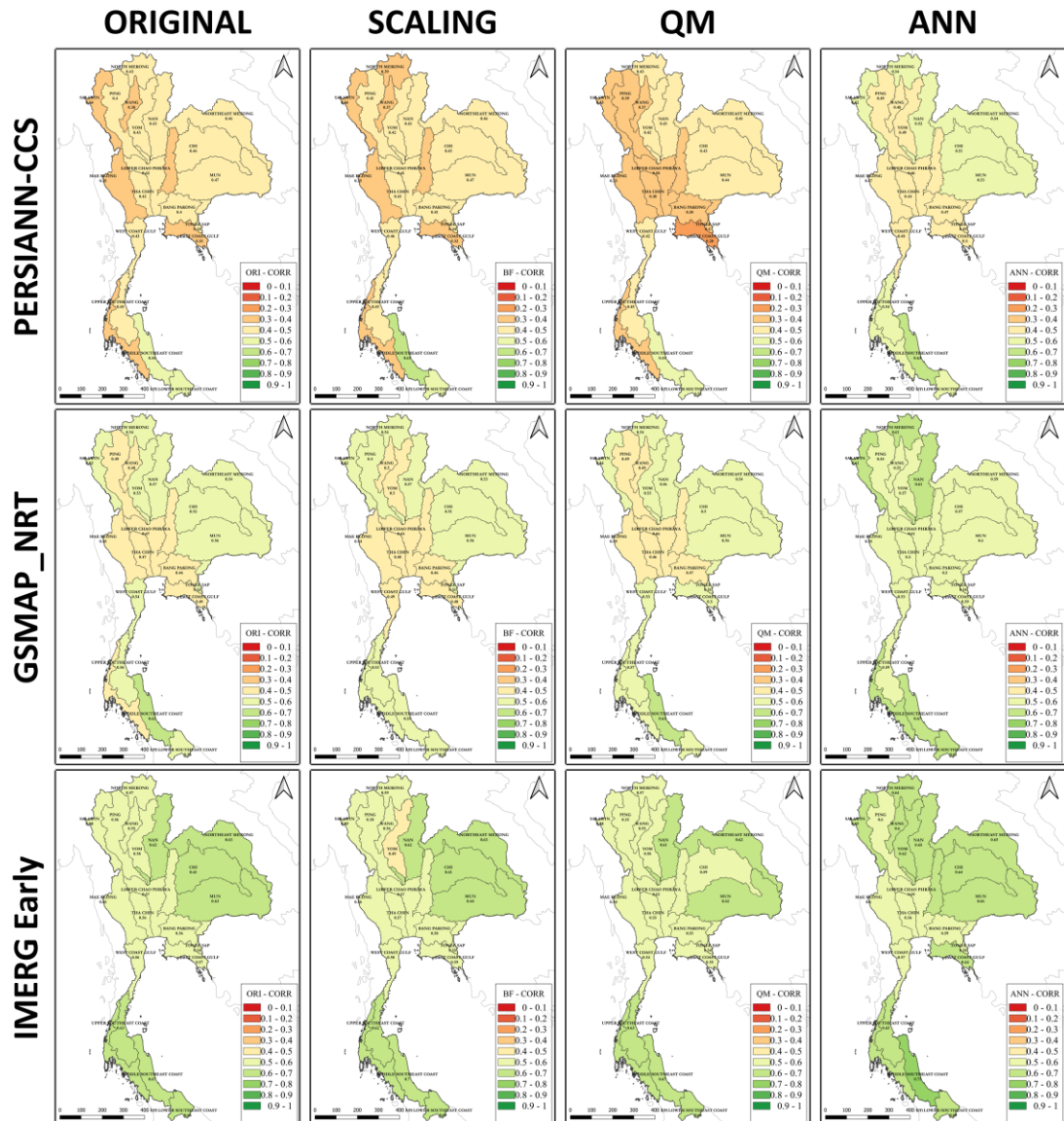


Figure 5-44. CORR of Adjusted SPE Products Daily Rainfall by Basin

Consistent to the results of the previous evaluations, the POD and FAR of some basins are reduced for GSMaP\_NRT and IMERG Early after applying the QM bias correction methods as illustrated in Figure 5-45 and Figure 5-46. Inversely, the ANN bias correction significantly increased the values of POD and FAR in some basins of GSMaP\_NRT and PERSIANN-CCS. As observed in Figure 5-47 the ANN corrected GSMaP\_NRT and PERSIANN-CCS showed lower ETS while the QM adjusted

GSMaP\_NRT and IMERG Early showed increased ETS. The improvements are more noticeable in the central, east, and some parts of the southern regions.

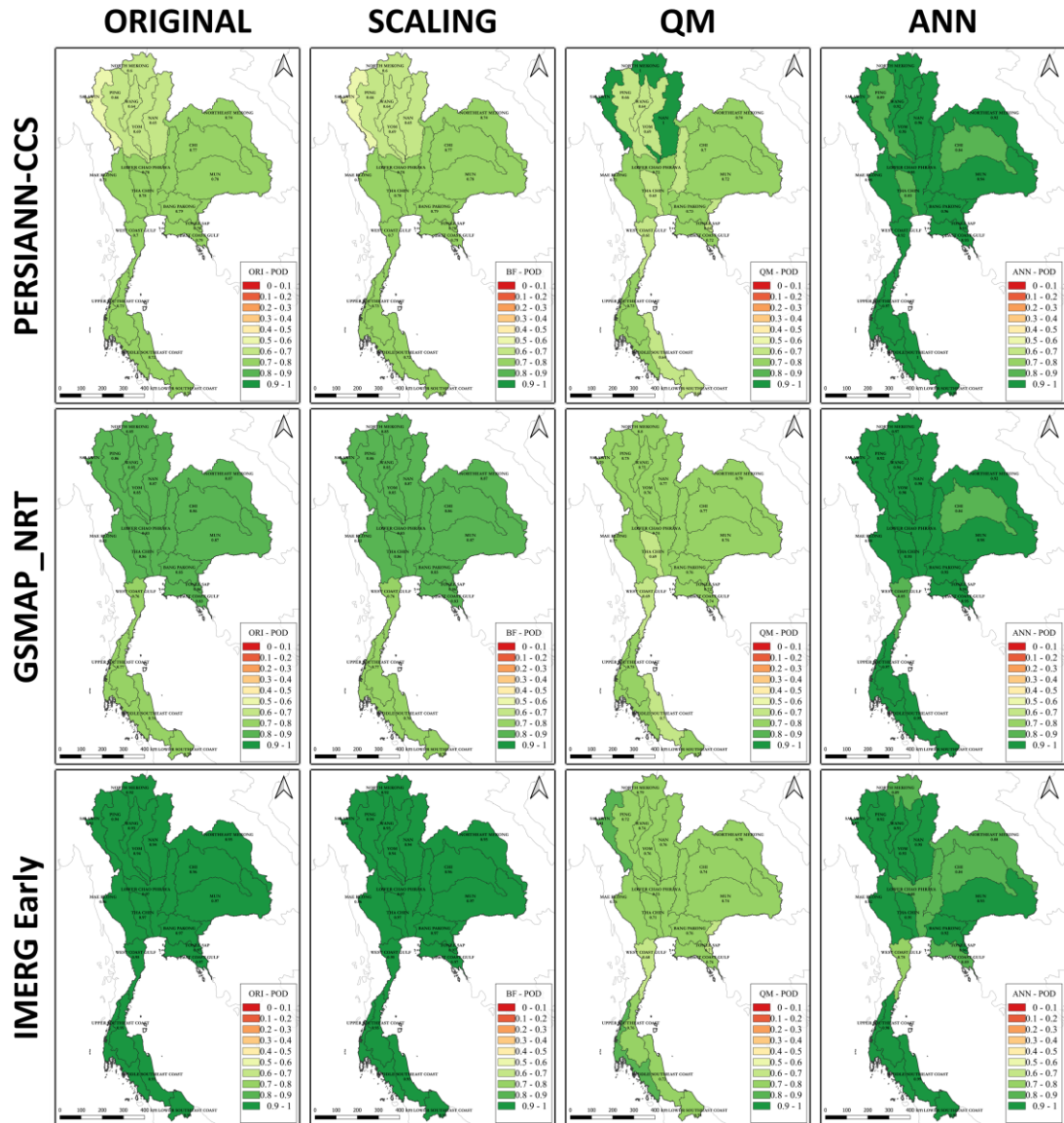


Figure 5-45. POD of Adjusted SPE Products Daily Rainfall by Basin

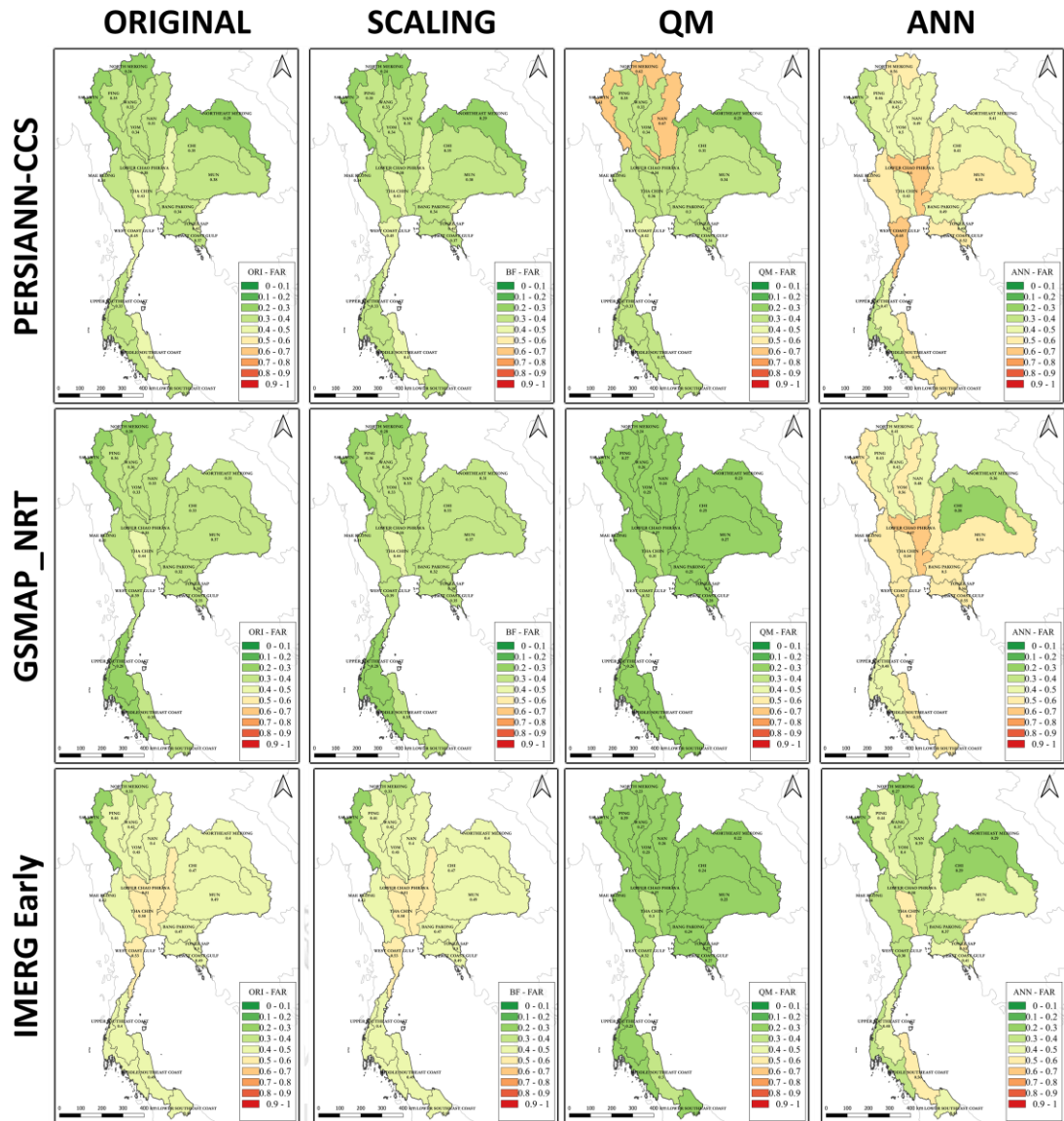


Figure 5-46. FAR of Adjusted SPE Products Daily Rainfall by Basin



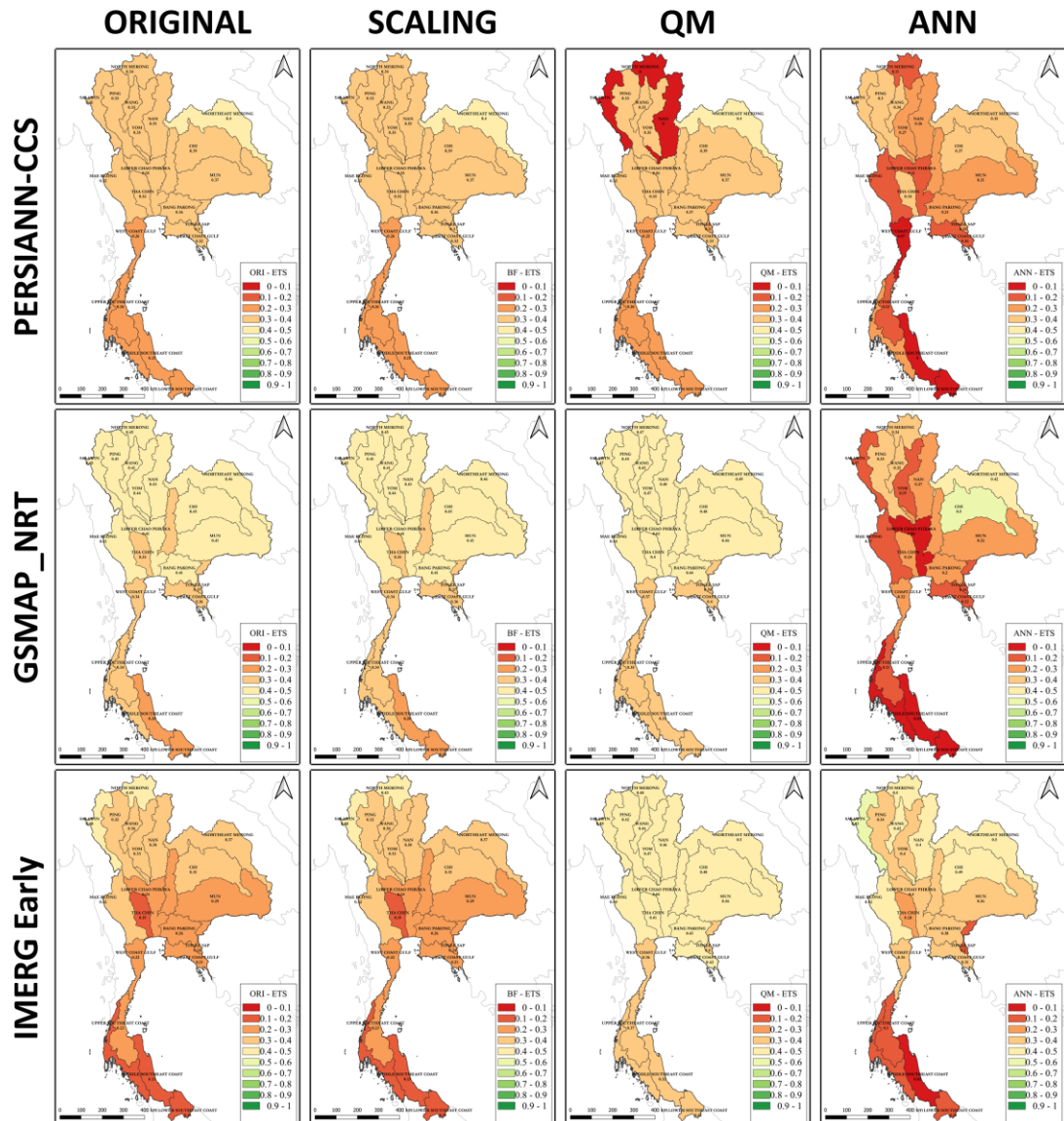


Figure 5-47. ETS of Adjusted SPE Products Daily Rainfall by Basin

### 5.3.5. Precipitation Analysis by Intensity

Figure 5-48 illustrates the bias of each original and adjusted SPE product by precipitation intensity. It is evident that the bias adjusted SPE products still follow the same pattern as the original datasets. However, the result is slightly different from the previous evaluations. In terms of no rain to moderate rain, the bias does not vary significantly from each other regardless of SPE product. On the other hand, the heavy and extreme rainfall reveals that the ANN bias correction method increases the

underestimation in these precipitation intensities. In reducing the underestimation of extreme rainfall, the scaling and QM correction methods provide better results. In the case of the extreme rainfall of GSMaP\_NRT, the scaling correction significantly reduces the bias because the original SPE products is generally underestimated. However, in observing Figure 5-49, it is noticeable that the scaling correction for GSMaP\_NRT still increases the errors for the extreme rainfall. QM correction is the only method that reduces the errors for the extreme rainfall. In any other precipitation range, the ANN method provides lower RMSE values. Furthermore, Figure 5-50 shows that the ANN correction also results in the highest correlation coefficient for each case.



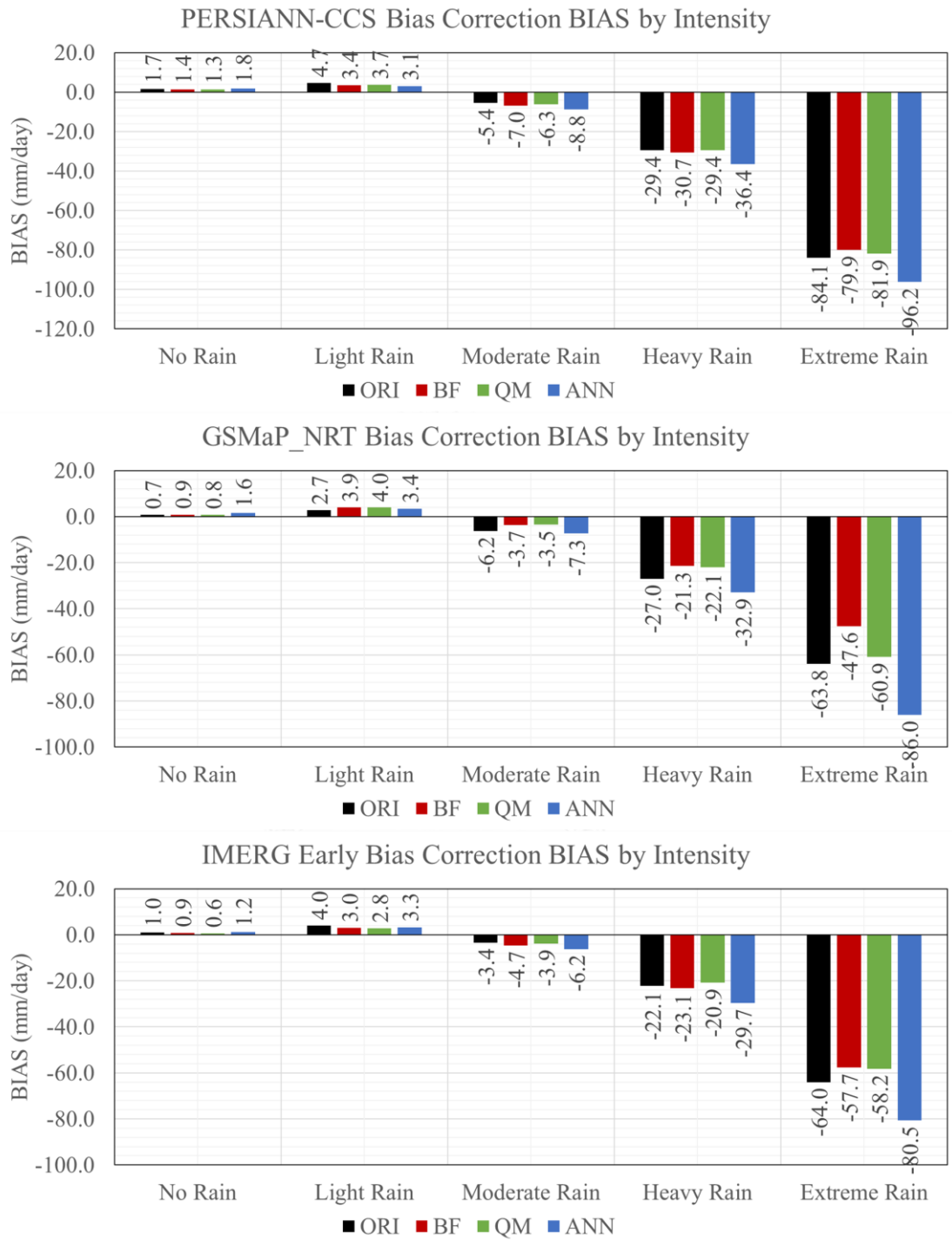


Figure 5-48. BIAS of Adjusted SPE Products Daily Rainfall by Basin



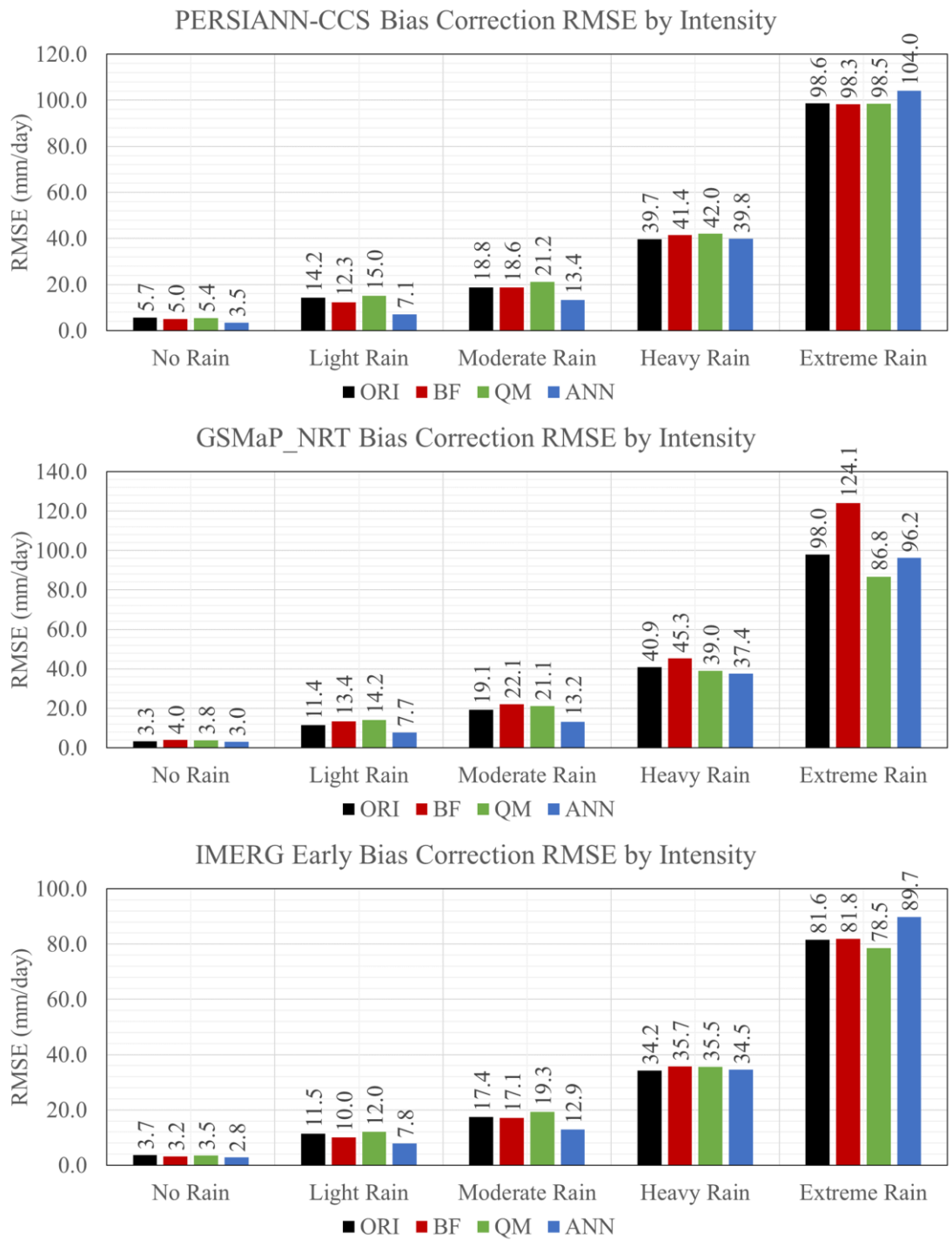


Figure 5-49. RMSE of Adjusted SPE Products Daily Rainfall by Basin

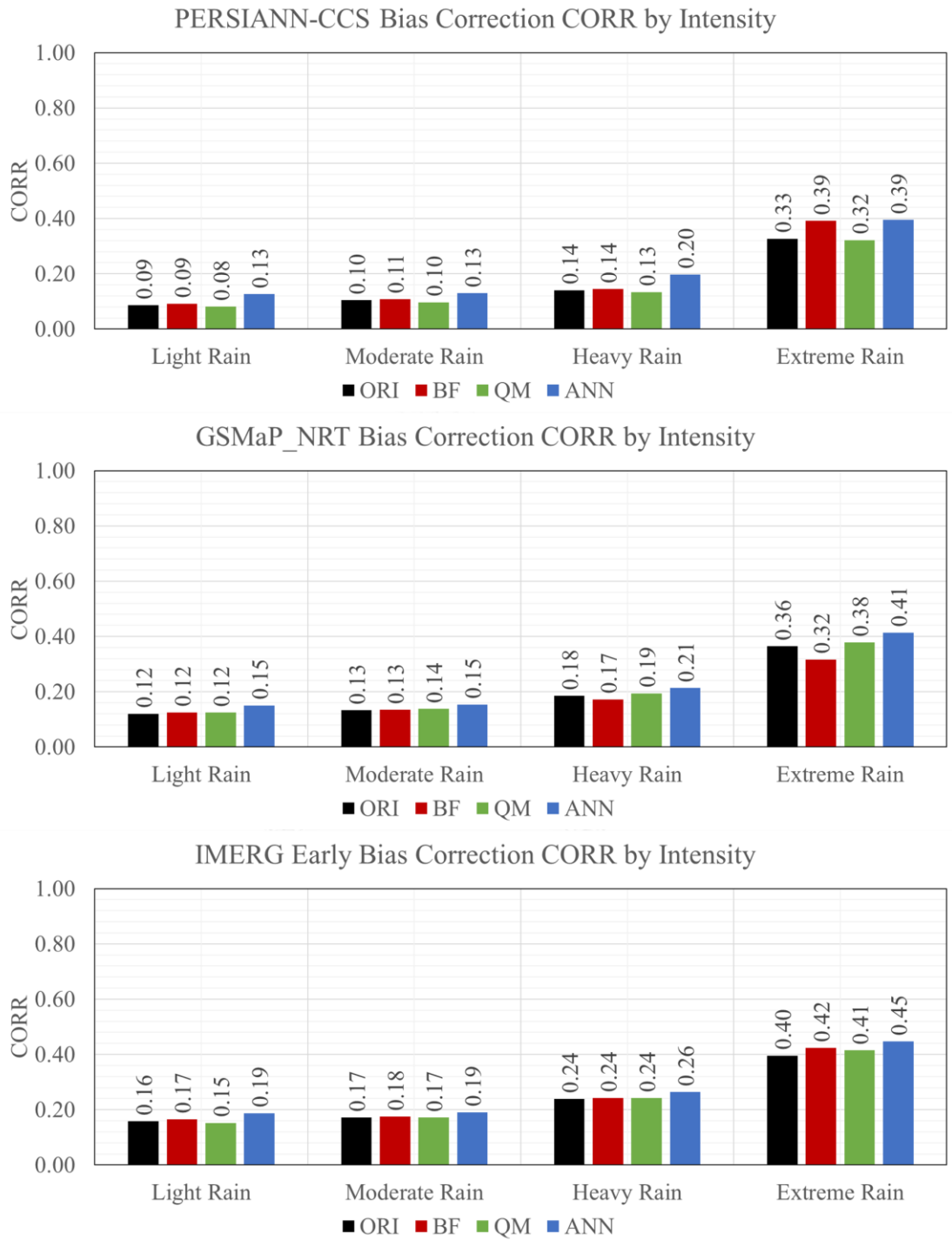


Figure 5-50. CORR of Adjusted SPE Products Daily Rainfall by Basin

#### 5.4. Comparison of Adjusted SPE Products

Table 5-1 summarizes the strong and weak points of each bias correction method applied in this study. Scaling correction can take advantage of its capability to consider space and time variations easily. Moreover, the method is fairly simple and easy to understand and execute. In addition, it is effective in dealing with overestimations even if the method is simple. However, it still has its disadvantages. Firstly, the scaling method in this study cannot improve detection skills as it only applies the bias factor through multiplicative means. Furthermore, as shown with the GSMaP\_NRT dataset, it is weak in dealing with underestimations where it would tend to increase high rainfall which may result in higher errors. Finally, there is little room for improvement in the methodology. Because of its simplicity, there are only limited ways to improve the method. One of the ways to improve the scaling is by including an additive factor which may be able to deal with detection skills.

As for the QM correction method, it is good at dealing with extreme rainfall intensities. It was able to successfully lower underestimation and RMSE for extreme rainfall. Furthermore, it is effective at reducing false alarms. Both of these advantages can be attributed to its methodology in mapping the satellite CDF to the gauge CDF. In addition, although it is more complex than scaling correction, the methodology is generally understandable with enough background on statistics. As such, there is still room for improvement for the method as other statistical methods may be incorporated in the approach. One of the key disadvantages of QM in this study is that it is less effective with non-extreme events. Another disadvantage is that similar to the case of reducing false alarms, the method can reduce correct hits and convert them into missing data.

Table 5-1. Summary of strong and weak points of each bias correction method

	<b>Advantages</b>	<b>Limitations</b>
<b>Scaling Correction</b>	Can consider space and time variations	Cannot improve detection skills
	Simple and not complicated to execute	Weak with underestimation
	Effective with dealing with overestimations	Little room for improvement in the methodology
<b>Quantile Mapping</b>	Good at dealing with extreme rainfall intensities	Ineffective with non-extreme events
	Effective at reducing false alarms	
	More complex than scaling but generally understandable	Lowers POD by turning real prediction to missing data
	Has room for improvement in the methodology	
<b>Artificial Neural Network</b>	Greatly reduces overall errors	Methodology is like a black box
	Effective at reducing non-extreme rainfall	Requires more data to execute more effectively
	Can be applied to all three SPEs	Weak against extreme events
	Extremely large room for improvement	Lowers detection skill by increasing false alarms

The ANN bias correction method has both great strong points and weak points. The most compelling attribute of the ANN correction is that it greatly reduces the overall error, especially with non-extreme rainfall. Moreover, it can be applied to all three SPEs used in the study. In addition, since the field and study of neural networks is still growing, there is a large room for improvement for this method such as using deep learning tools and methods. However, at its core, a neural network is still like a black box in which the structure itself may not give full insight of the model. Also, these networks require large amounts of data in order to accurately train the model and properly predict the target output. In addition, the ANN model developed in this study showed weakness in improving extreme rainfall events. False alarms were also

increased for PERSIANN-CCS and GSMaP\_NRT in trying to predict for hit. Additional data and information would be able to help in creating a better neural network for bias correction.

Finally, Table 5-2 lists the RMSE of each adjusted SPE product over each river basin in the country. In this study, the adjusted SPE with the lowest RMSE would be selected as the best performing SPE product and bias correction method. The lowest RMSE for all basin resulted from the ANN adjusted IMERG Early. In addition, Table 5-3 illustrates the normalized RMSE of each adjusted SPE product. Although some basins in the northern part have less RMSE values than the basins in southern part, the normalized RMSE shows that the resulting error is not significantly far from each other. When the error is observed relative to the standard deviation by basin, it gives a better insight on how the SPE actually performs.

Table 5-2. Basin RMSE (mm/day) for each adjusted SPE Product

REGION	BASIN	PERSIANN-CCS			GSMaP_NRT			IMERG Early		
		Scaling	QM	ANN	Scaling	QM	ANN	Scaling	QM	ANN
NORTH	NORTH MEKONG	13.0	12.0	9.6	11.4	11.0	9.0	9.9	10.5	8.7
	PING	10.3	10.9	8.3	9.6	9.9	8.0	8.3	9.1	7.6
	YOM	10.6	10.9	8.7	10.6	10.1	8.3	10.6	9.2	7.9
	WANG	10.5	10.8	8.3	9.8	9.6	8.0	8.5	8.8	7.6
	NAN	11.6	12.0	9.5	10.3	10.7	8.9	9.3	9.8	8.5
NORTHEAST	SALAWIN	11.9	10.7	8.3	10.3	9.2	7.7	8.8	8.8	7.4
	CHI	10.6	11.9	9.6	11.1	11.6	9.2	9.1	9.9	8.5
	MUN	10.7	12.1	10.0	10.6	11.2	9.5	9.2	10.0	8.9
	NORTHEAST MEKONG	12.5	13.5	10.9	12.3	12.5	10.5	10.5	11.2	9.8
	LOWER CHAO PHRAYA	11.3	12.7	9.9	12.5	12.5	9.7	9.7	10.6	9.0
CENTRAL	PASAK	9.9	11.3	8.7	9.6	10.5	8.2	8.1	9.1	7.7
	MAE KLONG	10.4	11.4	8.7	11.7	10.2	8.2	8.7	9.5	7.9
	THA CHIN	8.7	10.0	8.1	8.8	9.8	7.8	7.7	8.4	7.4
	BANG PAKONG	11.5	12.6	10.1	12.4	12.1	9.9	9.8	10.7	9.2
	TONLE SAP	9.5	10.6	8.7	9.4	9.8	8.3	8.8	9.4	8.1
EAST	EAST COAST GULF	16.8	19.9	14.4	17.2	17.0	13.5	13.6	15.3	12.7
	WEST COAST GULF	10.1	10.7	8.4	13.1	10.1	8.2	8.7	9.4	7.9
	MIDDLE SOUTHEAST COAST	16.1	16.0	13.4	24.0	15.4	12.6	13.8	13.9	12.0
	UPPER SOUTHEAST COAST	13.1	12.9	10.7	15.6	11.9	10.1	11.0	10.9	9.5
	SOUTHWEST COAST	18.2	20.2	15.0	19.2	17.5	14.2	14.5	15.6	13.2
SOUTH	LOWER SOUTHEAST COAST	17.9	19.0	15.7	26.1	17.8	15.0	15.8	16.0	14.0

Table 5-3. Basin Normalized RMSE for each adjusted SPE Product

REGION	BASIN	PERSIANN-CCS			GSMaP_NRT			IMERG Early		
		Scaling	QM	ANN	Scaling	QM	ANN	Scaling	QM	ANN
NORTH	NORTH MEKONG	1.14	1.05	0.83	0.99	0.96	0.78	0.86	0.92	0.76
	PING	1.06	1.13	0.85	0.99	1.02	0.82	0.85	0.94	0.78
	YOM	1.04	1.07	0.86	1.04	0.99	0.81	1.04	0.90	0.78
	WANG	1.09	1.12	0.87	1.02	1.00	0.83	0.88	0.92	0.79
	NAN	1.04	1.07	0.85	0.91	0.95	0.79	0.83	0.87	0.76
NORTHEAST	SALAWIN	1.23	1.11	0.86	1.06	0.95	0.80	0.91	0.91	0.76
	CHI	0.94	1.06	0.85	0.98	1.03	0.81	0.81	0.88	0.76
	MUN	0.92	1.04	0.86	0.91	0.96	0.81	0.79	0.86	0.76
	NORTHEAST MEKONG	0.96	1.03	0.83	0.94	0.95	0.80	0.80	0.85	0.75
	LOWER CHAO PHRAYA	1.00	1.13	0.88	1.10	1.11	0.86	0.86	0.94	0.80
CENTRAL	PASAK	1.02	1.16	0.89	0.99	1.08	0.84	0.83	0.93	0.79
	MAE KLONG	1.08	1.18	0.90	1.21	1.05	0.85	0.90	0.98	0.81
	THA CHIN	0.95	1.10	0.88	0.96	1.07	0.85	0.84	0.92	0.81
	BANG PAKONG	1.00	1.10	0.88	1.08	1.06	0.86	0.86	0.93	0.80
	TONLE SAP	0.95	1.06	0.87	0.94	0.98	0.83	0.88	0.94	0.81
EAST	EAST COAST GULF	1.03	1.21	0.88	1.05	1.04	0.82	0.83	0.93	0.77
	WEST COAST GULF	1.00	1.06	0.83	1.29	1.00	0.81	0.86	0.93	0.78
	MIDDLE SOUTHEAST COAST	0.91	0.91	0.76	1.37	0.88	0.72	0.79	0.79	0.68
	UPPER SOUTHEAST COAST	1.02	1.00	0.83	1.21	0.92	0.79	0.86	0.85	0.74
	SOUTHWEST COAST	1.03	1.14	0.85	1.08	0.98	0.80	0.82	0.88	0.74
LOWER SOUTHEAST COAST	0.90	0.96	0.79	1.31	0.90	0.76	0.80	0.80	0.70	

## CHAPTER 6

### Conclusions and Recommendations

#### 6.1. Conclusions

Satellite precipitation estimates are great supplementary data for rainfall quantification as these products provide coverage over the vast majority of the world. These space-borne radars can fill in the gaps in areas without dense rain gauge networks and ground radar stations. However, as shown in the literatures and results of this study, SPE products still have biases that should be corrected in order to be fully utilized.

In terms of the evaluation, each of the original SPE product has its strong points and weak points. It is observed that the precipitation is consistently underestimated as rainfall intensity increases. Furthermore, higher errors and lower correlations are more noticeable during the wet months and in high and extreme rainfall events. Moreover, higher errors can be observed in the coastal areas such as the southern and eastern parts of Thailand. As for the detection skill, the POD and FAR are better during wet months than the dry months. Likewise, the ETS of the SPE products is slightly lower during the wet season even though its values do not vary from each month significantly. PERSIAN-CCS and IMERG Early overestimate rainfall overall in any time scale while GSMaP\_NRT tended to underestimate precipitation. Furthermore, IMERG Early shows the best performance in terms of quantitative statistics. However, IMERG Early has the lowest ETS among the three SPES because there are higher amounts of false alarms.

For the bias correction calibration and validation phases, it can already be inferred which SPE products and bias correction method would work well together. It has been shown that QM and scaling correction have high RMSE values for



PERSIANN-CCS and GSMaP\_NRT respectively. This result implies that the methods may not work well together. On the other hand, the ANN correction method consistently shows lowered RMSE for all three SPE products. Overall, the ANN correction method shows consistently satisfactory results in terms of quantitative statistics. From the annual to daily timescale, the ANN correction bests the other two methods in terms of RMSE. Although the scaling correction has better bias reduction by month due to its methodology being able to consider monthly variations, the ANN correction still has the least errors. The same pattern applies with the analysis by basin. However, the ANN correction has some weaknesses in address detection skills. Although it lowers the errors, the POD and FAR for PERSIANN-CCS and GSMaP are increased which significantly decrease the ETS of both SPE products. One of the possible reasons why the detection skill of IMERG does not worsen unlike the other two may be attributed to the fact that it already has high POD and FAR. Furthermore, the ANN correction method lacks in addressing extreme rainfall. Based on the analysis by precipitation, the ANN correction greatly increases underestimation as well as the RMSE. On the other hand, the areas in which the ANN correction lacks are where QM correction proved to be more capable. Although the QM tends to reduce POD, it also reduces the FAR which improves ETS. Moreover, the QM consistently lowers the underestimation and RMSE in extreme rainfall intensities.

In terms of the correction methods, scaling correction is simple and it has the capability to easily consider spatiotemporal variations. Even with its simplicity, it is effectively reducing overestimations. However, the scaling method in this study cannot improve detection skills and it is weak in dealing with underestimations. As for the QM correction method, it deals with reducing both the biases and errors of extreme rainfall

intensities. It is also effective improving detection skills. However, the QM method in this study is less effective with normal rainfall events. As for the ANN, the bias correction method can greatly reduce the overall error, especially with non-extreme rainfall for all three SPEs used in the study. However, the model requires more data input in order to train the model. The ANN adjusted SPE products do not improve in the extreme rainfall events. Moreover, ANN aims to match between SPEs and observation while Scaling and QM aim to reduce the bias so ANN should not be compared directly with Scaling and QM.

The adjusted satellite precipitation estimate product with the least error for all basin is the ANN adjusted IMERG Early. Therefore, in this study, it is the best performing bias correction. However, it should be noted that this adjusted dataset still has its disadvantage in terms of its detection skills and its high error and bias in the extreme rainfall. The purpose of using the adjusted satellite precipitation should also be considered as each SPE product and correction method has its own specific qualities that makes it unique in certain scenarios. Understanding the basics of each methodology is beneficial in deciding which bias correction method should be applied as each one has its own advantages and limitations.

## 6.2. Recommendations

Further research is recommended in order to improve both the evaluation and correction. As for improving the evaluation, it may be possible to further specifically look into each region or basin in order to have a clearer understanding of the more detailed processes within each area. It would be beneficial to find a different perspective in evaluating the SPEs. Moreover, rain gauges located in mountainous areas are vital in improving the quality of SPEs.

As stated previously, each bias correction method has its own advantages to potentially improve its adjustments. As for the scaling correction, the resulting satellite values from an underestimated product increased its higher rainfall values. Therefore, this outcome should be considered when improving the scaling correction. Additionally, it may be possible to have an additive factor which would be able to address its weakness in its inability to improve detection skills, similar to the work of Gumindoga et al. (2016). In terms of the QM bias correction, this adjustment scheme did not perform well on non-extreme events. It would be recommended to separate the data to extreme and non-extreme data for the correction. Moreover, it may be possible to apply other statistical concepts such as multivariate CDF in order to account for non-rainfall factors such as in the ANN method. Similarly, although the ANN method has shown its capability in correcting the biases of satellite rainfall products, there are still numerous ways to improve the methodology. It would be recommended to apply deep learning techniques such as a 3D Convolutional Neural Networks (CNN) and take into account both spatial and temporal patterns in the training process. Since SPE datasets are grid files, taking advantage of these additional data points could potentially improve results.

Lastly, instead of simply conducting bias correction, it is possible to explore other options in utilizing SPE data, especially in near real-time applications. Some approaches include the merging of the SPE products with rain gauge measurements and/or other precipitation quantification. This approach may improve the prediction in areas with sparse gauge networks as more datasets may be utilized in the estimations.



## REFERENCES

- Abbot, J., & Marohasy, J. (2012). Application of artificial neural networks to rainfall forecasting in Queensland, Australia. *Advances in Atmospheric Sciences*, 29(4), 717-730.
- Alharbi, R., Hsu, K., & Sorooshian, S. (2018). Bias adjustment of satellite-based precipitation estimation using artificial neural networks-cloud classification system over Saudi Arabia. *Arabian Journal of Geosciences*, 11(17), 508.
- Amengual, A., Homar, V., Romero, R., Alonso, S., & Ramis, C. (2012). A statistical adjustment of regional climate model outputs to local scales: application to Platja de Palma, Spain. *Journal of Climate*, 25(3), 939-957.
- Ashouri, H., Hsu, K.-L., Sorooshian, S., Braithwaite, D. K., Knapp, K. R., Cecil, L. D., . . . Prat, O. P. (2015). PERSIANN-CDR: Daily precipitation climate data record from multisatellite observations for hydrological and climate studies. *Bulletin of the American Meteorological Society*, 96(1), 69-83.
- Behrangi, A., Khakbaz, B., Jaw, T. C., AghaKouchak, A., Hsu, K., & Sorooshian, S. (2011). Hydrologic evaluation of satellite precipitation products over a mid-size basin. *Journal of Hydrology*, 397(3-4), 225-237.
- Bui, H. T., Ishidaira, H., & Shaowei, N. (2019). Evaluation of the use of global satellite-gauge and satellite-only precipitation products in stream flow simulations. *Applied Water Science*, 9(3), 53.
- Coulibaly, P., & Evora, N. (2007). Comparison of neural network methods for infilling missing daily weather records. *Journal of Hydrology*, 341(1-2), 27-41.
- Deng, P., Zhang, M., Guo, H., Xu, C., Bing, J., & Jia, J. (2018). Error analysis and correction of the daily GSMaP products over Hanjiang River Basin of China. *Atmospheric Research*, 214, 121-134.
- Devi, S. R., Arulmozhivarman, P., Venkatesh, C., & Agarwal, P. (2016). Performance comparison of artificial neural network models for daily rainfall prediction. *International Journal of Automation and computing*, 13(5), 417-427.
- Du, K.-L., & Swamy, M. N. (2013). *Neural networks and statistical learning*: Springer Science & Business Media.
- Gao, J., Tang, G., & Hong, Y. (2017). Similarities and improvements of GPM dual-frequency precipitation radar (DPR) upon TRMM precipitation radar (PR) in global precipitation rate estimation, type classification and vertical profiling. *Remote sensing*, 9(11), 1142.
- Gumindoga, W., Rientjes, T., Haile, A., Makurira, H., & Reggiani, P. (2016). Bias correction schemes for CMORPH satellite rainfall estimates in the Zambezi River Basin. *Hydrology and Earth System Sciences Discussions*, 1-36.
- Habib, E., Haile, A. T., Sazib, N., Zhang, Y., & Rientjes, T. (2014). Effect of bias correction of satellite-rainfall estimates on runoff simulations at the source of the Upper Blue Nile. *Remote sensing*, 6(7), 6688-6708.
- Hong, Y., Hsu, K.-L., Sorooshian, S., & Gao, X. (2004). Precipitation estimation from remotely sensed imagery using an artificial neural network cloud classification system. *Journal of Applied Meteorology*, 43(12), 1834-1853.

- Hsu, K.-I., Gao, X., Sorooshian, S., & Gupta, H. V. (1997). Precipitation estimation from remotely sensed information using artificial neural networks. *Journal of Applied Meteorology*, 36(9), 1176-1190.
- Hu, Q., Li, Z., Wang, L., Huang, Y., Wang, Y., & Li, L. (2019). Rainfall spatial estimations: A review from spatial interpolation to multi-source data merging. *Water*, 11(3), 579.
- Huffman, G. J., Bolvin, D. T., Braithwaite, D., Hsu, K., Joyce, R., Xie, P., & Yoo, S.-H. (2015). NASA global precipitation measurement (GPM) integrated multi-satellite retrievals for GPM (IMERG). *Algorithm Theoretical Basis Document (ATBD) Version, 4*, 26.
- Huffman, G. J., Bolvin, D. T., Nelkin, E. J., Wolff, D. B., Adler, R. F., Gu, G., . . . Stocker, E. F. (2007). The TRMM multisatellite precipitation analysis (TMPA): Quasi-global, multiyear, combined-sensor precipitation estimates at fine scales. *Journal of hydrometeorology*, 8(1), 38-55.
- Hur, J., Raghavan, S. V., Nguyen, N. S., & Liong, S.-Y. (2016). Evaluation of high-resolution satellite rainfall data over Singapore. *Procedia Engineering*, 154, 158-167.
- Jakob Themeßl, M., Gobiet, A., & Leuprecht, A. (2011). Empirical - statistical downscaling and error correction of daily precipitation from regional climate models. *International Journal of Climatology*, 31(10), 1530-1544.
- Jamandre, C., & Narisma, G. T. (2013). Spatio-temporal validation of satellite-based rainfall estimates in the Philippines. *Atmospheric Research*, 122, 599-608.
- Japan Aerospace Exploration Agency. (2019). Data Format Description for Global Rainfall Map Realtime version (GSMaP\_NOW) and Gauge-calibrated Rainfall Product (GSMaP\_Gauge\_NOW).
- Joyce, R. J., Janowiak, J. E., Arkin, P. A., & Xie, P. (2004). CMORPH: A method that produces global precipitation estimates from passive microwave and infrared data at high spatial and temporal resolution. *Journal of hydrometeorology*, 5(3), 487-503.
- Joyce, R. J., & Xie, P. (2011). Kalman filter-based CMORPH. *Journal of hydrometeorology*, 12(6), 1547-1563.
- Karbalae, N., Hsu, K., Sorooshian, S., & Braithwaite, D. (2017). Bias adjustment of infrared - based rainfall estimation using passive microwave satellite rainfall data. *Journal of Geophysical Research: Atmospheres*, 122(7), 3859-3876.
- Kashiwao, T., Nakayama, K., Ando, S., Ikeda, K., Lee, M., & Bahadori, A. (2017). A neural network-based local rainfall prediction system using meteorological data on the Internet: A case study using data from the Japan Meteorological Agency. *Applied Soft Computing*, 56, 317-330.
- Katiraie-Boroujerdy, P.-S., Asanjan, A. A., Hsu, K.-I., & Sorooshian, S. (2017). Intercomparison of PERSIANN-CDR and TRMM-3B42V7 precipitation estimates at monthly and daily time scales. *Atmospheric Research*, 193, 36-49.
- Kenabatho, P., Parida, B., & Moalafhi, D. (2017). Evaluation of satellite and simulated rainfall products for hydrological applications in the Notwane Catchment, Botswana. *Physics and Chemistry of the Earth, Parts A/B/C*, 100, 19-30.
- Kidd, C., & Huffman, G. (2011). Global precipitation measurement. *Meteorological Applications*, 18(3), 334-353.

- Kirstetter, P. (2019). *Quantitative Precipitation Estimation (QPE): observations from radar, gauges and satellites for flood prediction*. Paper presented at the 12th International Precipitation Conference (IPC12), Irvine, California.
- Kubat, M. (2017). *An introduction to machine learning*: Springer.
- Kumar, A., Ramsankaran, R., Brocca, L., & Munoz-Arriola, F. (2019). A Machine Learning Approach for Improving Near-Real-Time Satellite-Based Rainfall Estimates by Integrating Soil Moisture. *Remote sensing*, *11*(19), 2221.
- Kundu, S., Khare, D., & Mondal, A. (2017). Future changes in rainfall, temperature and reference evapotranspiration in the central India by least square support vector machine. *Geoscience Frontiers*, *8*(3), 583-596.
- Lary, D. J., Remer, L., MacNeill, D., Roscoe, B., & Paradise, S. (2009). Machine learning and bias correction of MODIS aerosol optical depth. *IEEE Geoscience and Remote Sensing Letters*, *6*(4), 694-698.
- LeCun, Y., Bottou, L., Orr, G., & Muller, K.-R. (1998). Efficient backprop. *Neural Networks: Tricks of the Trade*. New York: Springer.
- Lee, W.-M. (2019). *Python machine learning*: John Wiley & Sons.
- Lekula, M., Lubczynski, M. W., Shemang, E. M., & Verhoef, W. (2018). Validation of satellite-based rainfall in Kalahari. *Physics and Chemistry of the Earth, Parts A/B/C*, *105*, 84-97.
- Li, N., Wang, Z., Chen, X., & Austin, G. (2019). Studies of General Precipitation Features with TRMM PR Data: An Extensive Overview. *Remote sensing*, *11*(1), 80.
- Maggioni, V., Meyers, P. C., & Robinson, M. D. (2016). A review of merged high-resolution satellite precipitation product accuracy during the Tropical Rainfall Measuring Mission (TRMM) era. *Journal of hydrometeorology*, *17*(4), 1101-1117.
- Mahmoud, M. T., Hamouda, M. A., & Mohamed, M. M. (2019). Spatiotemporal evaluation of the GPM satellite precipitation products over the United Arab Emirates. *Atmospheric Research*, *219*, 200-212.
- Mega, T., Ushio, T., Takahiro, M., Kubota, T., Kachi, M., & Oki, R. (2018). Gauge-adjusted global satellite mapping of precipitation. *IEEE Transactions on Geoscience and Remote Sensing*, *57*(4), 1928-1935.
- Musie, M., Sen, S., & Srivastava, P. (2019). Comparison and evaluation of gridded precipitation datasets for streamflow simulation in data scarce watersheds of Ethiopia. *Journal of Hydrology*, *579*, 124168.
- Najafi, M. R., Moradkhani, H., & Wherry, S. A. (2011). Statistical downscaling of precipitation using machine learning with optimal predictor selection. *Journal of Hydrologic Engineering*, *16*(8), 650-664.
- Nasrollahi, N., Hsu, K., & Sorooshian, S. (2013). An artificial neural network model to reduce false alarms in satellite precipitation products using MODIS and CloudSat observations. *Journal of hydrometeorology*, *14*(6), 1872-1883.
- Ngo-Duc, T., Matsumoto, J., Kamimera, H., & Bui, H.-H. (2013). Monthly adjustment of Global Satellite Mapping of Precipitation (GSMaP) data over the VuGia–ThuBon River Basin in Central Vietnam using an artificial neural network. *Hydrological Research Letters*, *7*(4), 85-90.
- Nguyen, P., Ombadi, M., Sorooshian, S., Hsu, K., AghaKouchak, A., Braithwaite, D., . . . Thorstensen, A. R. (2018). The PERSIANN family of global satellite

- precipitation data: A review and evaluation of products. *Hydrology and Earth System Sciences*, 22(11), 5801-5816.
- Nwankpa, C., Ijomah, W., Gachagan, A., & Marshall, S. (2018). Activation functions: Comparison of trends in practice and research for deep learning. *arXiv preprint arXiv:1811.03378*.
- Oostwal, E., Straat, M., & Biehl, M. (2020). Hidden unit specialization in layered neural networks: ReLU vs. sigmoidal activation. *Physica A: Statistical Mechanics and its Applications*, 125517.
- Rebala, G., Ravi, A., & Churiwala, S. (2019). *An introduction to machine learning*: Springer.
- Roodschild, M., Sardiñas, J. G., & Will, A. (2020). A new approach for the vanishing gradient problem on sigmoid activation. *Progress in Artificial Intelligence*, 9(4), 351-360.
- Saber, M., & Yilmaz, K. K. (2018). Evaluation and bias correction of satellite-based rainfall estimates for modelling flash floods over the Mediterranean region: application to Karpuz River Basin, Turkey. *Water*, 10(5), 657.
- Sachindra, D., Ahmed, K., Rashid, M. M., Shahid, S., & Perera, B. (2018). Statistical downscaling of precipitation using machine learning techniques. *Atmospheric Research*, 212, 240-258.
- Su, J., Lü, H., Zhu, Y., Cui, Y., & Wang, X. (2019). Evaluating the hydrological utility of latest IMERG products over the Upper Huaihe River Basin, China. *Atmospheric Research*, 225, 17-29.
- Sungmin, O., Foelsche, U., Kirchengast, G., Fuchsberger, J., Tan, J., & Petersen, W. A. (2017). Evaluation of GPM IMERG Early, Late, and Final rainfall estimates using WegenerNet gauge data in southeastern Austria. *Hydrology & Earth System Sciences*, 21(12).
- Swamynathan, M. (2019). *Mastering machine learning with python in six steps: A practical implementation guide to predictive data analytics using python*: Apress.
- Tan, M. L., & Santo, H. (2018). Comparison of GPM IMERG, TMPA 3B42 and PERSIANN-CDR satellite precipitation products over Malaysia. *Atmospheric Research*, 202, 63-76.
- Tao, Y., Gao, X., Hsu, K., Sorooshian, S., & Ihler, A. (2016). A deep neural network modeling framework to reduce bias in satellite precipitation products. *Journal of hydrometeorology*, 17(3), 931-945.
- Teutschbein, C., & Seibert, J. (2012). Bias correction of regional climate model simulations for hydrological climate-change impact studies: Review and evaluation of different methods. *Journal of Hydrology*, 456, 12-29.
- Thakur, P. K., Nikam, B. R., Garg, V., Aggarwal, S. P., Chouksey, A., Dhote, P. R., & Ghosh, S. (2017). Hydrological parameters estimation using remote sensing and GIS for Indian region: a review. *Proceedings of the National Academy of Sciences, India Section A: Physical Sciences*, 87(4), 641-659.
- Tian, Y., Peters-Lidard, C. D., Adler, R. F., Kubota, T., & Ushio, T. (2010). Evaluation of GSMaP precipitation estimates over the contiguous United States. *Journal of hydrometeorology*, 11(2), 566-574.



- Trinh-Tuan, L., Matsumoto, J., Ngo-Duc, T., Nodzu, M. I., & Inoue, T. (2019). Evaluation of satellite precipitation products over Central Vietnam. *Progress in Earth and Planetary Science*, 6(1), 54.
- Ushio, T., Sasashige, K., Kubota, T., Shige, S., Okamoto, K. i., Aonashi, K., . . . Kachi, M. (2009). A Kalman filter approach to the Global Satellite Mapping of Precipitation (GSMaP) from combined passive microwave and infrared radiometric data. *Journal of the Meteorological Society of Japan. Ser. II*, 87, 137-151.
- Vandal, T., Kodra, E., & Ganguly, A. R. (2019). Intercomparison of machine learning methods for statistical downscaling: the case of daily and extreme precipitation. *Theoretical and Applied Climatology*, 137(1-2), 557-570.
- Velasco, L. C. P., Serquiña, R. P., Zamad, M. S. A. A., Juanico, B. F., & Lomocso, J. C. (2019). Week-ahead Rainfall Forecasting Using Multilayer Perceptron Neural Network. *Procedia Computer Science*, 161, 386-397.
- Wang, X., Ding, Y., Zhao, C., & Wang, J. (2019). Similarities and improvements of GPM IMERG upon TRMM 3B42 precipitation product under complex topographic and climatic conditions over Hexi region, Northeastern Tibetan Plateau. *Atmospheric Research*, 218, 347-363.
- Wang, Z., Zhong, R., Lai, C., & Chen, J. (2017). Evaluation of the GPM IMERG satellite-based precipitation products and the hydrological utility. *Atmospheric Research*, 196, 151-163.
- Wilks, D. S. (2011). *Statistical methods in the atmospheric sciences* (Vol. 100): Academic press.
- Yang, Y., & Luo, Y. (2014). Evaluating the performance of remote sensing precipitation products CMORPH, PERSIANN, and TMPA, in the arid region of northwest China. *Theoretical and Applied Climatology*, 118(3), 429-445.
- Yang, Z., Hsu, K., Sorooshian, S., Xu, X., Braithwaite, D., & Verbist, K. M. (2016). Bias adjustment of satellite - based precipitation estimation using gauge observations: A case study in Chile. *Journal of Geophysical Research: Atmospheres*, 121(8), 3790-3806.
- Yuan, F., Wang, B., Shi, C., Cui, W., Zhao, C., Liu, Y., . . . Chen, T. (2018). Evaluation of hydrological utility of IMERG Final run V05 and TMPA 3B42V7 satellite precipitation products in the Yellow River source region, China. *Journal of Hydrology*, 567, 696-711.

**APPENDIX A:  
Table for Scaling Bias Factors**

*Table A-1. Scaling Factors for PERSIANN-CCS*

REGION	BASIN	JAN	FEB	MAR	APR	MAY	JUN	JUL	AUG	SEP	OCT	NOV	DEC
NORTH	NORTH MEKONG	13.14	5.42	2.46	1.76	1.46	0.90	1.00	1.18	1.66	2.87	7.09	7.12
	PING	2.67	3.33	1.23	0.89	1.05	0.80	0.66	0.71	1.17	1.92	2.55	5.96
	YOM	13.60	5.79	0.72	0.77	0.93	0.84	0.76	0.92	1.24	1.32	1.01	4.38
	WANG	11.61	14.85	1.43	1.21	1.12	0.96	0.74	0.88	1.25	1.86	2.33	3.37
	NAN	13.69	5.43	1.62	1.02	1.09	1.13	1.15	1.37	1.54	1.79	2.05	4.58
	SALAWIN	7.34	2.43	1.18	0.79	1.18	1.48	1.89	1.47	1.33	2.26	2.32	2.30
NORTHEAST	CHI	1.65	2.68	0.78	0.68	0.62	0.64	0.58	0.67	0.84	1.20	1.12	1.75
	MUN	2.87	1.27	0.63	0.53	0.67	0.58	0.66	0.65	0.88	0.98	0.77	0.22
	NORTHEAST MEKONG	4.20	3.43	1.25	0.73	0.80	0.65	0.75	0.83	1.09	1.59	1.65	1.53
	LOWER CHAO PHRAYA	3.39	3.83	1.45	0.56	0.53	0.61	0.56	0.56	0.84	0.91	0.73	0.78
CENTRAL	PASAK	2.17	2.01	0.92	0.59	0.60	0.67	0.62	0.61	0.96	1.26	1.06	1.67
	MAE KLONG	1.50	2.34	1.30	0.70	0.74	0.60	0.85	0.80	0.70	1.05	1.03	1.18
	THA CHIN	2.58	2.08	0.93	0.43	0.53	0.42	0.38	0.40	0.69	0.87	0.69	0.99
	BANG PAKONG	2.43	1.33	0.57	0.40	0.55	0.66	0.87	0.76	0.90	0.83	0.84	0.36
EAST	TONLE SAP	1.84	1.03	0.33	0.44	0.49	0.52	0.66	0.73	0.69	0.90	0.96	0.69
	EAST COAST GULF	4.63	3.11	1.23	0.54	0.66	0.80	1.16	0.77	1.02	0.95	0.64	0.53
	WEST COAST GULF	4.47	1.54	1.53	0.51	0.66	0.51	0.60	0.42	0.55	0.93	0.80	0.35
SOUTH	MIDDLE SOUTHEAST COAST	3.20	2.05	0.92	0.68	0.53	0.67	0.49	0.65	0.71	0.75	1.04	1.55
	UPPER SOUTHEAST COAST	2.14	2.70	1.24	0.52	0.66	0.85	0.90	1.04	0.96	0.68	0.71	0.95
	SOUTHWEST COAST	1.28	0.87	0.74	0.55	0.82	1.56	1.35	1.94	1.50	1.17	0.65	0.88
	LOWER SOUTHEAST COAST	2.61	2.65	1.39	0.64	0.62	0.57	0.67	0.82	0.75	0.79	0.89	1.60

Table A-2. Scaling Factors for GSMaP\_NRT

REGION	BASIN	JAN	FEB	MAR	APR	MAY	JUN	JUL	AUG	SEP	OCT	NOV	DEC
NORTH	NORTH MEKONG	4.70	4.71	1.48	1.51	1.95	1.34	1.04	1.34	1.60	2.70	3.79	3.70
	PING	2.84	3.62	1.06	1.10	1.55	1.27	0.82	0.94	1.35	2.12	2.91	6.97
	YOM	7.16	3.99	0.84	1.20	1.45	1.32	0.95	1.14	1.53	1.85	1.34	4.60
	WANG	3.01	8.30	1.72	1.38	1.66	1.34	0.91	1.09	1.27	2.12	2.74	6.21
	NAN	4.91	4.85	1.35	1.21	1.40	1.31	1.19	1.59	1.59	1.91	2.24	3.10
	SALAWIN	4.50	3.33	1.28	0.94	1.45	1.95	1.92	1.93	1.40	2.06	2.86	3.54
NORTHEAST	CHI	2.39	2.18	1.16	1.10	1.16	1.33	1.00	1.06	1.26	1.30	1.64	16.37
	MUN	2.77	2.27	1.02	1.06	1.33	1.33	1.12	1.06	1.24	1.17	1.37	5.76
	NORTHEAST MEKONG	2.71	3.00	1.27	1.04	1.26	1.06	1.03	1.12	1.33	1.52	1.80	4.53
	LOWER CHAO PHRAYA	3.84	3.90	1.64	1.18	1.07	1.16	0.90	0.91	1.16	1.23	1.36	2.93
CENTRAL	PASAK	3.60	2.80	1.44	1.11	1.09	1.33	1.04	1.00	1.45	1.42	1.35	10.60
	MAE KLONG	2.13	2.71	1.64	1.07	1.18	1.24	1.24	1.28	0.98	1.39	1.89	5.02
	THA CHIN	0.61	1.09	1.14	0.86	1.06	1.06	0.70	0.76	0.99	1.29	0.92	1.18
	BANG PAKONG	1.96	2.31	1.16	0.87	1.27	1.35	1.41	1.13	1.21	1.22	1.48	2.41
EAST	TONLE SAP	2.24	1.83	0.81	0.88	1.22	1.24	1.07	1.29	1.11	1.43	1.73	6.65
	EAST COAST GULF	2.78	3.70	1.46	0.92	0.94	1.11	1.20	0.90	1.03	1.16	1.03	3.13
	WEST COAST GULF	3.49	1.53	1.47	0.70	0.82	0.81	0.74	0.67	0.64	0.97	0.81	1.58
SOUTH	MIDDLE SOUTHEAST COAST	2.27	1.87	1.05	1.13	0.81	0.95	0.76	1.03	0.91	0.87	0.91	1.64
	UPPER SOUTHEAST COAST	1.83	2.17	1.64	0.93	0.96	1.10	1.09	1.18	1.11	0.72	0.58	0.96
	SOUTHWEST COAST	1.39	1.05	1.08	1.08	1.25	1.76	1.53	2.13	1.50	1.32	0.64	1.02
	LOWER SOUTHEAST COAST	1.99	2.68	1.50	0.96	0.79	0.79	0.77	1.09	0.94	0.85	0.70	1.20

Table A-3. Scaling Factors for IMERG Early

REGION	BASIN	JAN	FEB	MAR	APR	MAY	JUN	JUL	AUG	SEP	OCT	NOV	DEC
NORTH	NORTH MEKONG	2.07	1.05	0.43	0.72	1.08	0.99	0.78	0.97	1.20	1.66	1.79	0.76
	PING	1.44	0.82	0.27	0.53	1.06	1.00	0.66	0.71	1.06	1.39	1.31	1.18
	YOM	4.68	0.99	0.32	0.56	0.86	0.96	0.71	0.86	1.03	1.00	0.74	1.72
	WANG	2.30	1.69	0.43	0.59	1.00	1.15	0.74	0.82	1.22	1.30	1.19	1.32
	NAN	2.07	1.22	0.37	0.60	0.94	1.17	0.97	1.08	1.13	1.20	0.98	1.11
	SALAWIN	1.58	1.71	0.41	0.46	1.04	1.45	1.35	1.22	1.15	1.48	1.59	0.73
NORTHEAST	CHI	0.70	0.87	0.61	0.75	0.69	0.90	0.78	0.83	0.92	1.01	1.02	1.51
	MUN	0.88	0.72	0.50	0.73	0.84	0.88	0.87	0.86	0.91	0.86	0.79	0.36
	NORTHEAST MEKONG	0.93	1.14	0.62	0.57	0.79	0.79	0.79	0.83	0.95	1.13	1.08	1.31
	LOWER CHAO PHRAYA	1.49	0.78	0.65	0.65	0.71	0.80	0.73	0.75	0.88	0.87	0.67	0.61
CENTRAL	PASAK	1.05	0.61	0.50	0.55	0.63	0.91	0.79	0.81	1.04	1.03	0.92	1.11
	MAE KLONG	0.73	0.55	0.55	0.57	0.89	0.94	0.94	0.81	0.85	1.09	1.59	1.10
	THA CHIN	0.58	0.50	0.48	0.51	0.82	0.78	0.60	0.66	0.73	0.86	0.70	0.40
	BANG PAKONG	0.88	0.63	0.47	0.48	0.75	0.95	1.06	1.00	0.93	0.87	0.94	0.35
	TONLE SAP	1.27	0.57	0.34	0.62	0.79	0.93	0.86	0.96	0.80	1.02	1.51	0.87
EAST	EAST COAST GULF	1.41	0.94	0.67	0.68	0.90	1.16	1.17	0.96	1.07	0.98	0.74	0.69
	WEST COAST GULF	2.81	0.49	0.64	0.46	0.77	0.74	0.66	0.49	0.60	1.08	0.94	0.60
	MIDDLE SOUTHEAST COAST	2.24	0.90	0.58	0.72	0.77	0.84	0.61	0.72	0.72	0.83	1.11	1.41
	UPPER SOUTHEAST COAST	1.90	1.08	0.70	0.59	0.80	0.96	0.85	0.89	0.77	0.68	0.84	1.03
SOUTH	SOUTHWEST COAST	1.05	0.64	0.65	0.71	1.14	1.63	1.25	1.60	1.20	1.11	0.80	0.96
	LOWER SOUTHEAST COAST	2.57	1.39	0.84	0.67	0.71	0.64	0.70	0.89	0.76	0.90	1.05	1.56

## APPENDIX B: CDFs from Quantile Mapping

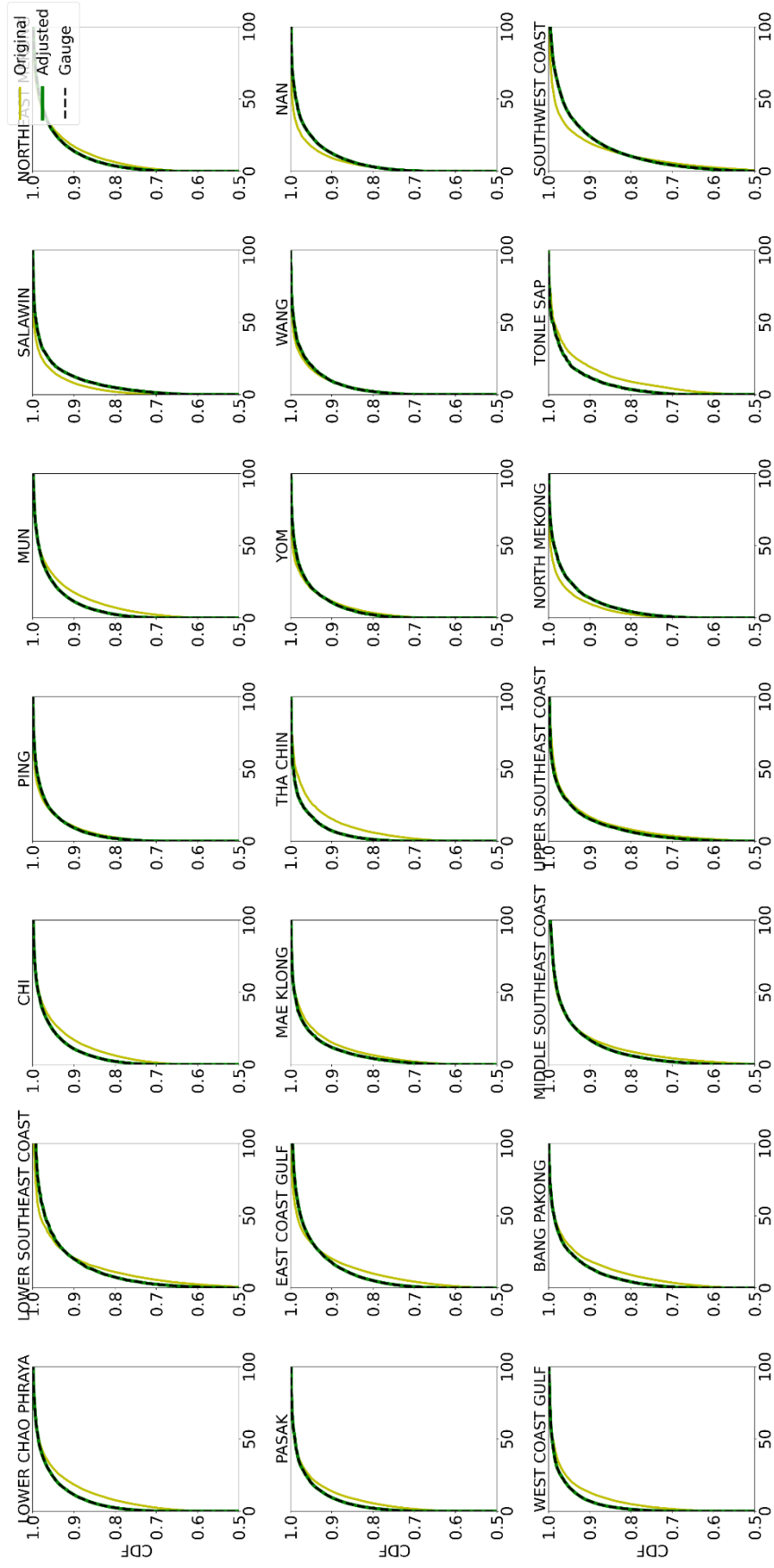


*Figure B-1. PERSIANN-CCS CDF by Basin*

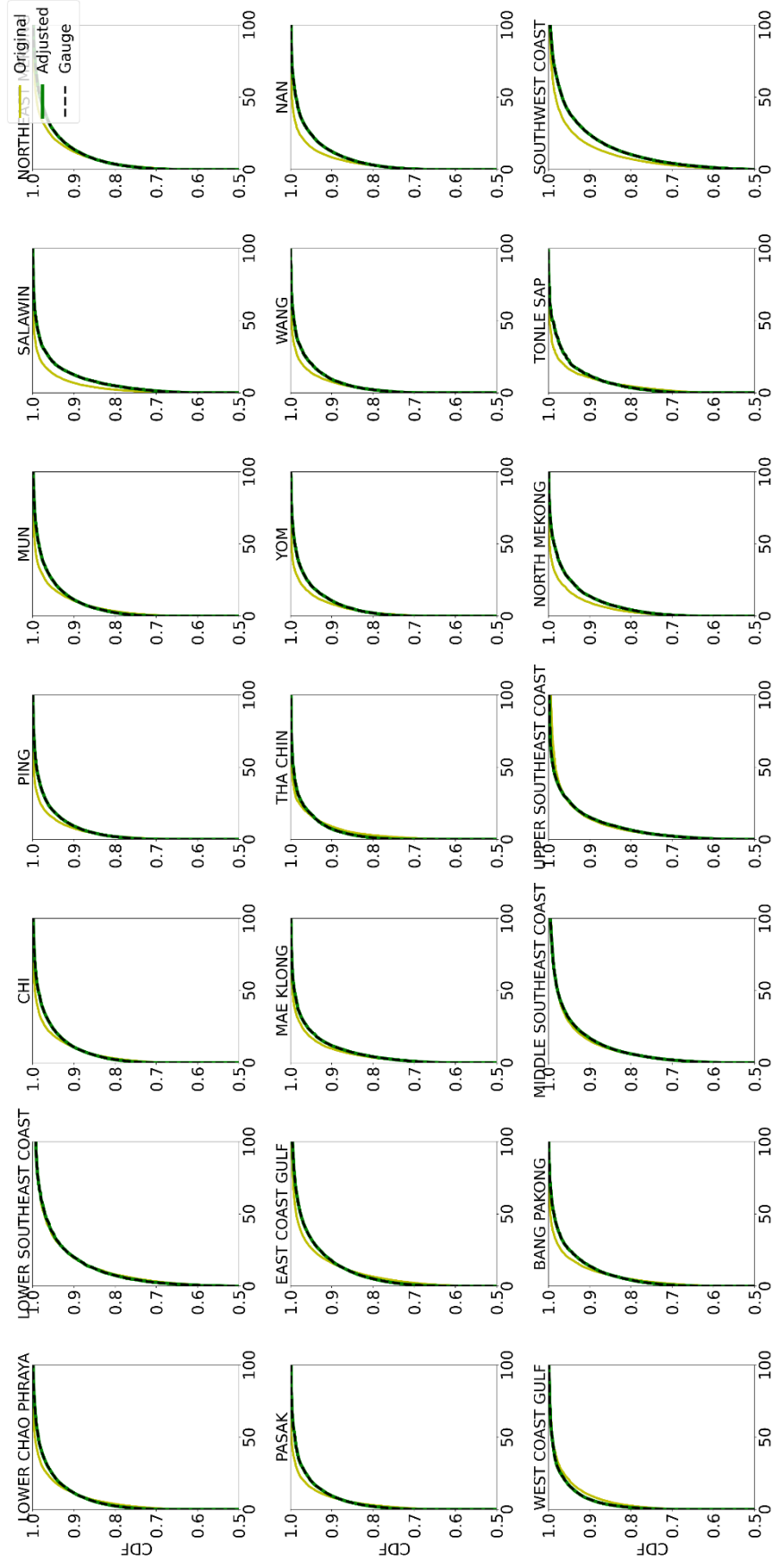


Figure B-2. GSMaP\_NRT CDF by Basin

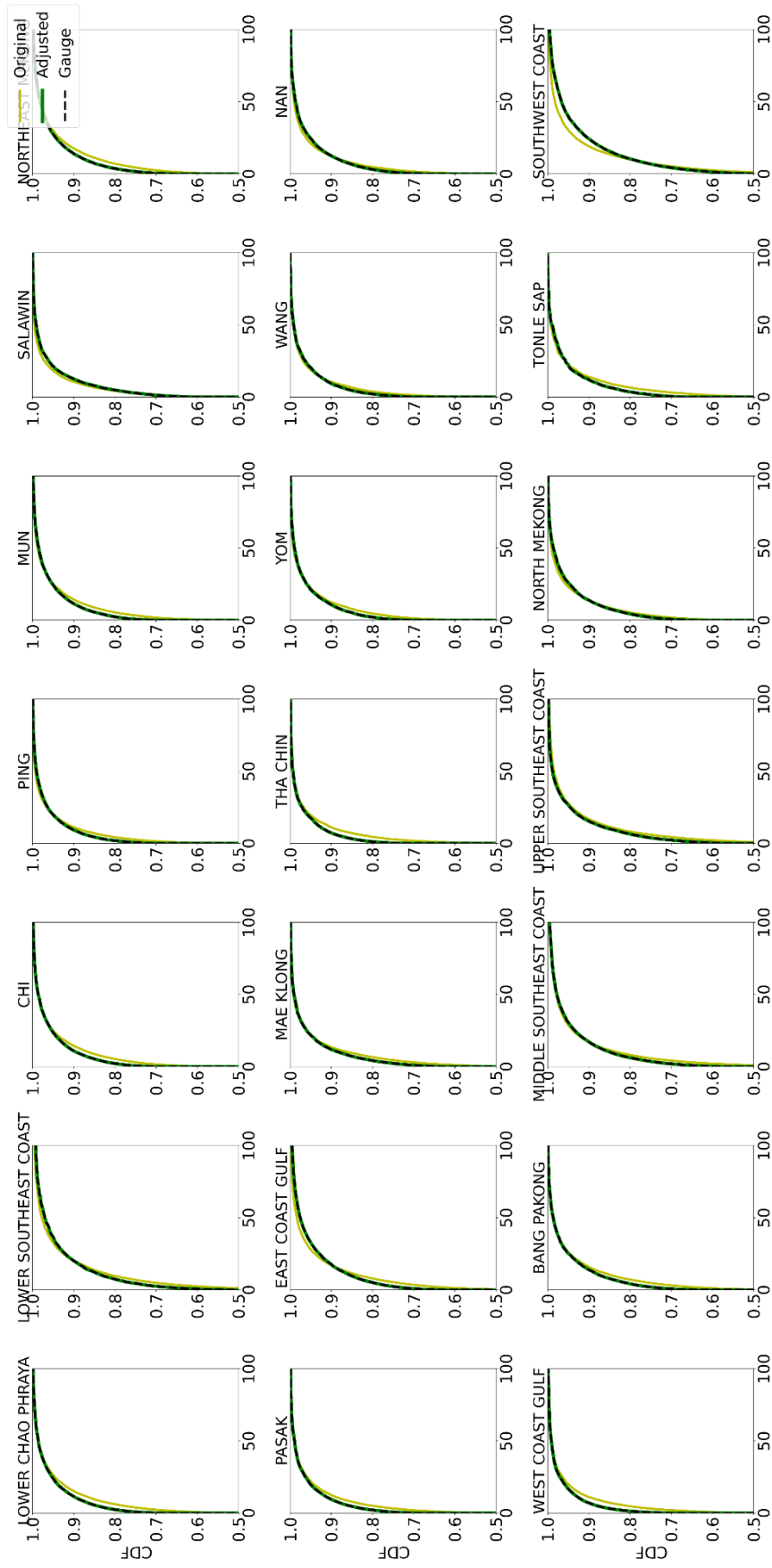


Figure B-3. IMERG Early CDF by Basin

## VITA

**NAME** Nelson Stephen Lising Ventura

**DATE OF BIRTH** 12 February 1996

**PLACE OF BIRTH** Calamba, Laguna, Philippines

**INSTITUTIONS ATTENDED** De La Salle University (2012 - 2017)

**HOME ADDRESS** 29/11 Chuea Phloeng Rd., Thung Maha Mek, Sathorn, Bangkok 10120

**PUBLICATION** Ventura, N. S. L., & Ruangrassamee, P. (2019). Cross Validation of Spatial Interpolated Rain Gage and Satellite-Based Rainfall over Chao Phraya River Basin Thailand. THA 2019 International Conference on "Water Management and Climate Change towards Asia's Water-Energy-Food Nexus and SDGs", (pp. 415-420). 23-25 January 2019. Bangkok, Thailand.